5-2014

Uniform Temperature Predictions and Temperature Gradient Effects on I-Girder and Box Girder Concrete Bridges

Edyson Rojas
Utah State University

Utah State University
MERRILL-CAZIER LIBRARY

UNIFORM TEMPERATURE PREDICTIONS AND TEMPERATURE GRADIENT EFFECTS

ON I-GIRDER AND BOX GIRDER CONCRETE BRIDGES

by

Edyson Rojas

A thesis submitted in partial fulfillment
of the requirements for the degree

of

MASTER OF SCIENCE

in

Civil and Environmental Engineering
(Structural Engineering and Mechanics)

Approved:

_____   _____
Paul J. Barr   James A. Bay
Major Professor   Committee Member

_____   _____
Marvin W. Halling   Mark McLellan
Committee Member   Vice President for Research and
                                              Dean of the School of Graduate
                                              Studies

UTAH STATE UNIVERSITY
Logan, Utah

2014

ABSTRACT

Uniform Temperature Predictions and Temperature Gradient

Effects on I-Girder and Box Girder Concrete Bridges

by

Edyson Rojas, Master of Science

Utah State University, 2014

Major Professor: Dr. Paul J. Barr
Department: Civil and Environmental Engineering

In order to more accurately quantify the behavior and degradation of bridges throughout their service life, the Federal Highway Administration lunched the Long-Term Bridge Performance Program. As part of this program an I-girder, integral abutment bridge near Perry, Utah and a two span, box-girder bridge south of Sacramento, California were instrumented with foil strain gauges, velocity transducers, vibrating wire strain gauges, thermocouples, and tiltmeters.

In this research study, data from the thermocouples was used to calculate average bridge temperature and compare it to the recommended design criteria in accordance to the 2010 LRFD Bridge Design Specifications of the American Association of State Highway and Transportation Officials (AASHTO). The design maximum average bridge temperature defined in the 2010 LRFD Bridge Design Specifications was exceeded for both bridges. The accuracy of the 1991 Kuppa Method and the 1976 Black and Emerson Method to estimate the average bridge

temperature based on ambient temperature was studied and a new method that was found to be more accurate was proposed. Long-term predictions of average bridge temperature for both bridges were calculated. Temperature gradients were measured and compared to the 2010 AASHTO LRFD Bridge Design Specifications and the 1978 Priestley Method. Calculated flexural stresses as a function of maximum positive and negative temperature gradients were found to exceed the service limit state established in the 2010 AASHTO LRFD Bridge Design Specifications in the case of the California bridge.

(139 pages)

PUBLIC ABSTRACT

Uniform Temperature Predictions and Temperature Gradient

Effects on I-Girder and Box Girder Concrete Bridges

The Federal Highway Administration (FHWA) created the Long-Term Bridge Performance (LTBP) program with the objective of acquiring quality scientific data for in-service bridge performance throughout the United States. This information will be used to improve the practices of bridge design and maintenance. To accomplish this objective, a variety of sensors were installed on a bridge south of Sacramento, California and a bridge near Perry, Utah. Data from the sensors is constantly gather and analyzed.

This research analyzed the data from the temperature sensors in order to investigate the effect of temperature changes in the California and Utah bridges over a period of more than two years. Maximum and minimum average bridge temperatures over time are determined and compared to current code specifications. Long-term bridge temperature estimations are calculated based on ambient historical data and were found to exceed code specifications. Temperature-induced stresses exceeded the code limits for the California bridge and were close to the limit in the case of the Utah bridge.

Edyson Rojas

ACKNOWLEDGMENTS

CONTENTS

LIST OF TABLES

LIST OF FIGURES

LIST OF EQUATIONS

LIST OF NOTATIONS

k .... Isotropic thermal conductivity coefficient W/m °C (Btu/(h ft °F))

Q .... Rate of heat per unit volume generated within the body W/m^3 (Btu/(h ft^3))

P .... Density kg/m^3 (lb/ft^3)

C .... Specific heat J/(kg °C) (Btu/(lb °F))

Q .... Boundary heat input or loss per unit area W/m^2 (Btu/(h ft^2))

[N] .... Linear shape functions

$\{T\}^e$ .... Column vector of four or two nodal temperature for an interior or boundary element, respectively

T(y) .... Temperature at a distance y from the centroid of the section

b(y) .... Width of section at distance y from the centroid

α .... Coefficient of thermal expansion (11×10^{-6}/°C)

E .... Modulus of elasticity

$T_{MaxDesign}$ .... Maximum design average bridge temperature.

$T_{MinDesign}$ .... Minimum design average bridge temperature.

T_{AvgMax} .... Maximum average bridge temperature.

T_{AvgMin} .... Minimum average bridge temperature.

$T_{MaxAir1}$ .... Maximum air temperature of the hottest day.

$T_{MaxAir2}$ .... Maximum air temperature of the day before the hottest day.

$T_{MinMaxAir1}$ .... Minimum air temperature of the hottest day.

$T_{MinMaxAir2}$ .... Minimum air temperature of the day before the hottest day.

$T_{MinAir1}$ .... Minimum air temperature of the coldest day.

$T_{MinAir2}$ .... Minimum air temperature of the day before the coldest day.

$T_{MaxMinAir1}$ .... Maximum air temperature of the coldest day.

$T_{MaxMinAir2}$ .... Maximum air temperature of the day before the coldest day.

n .... Total number of months.

x_i .... Measured average bridge temperature for a particular month.

y_i .... Predicted average bridge temperature for a particular month.

ε_b .... Real strain at the bottom of the cross-section.

ε_t .... Real strain at the top of the cross-section.

y_n .... Distance from the bottom to the centroid of the nth layer.

A_n .... Area of the nth layer.

h .... Height of the cross-section.

ε_{fn} .... Free strain at an nth layer.

ε_{Rn} .... Real strain at an nth layer.

ε_{sen} .... Strain due to self-equilibrating stresses at an nth layer.

σ_{sen} .... Self-equilibrating stress at an nth layer.

Φ .... Rotation.

L .... Length of the bridge.

M .... Internal moment at examined cross-section.

σ_{cn} .... Continuity stress at the nth layer of the examined cross-section.

y_c .... Distance from the bottom to the centroid of the cross-section.

I .... Moment of inertia of the cross-section.

y_n .... Distance from the bottom to the centroid of the nth layer.

σ_{Tn} .... Total stress at the nth layer of the examined cross-section.

f'c.......................Specified compressive strength of concrete.

CHAPTER 1

INTRODUCTION

<u>Context</u>

A bridge is an essential component in the overall transportation system, allowing commerce and connecting regions that otherwise would be difficult to reach. These reasons make functioning bridges a critical asset in the creation and sustenance of a develop society. The critical nature of bridges necessitates an accurate design and construction that will serve society for decades without significant damage.

One of the greatest concerns when designing a bridge are loads that can quickly take it out of service or cause failure to the structure. However, small defects affecting the bridge, over a long period of time, can have equally devastating effects on the structure and greatly reduce its service life. Small cracks on concrete bridges, that don't pose an imminent threat to the structural integrity of the bridge, can allow water, snow and salt to percolate into the element and reach the reinforcement; corroding the steel and affecting the overall performance and safety of the structure.

<u>Temperature Effects</u>

Changes in temperature throughout the day cause expansion and contraction on a bridge as it heats up and cools down. When the movement is restrained, expansion and contraction produces flexural deformations and stresses on the

super-structure that can cause cracks, which can lead to a reduction in the overall service life of the bridge. A uniform average change in temperature on a bridge results in axial deformations. Depending on the support conditions, this behavior will result in stresses that need to be taken in account in the design. Furthermore, non-linear temperature changes throughout the depth of the super-structure causes flexural deformation and stresses that also pose a threat to the girders and deck.

The LRFD Bridge Design Specifications (2010) of the American Association of State Highway and Transportation Officials (AASHTO) defines the design uniform temperature ranges for concrete and steel bridges, using two methods. Procedure A classifies bridges as steel or aluminum, concrete and wood and assigns a climate zone as either moderate or cold. A table provides the recommended temperature range for each combination of bridge type and climate zone. Procedure B determines the maximum and minimum design bridge temperatures for concrete and steel girder bridges with concrete decks. These design temperatures are obtained using contour maps for each bridge type.

For the design temperature gradients, the AASHTO LRFD Bridge Design Specifications (2010) provides a map of the United States divided into four regions. For each region a temperature T1 and T2 value is provided, which defines the design positive temperature gradient. These temperature values are presented without differentiating between concrete and steel bridges; or the absence or presence of an asphalt overlay. To determine the negative design temperature gradient, the positive design temperature gradient is multiplied by a factor that depends on the presence or absence of asphalt overlay.

Another temperature gradient often utilized by engineers was proposed by Priestley (1978) which was implemented in the New Zealand Design Code. The positive temperature gradient has a temperature T defined at the top of the cross section. The value of T is dependent on the presence or absence of an asphalt overlay and decreases to zero following a fifth order curve.

This research uses the recorded changes in temperature on an I-girder concrete bridge in Perry, Utah and a concrete box-girder bridge south of Sacramento, California. Multiple sensors monitored the changes in temperature at 15 minutes intervals for a period of two years and five months. Using the temperature measurements, uniform temperatures and temperature gradients were calculated. The measured values were compared to the methods described in the AASHTO LRFD Bridge Design Specifications (2010) and the Priestley Method (1978). The comparison was used to determine the accuracy of the current codes in predicting the temperature changes that affect concrete bridges and subsequently the calculated effects of such changes on the bridge's structure.

<u>Research Objectives</u>

The goals of the research were defined as:

- Obtain and analyze temperature data from the two instrumented bridges, in order to quantify temperature changes in the super-structures of a concrete I-girder and concrete box girder bridge.

- Utilize recorded sensor data along with the location and bridge geometry to calculate changes in average bridge temperature and quantify the maximum and minimum temperatures that the bridges experienced.

- Evaluate the accuracy of the maximum and minimum uniform design temperature defined in the AASHTO LRFD Bridge Design Specifications (2010) by comparing the code predicted values to the measured values.

- Determine the measured positive and negative temperature gradients to which the bridges are exposed.

- Compare the shape and magnitude of the measured positive and negative temperature gradients to the gradients recommended by the AASHTO LRFD Bridge Design Specifications (2010) and the Priestley Method (1978).

- Calculate the stresses on the cross-section due to the measured positive and negative maximum temperature gradients.

- Determine if the presence of asphalt overlay on the I-girder concrete bridge has an influence on the temperature gradients to which the bridge is exposed.

Scope and Organization

The results of this research project were organized into six chapters. Previous research done in the area of temperature effect on concrete bridges is summarized in Chapter 2. In addition, the Kuppa Method (Kuppa and Roeder 1991) and the Black and Emerson Method (Emerson 1976) used for calculating the

average bridge temperature as a function of the ambient temperature are presented in this chapter. Chapter 3 presents a detailed description of the location and physical characteristics of the Utah and California Bridge used in this study. Figures are presented showing number of spans, length of spans and cross-sectional dimensions. The location and type of sensors installed on the bridge are also described in detail.

Chapter 4 describes the recommended procedures defined in the AASHTO LRFD Bridge Design Specifications (2010) to determine the maximum and minimum design average bridge temperatures. In addition, the procedure used in this research study to calculate the average bridge temperature for the instrumented bridges based on the measurements from the installed sensors is described. Results of the maximum and minimum measured average bridge temperature are presented and comparisons are made to the Kuppa Method (1991) and the Black and Emerson Method (1976). Finally a new method for predicting the average bridge temperature based on the ambient temperature is proposed and long-term predictions of the maximum and minimum average bridge temperatures are calculated using the Kuppa Method (1991), the Black and Emerson Method (1976) and the proposed new method with data provided by the National Oceanic and Atmospheric Administration (NOAA).

Chapter 5 reviews the Priestley Method (1978) and the method used in the AASHTO LRFD Bridge Design Specifications (2010) to calculate the design temperature gradients. A subsequent description of the procedure used to determine the measured temperature gradient is presented and compared with the

AASHTO (2010) and Priestley (1978) methods. A discussion on the overall shape of the measured temperature gradients and how to quantify it is presented. This chapter also presents the procedure to calculate the flexural stresses induced by non-linear temperature gradients. Finally, the stresses due to the maximum measured positive and negative temperature gradients are presented for both instrumented bridges and the results are compared to the limits established in the AASHTO LRFD Bridge Design Specifications (2010).

The last chapter presents a summary of the results of this research study.

CHAPTER 2

LITERATURE REVIEW

Temperature loads are not given much importance on the day to day design and maintenance of bridges, but they can have significant effects on the lifespan of the bridge structure. This chapter presents previous research in the area of temperature effects on concrete bridges.

Temperature Variation in Concrete Bridges (Mamdouh M. Elbadry and Amin Ghali 1983)

The continuous variation of temperature induces complex thermal stresses on the structure of bridges. The cross section, exposed surfaces, thermal properties of the material, orientation, and location of the bridge; as well as the environmental conditions affect the changes in temperature in the structure of the bridge. This temperature variation directly produces the magnitude and variation of the thermal stresses.

Is often assumed that the temperature does not change longitudinally along the length of a bridge with constant cross section. However, the temperature has been found to vary significantly through the width and depth of the cross section. Thus, at any time t the temperature distribution is a two-dimensional problem; T = T(x,y,t). The authors used two-dimensional finite elements to determine time dependent temperature variations and effects for a given geographic location and climatological conditions; for the cross section of concrete bridges with arbitrary geometry and orientation.

To properly model the thermal behavior of a bridge, the boundary conditions must be carefully considered. The heat gain or loss due to surface convection and radiation from or to the atmosphere and solar radiation are particularly important. The authors considered the solar radiation dependent on the angle of altitude of the sun which changes with time of day and the seasons. The radiation and convection depend on the temperatures of the surface and the air that varies with time. The differences between the outside and inside air of a box-girder bridge were also considered.

The change in temperature T at any time t through a bridge cross section is define by the Fourier heat flow equation.

$$k \left(\frac{d^2T}{dx^2} + \frac{d^2T}{dy^2} \right) + Q = \rho c \frac{dT}{dt} \qquad \text{Equation 1}$$

where

k = isotropic thermal conductivity coefficient W/m °C (Btu/(h ft °F))

Q = rate of heat per unit volume generated within the body W/m^3 (Btu/(h ft^3))

P = density kg/m^3 (lb/ft^3)

c = specific heat J/(kg °C) (Btu/(lb °F))

For the energy transferred to or from the boundary surface by the surrounding media, the boundary conditions can be define as

$$k \left(\frac{dT}{dx} n_x + \frac{dT}{dy} n_y \right) + q = 0 \qquad \text{Equation 2}$$

in which

n_x and n_y = direction cosines of the unit outward normal to the boundary surface

q = boundary heat input or loss per unit area W/m^2 (Btu/(h ft^2))

The authors used two types of finite elements to discretize the cross section of a typical bridge. Fictitious linear one-dimensional elements were used to represent the boundaries, and bilinear quadrilateral interior elements. Within a finite element e, the temperature can be approximated by

$$T(x, y, t)^e = [N]\{T\}^e \qquad \text{Equation 3}$$

where

[N] = linear shape functions

$\{T\}^e$ = column vector of four or two nodal temperature for an interior or boundary element, respectively

To calculate the longitudinal temperature stresses of a simply supported bridge, it can be assumed that the bridge acts as a beam, by

$$\sigma = -E\,\alpha\,T - \left(\frac{N_0}{A} + \frac{M_{0x}}{I_x}y + \frac{M_{0y}}{I_y}x\right) \qquad \text{Equation 4}$$

where moments, forces, distances and moments of inertia are referenced to the centroid of the bridge cross section. The distance y is measured positive down and x positive to the right. The value of N_0, M_{0x}, and M_{0y} are resultants of the stress σ_0=-EαT that would be required if the strain due to temperature is artificially restrained. The longitudinal stresses, σ, are zero when the temperature distribution over the cross section is plane.

$$N_0 = \iint \sigma_0 \, dx \, dy \qquad \text{Equation 5}$$

$$M_{0x} = \iint \sigma_0 y \, dx \, dy \qquad\qquad \text{Equation 6}$$

$$M_{0y} = \iint \sigma_0 x \, dx \, dy \qquad\qquad \text{Equation 7}$$

The curvatures ψ_x and ψ_y due to temperature, induced in the horizontal and vertical directions, respectively, are

$$\psi_x = -\frac{M_{0x}}{EI_x} \qquad\qquad \text{Equation 8}$$

$$\psi_y = -\frac{M_{0y}}{EI_y} \qquad\qquad \text{Equation 9}$$

When the curvature ψ_x is restrained, statically indeterminate reactions and internal forces develop which produce continuity stresses. These additional stresses develop in continuous bridges. The continuity stresses must be added to the stresses σ defined previously.

The temperature distribution that produces the largest temperature stresses where found to develop during the summer months when the solar radiation is maximum. This is also a time when the wind speed is minimum and the daily range in ambient temperature is large. During this time unfavorable conditions can also appear. The temperature stresses were found to be more prominent with the presence of an asphalt deck overlay.

The authors determined that as the cross section of the bridge increases, the temperature stresses also increase. They considered solid slab, cellular slabs, and box-girder bridges and found that, for the same conditions, the curvature, temperature stresses and distribution did not vary that much.

Thermal Stresses and Cracking of Concrete Bridges (Elbadry and Ghali 1986)

A bridge deck continuously gains and losses heat from solar radiation, re-radiation to the sky, and convection to or from the surrounding atmosphere. Temperature variations induced by these sources depend on geometry, location, and orientation of the bridge, on climatological conditions, and on thermal properties of the material and exposed surfaces.

Solar radiation impinging on the surfaces is partly absorbed and partly reflected. Absorbed energy heats the surface and produces a temperature rise through the deck. The amount of absorbed radiation depends on the nature and color of the surface. Some of this absorbed is lost to the air by convection and re-radiation from the surface. The amount of heat lost or gained by convection depends upon wind velocity humidity and the difference in temperature between the air and the surface.

Because these boundary conditions vary continuously with time and because the conductivity of concrete is relatively low, variation of temperature through a bridge cross section in nonlinear.

Temperature variations that develop in bridge structures due to changing weather conditions are generally nonlinear. In a statically determinate bridge, nonlinear temperature variations produce stresses in the longitudinal direction of the span. These stresses are self-equilibrating since their resultants are equal to zero and no change in reactions occurs. In a statically indeterminate bridge, additional continuity stresses develop in the longitudinal direction due to restrained movement whether the variation of temperature is linear or nonlinear.

Temperature stresses can also be induced in the transverse direction of a bridge cross section and produce longitudinal cracks on the bridge.

Priestley also noted that in wide multicell box-girder bridges, transverse curvature due to temperature induces upward movement at the internal support. This results in a substantial increase of reactions at the outer bearings and may cause the deck to separate from some of its bearings. See Figure 1.
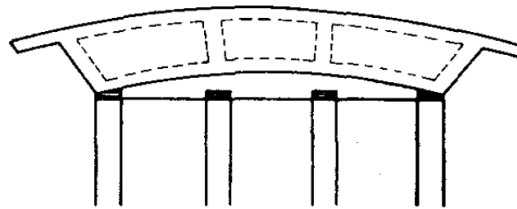
Figure 1. Overloading of bearing due to transverse thermal curvature.

As for the longitudinal cross section of the bridge, when the surface of the bridge is warmer than the bottom it results in an upward deflection. Conversely, when the bottom is warmer than the surface it results in a downward deflection.

Stresses caused by temperature gradients in statically determinate bridges can be of two forms. Tensile stresses in the central part of the height and compressive stresses at the top and bottom fibers. This occurs when the temperature of the middle part of the section is lower than the average temperature of the cross section.

The reverse occurs, with tensile stresses at the surfaces and compressive stresses in the central part, when the temperature of the middle part is higher than the average temperature of the cross section. The tensile stresses in this case, when

added to stresses form other loading conditions, may be high enough to cause cracking at one or the other of the exterior surfaces.

For statically indeterminate bridges the curvature due to temperature will be restrained and statically indeterminate reactions and continuity moments will develop. The resulting stresses, referred to as continuity stresses, are produced whether the temperature distribution is linear or nonlinear and must be added to the self-equilibrating stresses to obtain the total thermal stresses.

Tensile stresses due to temperature can be high enough to cause cracking. This cracking produces stress redistribution and substantial relief of temperature stresses. Use of partial prestressing is recommended to reduce thermal stresses and control thermal cracking by provisions of sufficient amounts of non-prestressed steel.

Thus, the author stated that temperature must be considered in design, particularly in deciding the amount and detailing of non-prestressed reinforcement, to insure satisfactory serviceability of concrete bridge.

<u>Thermal Movement Design Procedure for Steel and Concrete Bridges (Charles W. Roeder 2002)</u>

Bridges expand and contract due to change in temperature. This movement is accommodated by the use of bearings and expansion joints or by deformation of the piers and abutments with integral construction. Overall bridge movements are computed using Equation 10:

$$\Delta = \alpha \cdot L \cdot \Delta T \qquad\qquad \text{Equation 10}$$

Research has shown that bridge expansion and contraction depend upon change in average bridge temperatures rather than air temperature. The actual calculation of the bridge temperature distribution is quite complex, but two simplified methods [the Emerson Method (1976) and Kuppa Method (1991)] for estimating the average temperature were noted.

Bridge temperatures vary through the bridge cross section as a function of time. Temperature differences are a function of radiation, convection, and conduction heat flow; and these three mechanisms all contribute to the time dependent cross sectional variation. Accurate determination of the bridge temperature requires consideration of all three components of heat flow in addition to other information including the cloud cover, air temperature, wind speed, angle of the sun, time of day, orientation of the structure with respect to the sun, geometry and materials of the bridge.

Kuppa and Roeder (1991) used analytical methods developed and initially verified by others to perform a heat flow analysis of both steel and concrete bridges in a wide range of climates. Kuppa and Roeder's (1991) calculations focused on near extreme events, since these events control thermal design. Kuppa and Roeder (1991) showed that temperature distribution within the bridge varies as a function of time and bridge type. The average temperature, T_{Avg}, is based on equilibrium principles, and is integrated over the bridge cross section, and is provided as equation 11,

$$T_{Avg} = \frac{\sum A_i \, E_i \, \alpha_i \, T_i}{\sum A_i \, E_i \, \alpha_i} \qquad\qquad \text{Equation 11}$$

where i represents the different temperature or material segments (or layers) of the bridge, A_i is the cross sectional area of the ith segment, E_i is the elastic modulus of the ith segment, α_i is the coefficient of thermal expansion of the ith segment, and T_i is the temperature of the ith segment. Kuppa and Roeder's (1991) calculations included all bridge properties as well as conduction, convection, and radiation heat transfer. Kuppa considered actual air temperature, cloud cover, precipitation, and wind velocity, since data was taken from US sites where complete climate data was available.

These calculations indicated that the extreme maximum and minimum average bridge temperatures depend upon the four day averages of the high and low air temperature, respectively. That is, the extreme maximum average bridge temperature, T_{AvgMax}, depends upon the average high air temperatures for four consecutive days in the hottest part of the summer, and the extreme minimum average bridge temperature, T_{AvgMin}, depends on the average of the low air temperature for four consecutive days in the coldest part of the winter. The four day averages were the same for both bridge types, but different relationships were noted for steel bridges with concrete decks, concrete girder bridges and concrete box girder bridges. The correlation was determined by a regression analysis of data obtained from detailed analysis for a number of locations in the US.

For concrete bridges, the Kuppa Method (1991) suggests that

$$T_{AvgMax} = \frac{T_{MaxAir1} + T_{MaxAir2} + T_{MaxAir3} + T_{MaxAir4}}{4} \, 0.953 + 4.6 (°F) \quad \text{Equation 12}$$

$$T_{AvgMin} = \frac{T_{MinAir1} + T_{MinAir2} + T_{MinAir3} + T_{MinAir4}}{4} \, 1.186 + 17.24 \quad (°F) \quad \text{Equation 13}$$

Slight differences were noted for concrete box girder bridges and bridges with precast concrete girders, but these differences are not large enough to warrant separate design limits.

The Black and Emerson Method (1976) were based upon a correlation between the measured daily minimum average temperature, T_{AvgMin}, of the bridge and the mean of the measured night time low and previous day high shade temperatures, $T_{ShadePrevHigh}$ and $T_{NightLow}$, for a two day period. T_{AvgMin} for a given day was then correlated to the 2 day average of the night time low and previous day high shade temperature through and empirical equation. This equation for concrete bridges can be approximately expressed,

$$T_{AvgMin} = \frac{T_{MaxAir1} + T_{MaxAir2} + T_{MinAir1} + T_{MinAir2}}{4} \, 1.14 + 10.96 \qquad (°F) \qquad \text{Equation 14}$$

The average minimum bridge temperature occurs early in the morning while the bridge is approaching a thermal equilibrium state. Emerson (1976) estimated the average maximum bridge temperature by adding a temperature range to the minimum value for that day. Emerson (1976) observed that the maximum daily range of the average bridge temperature depended upon the type of bridge, season of the year, and the cloud cover. Table 1 illustrates these maximum temperature ranges for concrete bridges.

Table 1. Maximum daily temperature ranges for concrete bridges.

	Daily Temperature Range °F (°C)		
	Clear and Sunny	Cloudy, but not overcast	Overcast / rain, snow
Winter	5.4 (3)	1.8 (1)	0 (0)
Spring/Autumn	10.8 (6)	5.4 (3)	1.8 (1)
Summer	10.8 (6)	7.2 (4)	3.6 (2)

The Emerson Method (1976) is based upon air temperatures in the shade rather than normal weather station data or normal air temperatures. The shade air temperatures are measured under a bridge in a sheltered location, and as a result shade temperatures have less extreme variations than the normal air temperature. Therefore, the use of air temperature always overestimates the magnitude of bridge movements by the Emerson Method (1976).

<u>Measurements of thermal gradients and their effects on segmental concrete bridge</u>

<u>(Carin L. Roberts-Wollman, John E. Breen, Jason Cawrse 2002)</u>

To gain a better understanding of the effects of thermal gradients on segmental box girder bridges, a field study of several spans of the San Antonio "Y" project started in 1989 (Roberts et al. 1993). The San Antonio "Y" project was an upgrade to the intersection of interstate highways I-35 and I-10 in downtown San Antonio.

Three spans of the bridge were instrumented as part of the study. Eight thermocouples through the depth of an external girder (segment 44A-15) were connected to a data logger. The temperatures were recorded every half-hour for two and a half years. Segment 44A-15 was located in one of the end spans of a three span

continuous bridge. Span A42 had a length of 35 m (114.83 ft) and the other two spans (A43 and A44) had a length of 33.5 m (109.91 ft). A taut wire baseline deflection measurement system was installed on spans A43 and A44 (Roberts et al. 1993).

The maximum positive temperature difference, define as the difference between the top thermocouple [25 mm (0.98 in.) below the top of the deck] and the coolest web thermocouple reading, was recorded daily. The temperature gradients were recorded without an asphalt overlay (July 25, 1992 – March 25, 1993) and after a 50 mm (1.97 in.) topping was placed (March 26, 1993 – December 16, 1994).

The authors compared the measured temperature gradients with the AASHTO LRFD Bridge Design Specifications (1994) and the AASHTO Guide Specifications for Design and Construction of Segmental Concrete Bridges (1999) for both surface conditions. The maximum positive thermal gradient was recorded at 12 °C (21.6 °F) without asphalt overlay, and 16 °C (28.8 °F) with the 50 mm (1.97 in.) topping. For both cases the measured gradients were below both AASHTO specifications and the shape of the measured gradients were closer to the shape of the trilinear gradient from the AASHTO Standard Specifications for Highway Bridges (1989).

The authors compared the shape of the measured temperature gradients for many days with a curve starting with the temperature at the top of the deck and following the fifth order curved proposed by Priestley (1978). The authors found that on days of high solar radiation following several days of little sunshine the temperature dropped faster with depth than a fifth-order curve. When climatic

conditions where relatively uniform the measured gradients followed closely a fifth-order curve. On days of very low sun radiation combined with the passage of a cold front, the measured temperature gradients dropped less with depth than a fifth-order curve. The authors concluded that for the majority of the days the measured gradient followed the shape of a fifth-order curved and the coolest web temperature occurred 1,220 mm (48.03 in.) below the top of the deck.

Since the first the thermocouple was located 25 mm (0.98 in.) below the top of the deck, the authors used a fifth-order curve (Equation 15) to extrapolate the temperature at the surface of the bridge. However, the extrapolated temperature gradient didn't exceed the design gradients of the AASHTO LRFD Bridge Design Specifications (1994) and the AASHTO Guide Specifications for Design and Construction of Segmental Concrete Bridges (1999).

$$T_{(y)} = T \cdot \left(\frac{y}{1220}\right)^5 \; where \; y \; is \; in \; mm \qquad \text{Equation 15}$$

The maximum negative temperature gradients were -8.5 °C (-15.3 °F) without an asphalt overlay and -6 °C (-10.8 °F) with the topping. The magnitudes of the measured gradients were smaller than the AASHTO LRFD Bridge Design Specifications (1994), but a little bit bigger than the AASHTO Guide Specifications for Design and Construction of Segmental Concrete Bridges (1999). The shape of the measured negative gradients was similar to both AASHTO Specifications near the deck, but very different towards the bottom of the cross-section. A fifth-order parabolic shape with the zero point 610 mm (24.02 in.) below the top of the deck

proved to predict very well the shape of the measured negative temperature gradients for the zone close to the deck.

Potgieter and Gamble (1983) proposed equations to predict temperature gradients based on daily ambient temperature variations, wind speed, and ambient climatic conditions of solar radiation. The authors used data from a station of the National Weather Service located 10 km (6.21 mi.) north of the bridge, an equation to calculate the theoretical solar radiation that hits the atmosphere proposed by Duffie and Beckman (1980), and an equation to calculate the daily solar radiation that reaches the ground (or bridge) as inputs for the Potgieter and Gamble (1983) equations. Comparing the measured positive temperature gradients with the Potgieter and Gamble (1983) Method, the authors concluded that the Potgieter and Gamble (1983) Method predicted the trends well but constantly overestimated the magnitude of the positive temperature gradient for the bridge with and without the asphalt overlay.

The authors found that the average ambient air temperature for the current and previous two days (the three day average) is, on average, 99.8% of the coolest web temperature of the day with a coefficient of variation of 4.3%. An additional observation was that during spring and fall the extrapolated temperature at the top of the deck was very similar to the daily high temperature, however, during spring and summer the temperature at the top of the deck was higher than the daily high temperature.

Based on these observations the authors made a modification to the Potgieter and Gamble Method (1983) and created a simplified equation to predict

the temperature gradient. The Potgieter and Gamble Method (1983) predicts the temperature gradient 3.9 °C above, on average, with a standard deviation of 3.9 °C. With the modification, the Potgieter and Gamble Method (1983) predicts the temperature gradient 1.6 °C below, on average, with a standard deviation of 2.9 °C. The simplified equation predicts the temperature gradient 0.6 °C below, on average, with a standard deviation of 3.2 °C. The authors noticed that all the methods yield better results when the climatic conditions are relatively stable.

The authors performed two, one-day studies, in which they measured temperature and deflection every hour starting early in the morning until passed sunset. With this information the authors generated gradients with the difference between the first reading in the morning and the warmest temperature in the afternoon. Using Equation 16 to determine the moment that would develop in a fully restrained system subjected to these gradients; deflections can be calculated by applying those moments to the ends of the actual structural system.

$$M = \alpha \, E \int T_{(y)} b_{(y)} y \, dy \qquad \text{Equation 16}$$

where

T(y) = temperature at a distance y from the centroid of the section

b(y) = width of section at distance y from the centroid

α = coefficient of thermal expansion (11×10^{-6}/°C)

E = modulus of elasticity

The calculated deflections matched almost perfectly the measured deflections for the two studies.

Investigation of thermal gradient effects in the I-35W St. Anthony Falls Bridge

(Brock D. Hedegaard, Catherine E. W. French, Carol K. Shield 2012)

During the day the cross section of a concrete element can heat of cool nonuniformly due to the low thermal conductivity of the material. This produces gradients that are typically bigger through the depth of the cross section. When the top surface is hotter than the web this is defined as a positive thermal gradient. A negative thermal gradient occurs when the top surface is colder than the webs. According to Hedegaard et al. (2012) the positive thermal gradients are generally observed on hot, clear and sunny afternoons with high solar radiation in the early summer months, typically between 2:00 and 4:00 PM. And negative thermal gradients typically occur in early mornings throughout the year, usually between 5:00 and 8:00 AM.

When a positive thermal gradient is affecting a structure the top surface will expand more than the bottom, this will induce an upward deflection. The opposite happens when a negative thermal gradient is acting on the structure. When temperature gradients are applied axial and bending stresses are induced due to restrains associated with boundary conditions. If the thermal gradient affecting the structure is nonlinear, to comply with the Bernoulli beam bending assumption that plane sections remain plane, compatibility stresses will be generated. Hedegaard et al. (2012) say that the stresses induced by thermal gradients can be larger than those induce by vehicle live loading.

Potgieter and Gamble (1983) constructed a finite difference heat flow model and complemented their numerical study with field measurements from the

Kishwaukee River Bridge, located near Rockford, Illinois. Imbsen et al. (1985) advanced the work of Potgieter and Gamble, in what was later adapted into the AASHTO LRFD Bridge Design Specifications (AASHTO 2010). The design gradients are given as the temperature difference of the cross-section from the temperature in the webs.

The design gradient from the New Zealand Code (Priestley 1978), is a fifth-order curve decreasing from maximum gradient temperature T_0 at the top of the deck to zero at a depth of 1200 mm (47.2 in) defined by

$$T_{grad}(y) = T_0 \left(\frac{y}{1200}\right)^5, y \ (mm) \hspace{3cm} \text{Equation 17}$$

where y is defined positive up from the point 1200 mm (47.2 in) below the top surface. The specified maximum gradient temperature T_0 for plain concrete deck with no asphalt overlay in New Zealand is equal to 32°C (57.6°F). For a concrete deck with 76.2 mm (3 in.) asphalt overlay, T_0 is 16.76°C (30.17°F). The fifth-order curve is applied through the depth of the webs and for decks above unenclosed air. For decks above enclosed air cells in box girders, a linear gradient is prescribed with a top gradient temperature equal to T_0 and, for plain concrete decks with no asphalt overlay, temperature decreasing at a rate of 1°C per 20 mm (1°F per 0.44 in). The bottom gradients tail temperature is specified as 1.5°C (2.7°F), decreasing linearly to zero over a height of 200 mm (7.9 in.) measured up from the bottom of the section. There is no design negative thermal gradient specified in the New Zealand Code (Priestley 1978).

Shushkewich (1998) investigated the measured thermal gradients of the North Halawa Valley Viaduct, a cast-in-place concrete box girder bridge in Hawaii. Positive and negative thermal gradients were found to correspond well with AASHTO (1998) proposals, which are identical to the thermal gradient provisions in AASHTO LRFD (2010). Thompson et al. (1998) considered the "Ramp P' structure, a curved precast segmental concrete box girder bridge on highway US 183 in Austin, Texas. Gradients were measured both with and without 50 mm (2 in.) blacktop covering. Measured gradients were typically lower than those specified in AASHTO LRFD (1994), which had an identical positive design gradient to ASSHTO LRFD (2010) but used a multiplier of -0.5 instead of -0.3 for defining the negative gradient. However, it was stated that more data was needed to construct a sound statistical comparison. Roberts-Wollman et al. (2002) investigated thermal gradients in precast segmental concrete box girders in the San Antonio "Y" Project. The concluded that typical positive gradients could be approximated by a fifth-order curve similar to that presented in Priestly (1978). They also stated that the ASSHTO LRFD (1994) positive and negative design gradients were conservative.

For three years Hedegaard et al. (2012) measured the thermal gradients through the section of a post-tensioned concrete box girder bridge, the I-35W St. Anthony Falls Bridge in Minneapolis, Minnesota. The authors compared there measurements to various design gradients and found that a fifth-order curve best matched the shape of the gradients. Hedegaard, French and Shield (2012) compared the response of the structure to the largest measured thermal gradient to the deformation and stresses of design gradients applied to a finite element model. And

found that the measured structural response was best predicted when the finite element model is exposed to a fifth-order design thermal gradient scaled to match maximum top surface temperature values proposed by AASHTO LRFD Bridge Design Specifications for the region. Stresses and deformations from the finite element model with the AASHTO LRFD bilinear design gradients applied were considerably lower than those derived from measured results.

<u>Experimental Study of Thermal Actions on a Solid Slab Concrete Deck Bridge: Validation by Measured Displacements and Comparison with Eurocode 1 Specifications (Hugo Corres Peiretti, Javier I. Ezeberry Parrotta, Amets Berecibar Oregui, Alejandro Perez Caldentey, Freddy Ariñez Fernandez 2012)</u>

The European Committee for Standardization Eurocode 1 (2004) represents the thermal effects on structures with four constituent components and considers them as variable indirect actions. The constituent components are the following:

- Uniform component of temperature ΔT_u.

- Temperature difference component that varies linearly along the vertical axis of the cross section: ΔT_{My}.

- Temperature difference component that varies linearly along the width of the element: ΔT_{Mz}.

- A non-linear variation of temperature along the vertical axis of the cross section: ΔT_E.

Combining these temperature components, the Eurocode 1 (2004) permits two procedures to assess the thermal effects on a structure. These procedures are:

- The uniform temperature ΔT_u component applied at the centroid of a section plus a linear gradient component ΔT_M.

- The uniform temperature ΔT_u component applied at the centroid of a section plus a non-linear gradient component, define as the sum of ΔT_E and ΔT_M.

When analyzing at the global response of the structure to the thermal load, both methods yield the same results. But when we look at the local effects of temperature by analyzing one section; the second method, which includes the non-linear ΔT_E component, takes into account the self-equilibrating stresses which only have a local influence.

Corres Peiretti et al. (2012) measured the temperatures that developed in a four spans and 64 meters (210 ft) long solid slab prestressed concrete bridge deck in the province of Avila, Spain. The super-structure of the bridge is rigidly connected to the columns and abutments.

To measure the thermal effects on the bridge various cross sections of the bridge were chosen and twelve thermistors and vibrating wire strain gauges were installed in each section. One joint meter (JM) was installed at each end of the bridge to measure the overall expansion and contraction of the super-structure. To relate the bridge temperature to the ambient shade air temperature and the Eurocode 1 (2004), a weather station that measures ambient temperature and humidity was installed under the bridge. Also the Spanish National Meteorological Institute provided temperature and humidity readings from a station 4 km (2.5 miles) away from the bridge location.

The collected data covers four years, divided into several periods that go from 2008 to 2012. The information was collected at different intervals for each period; these intervals range from 1 to 24 hours. The data from November 19, 2009 to May 13, 2010 was lost. As for the sensors, only section S-5 has all sensors working; all the other sections have lost some sensors.

Corres Peiretti et al. (2012) compared the measured data with the values given by the Eurocode 1 (2004) for the specific location and bridge type studied. During the four years of the study the maximum and minimum uniform temperatures were 44.5 °C (112.1 °F) and -3.3 °C (26.06 °F), respectively. While the Eurocode 1 (2004) establishes a maximum uniform temperature of 46.6 °C (115.88 °F) and a minimum uniform temperature of -13.6 °C (7.52 °F). This difference could be explained by the fact that the values of the Eurocode 1 (2004) are based on a return period of 100 years and the measured data only covers four years.

The Eurocode 1 (2004) determines the maximum and minimum uniform temperature components by taking the maximum and minimum shade air temperatures for a return period of 100 years and adding 2 °C (35.6 °F) and 8 °C (46.4 °F) respectively. The authors found that there is a direct correlation between the shade air temperature and the uniform temperature component, but that the relation given by the Eurocode 1 (2004) is unfit for the particular bridge studied.

Crespo (2005) and Ortega et al. (2010, 2011) have studied the uniform temperature component on different locations and bridge types than the bridge studied by Corres Peiretti et al. (2012) and concluded that the uniform temperature

determine by their measurements matched rather well the temperatures predicted by the Eurocode 1 (2004) for their specific bridges.

The difference in the uniform temperature determined by the Eurocodthe 1 (2004) and the one measured by Corres Peiretti et al. (2012) could be because, according to available information, the specifications established in the Eurocode 1 (2004) are derived from locations where the daily thermal variation was no greater than 10 °C (50 °F). In addition, on the bridge studied by the authors the daily shade air temperature variations reached values as high as 18 °C (64.4 °F).

The foundations of the abutments of the bridge studied by Corres Peiretti et al. (2012) are designed to minimize the resistance to horizontal movements. Also the effects of creep and shrinkage decrease as the age of the structure increases and for a structure that has been in service for more than a year, the movements due to creep and shrinkage over the course of a week can be consider negligible in comparison to the thermal movements. So the authors assume that comparing the movements measured by the joint meters with the theoretical movements calculated with the uniform temperatures would be a good way to validate the quality of the temperature data gathered.

The movements measured by the joint meters almost perfectly match the movements calculated with the measured uniform temperature data. Confirming not only that the measured temperature data is of great quality, but also that, for this specific bridge, the axial movements are not affected by the lateral earth pressure of the backfill behind the abutments.

CHAPTER 3

BRIDGE DESCRIPTIONS

The Federal Highway Administration (FHWA) created the Long-Term Bridge Performance (LTBP) program with the objective of acquiring quality scientific data about the bridges in operation in the United States. This information will be used to improve the practices of bridge design and maintenance. To accomplish this objective information that represents the variety of bridge types, site conditions and administration agencies present in the United States is required. The California Bridge is located in a hot-dry climatic zone, while the Utah Bridge is within a cold-dry zone as defined by the Department of Energy. The diversity of environmental conditions in combination with the fact that the two bridges have different number of span, structure types and are administrated by different agencies fits the purpose of the Long-Term Bridge Performance (LTBP) program of representing the diversity of the National Bridge Inventory.

The California Bridge

Built in 1975, the Lambert Road Undercrossing is a bridge under the jurisdiction of the California Department of Transportation (Caltrans) numbered 24-0287L. The bridge is part of the southbound side of the Interstate 5 (I-5) Highway. Located 20 miles south of Sacramento CA, the bridge crosses Lambert Road and a dirt irrigation canal that runs on the north side parallel to Lambert road. A more general location is given by latitude 38.320845 and longitude -121.465681. Figure 2 shows an aerial view of the Lambert Road Bridge taken using Google Maps (2013a).

Figure 2. Aerial view of the 24-0287L Bridge (blue marker). North up.

The Lambert Road Bridge provides two lanes of traffic to an Average Daily Traffic (ADT) of 24500 vehicles with 21% trucks. The overall length of the bridge is 78.64 m (258 ft) and is built on an 8° skew. The bridge consists of two continuous spans with an equal lengths of 39.32 m (129 ft) separated by a reinforced concrete column that varies in dimensions from 3657.6 mm by 1066.8 mm (144 in. by 42 in.) at the base to 5486.4 mm by 1066.8 mm (216 in. by 42 in.) at the top. At the ends,

the bridge is supported with reinforced concrete open ended hinged diaphragm abutments. The foundations of both the column and the abutments are cast-in-drilled-hole concrete drilled shafts. Figures 3 and 4 show a plan view and cross-section of the bridge, respectively.
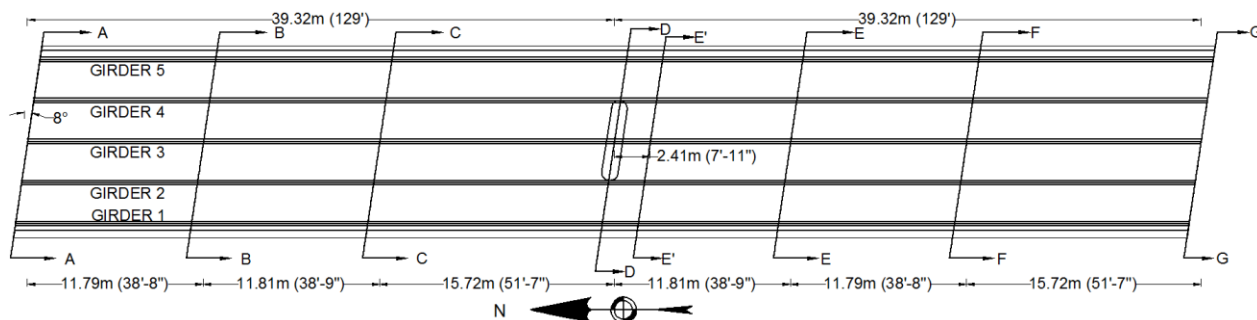
Figure 3. Plan view of the California bridge.
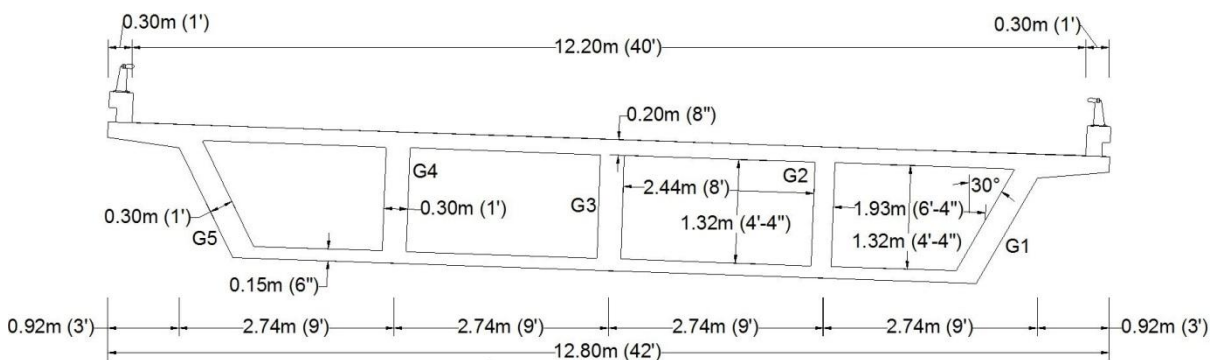
Figure 4. Typical cross-section of the California bridge.

The superstructure consists of post-tensioned cast-in-place concrete box-girders with four cells. The surface of the deck was treated with an epoxy seal. The overall width of the bridge is 12.80 m (42 ft) with a 0.30 m (1 ft) barrier on each side, making the overall roadway width 12.20 m (40 ft). The deck has an overhang distance of 0.92 m (3 ft) from the edge of the exterior girders and is 200 mm (8 in.)

thick in average. The bottom flange of the box-girder is 150 mm (6 in.) thick. The inner cells are 2.44m by 1.32m (8 ft by 4 ft 4 in.), the other two outer cells are 1.93m (6 ft 4 in.) in average by the same height. There are five 0.30m (1 ft) thick girders; and outer two are inclined 30° from the vertical. The specified compressive strength of the concrete (f'c) is 24.13MPa (3.5 ksi) and it is reinforced with mild steel and post-tensioning strands.

The post-tensioning on the bridge was done by placing the strands in a parabolic profile through the length of each span. The force on the strands was 7.52 kN (1.69 kips) including stress and friction losses.

The Utah Bridge

Built in 1976, the Perry Bridge is under the jurisdiction of the Utah Department of Transportation (UDOT) numbered 3F 205. The bridge is part of the northbound side of the Interstate 15 (I-15) Highway. Located 2.41Km (1.5 miles) west of Perry UT. The bridge crosses Cannery Road a small dirt road that gives access to the agricultural fields west of the highway. A more general location is given by latitude 41.457083 and longitude -112.055186. Figure 5 shows and aerial view of the bridge taken using Google Maps (2013b).

Figure 5. Aerial view of the 3F 205 Bridge (blue marker). North up.

Expanding over a single 24.90m (81 ft 8 in.) span, the Perry Bridge provides two lanes of traffic to an Average Daily Traffic (ADT) of 22255 vehicles with 29% trucks. With no skew, the bridge is supported at the ends by reinforced concrete integral abutments supported on piles made with 344MPa (50 ksi) steel tubes filled with reinforced concrete. Four types of reinforced concrete filled steel piles where used, two with 0.30m (12 in.) and 0.36m (14 in.) constant diameters. And the other two types are tapered tubes with diameters of 0.36m (14 in.) to 0.20m (8 in.) and 0.30m (12 in.) to 0.20m (8 in.). Figures 6 and 7 show a plan view and cross-section of the bridge, respectively.

Figure 6. Plan view of the Utah bridge.
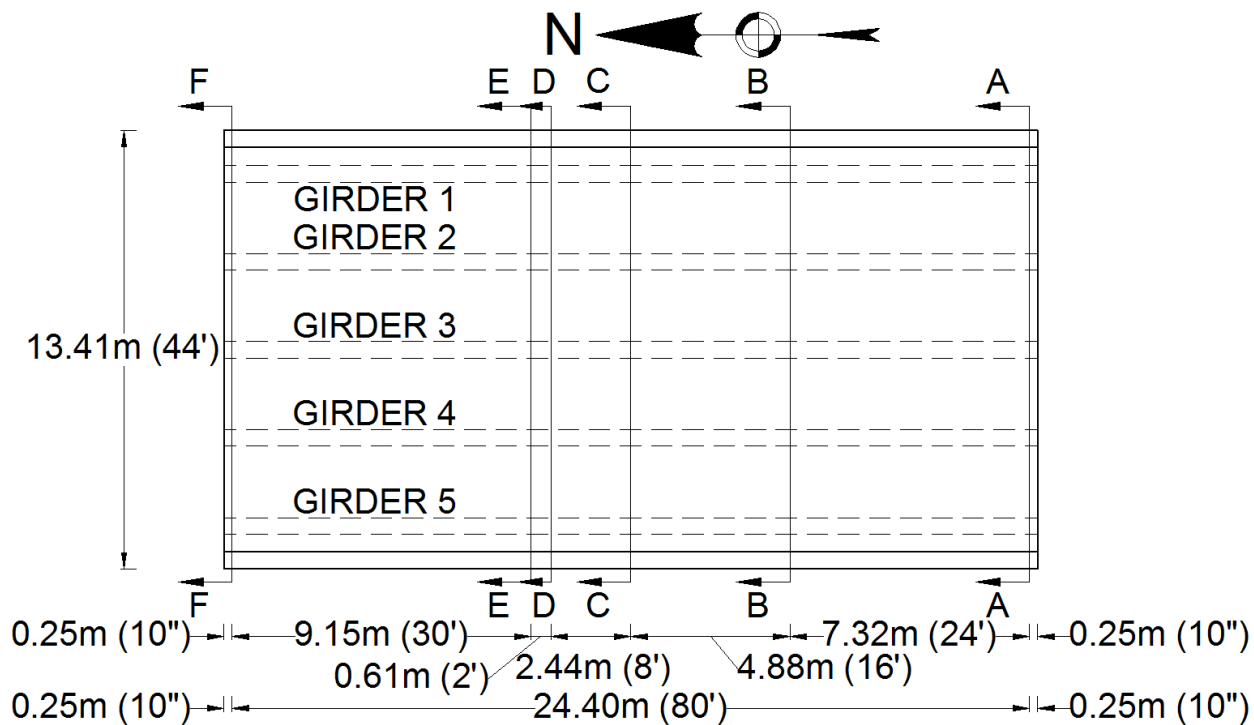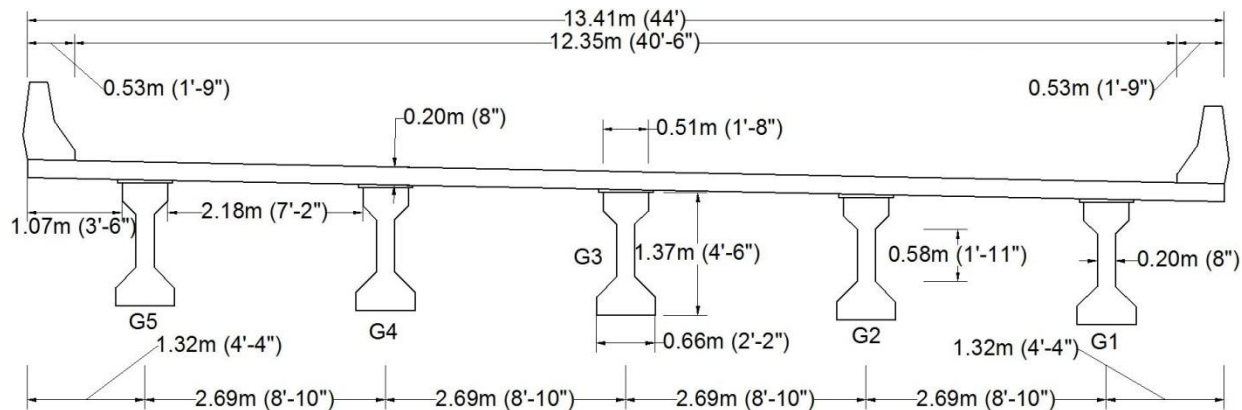

Figure 7. Typical cross-section of the Utah bridge.

The superstructure consists of five AASHTO type IV pre-stressed concrete girders. Figure 8 shows the geometry of the type IV girder. The overall height of the girders is 1.37m (4.5 ft), with a web height of 0.58m (1 ft 11 in.) by 0.20m (8 in.) thick. The top and bottom flanges are 0.51m (1 ft 8 in.) and 0.66m (2 ft 2 in.) wide,

respectively. The surface of the deck covered with a 76mm (3 in.) asphalt overlay. The overall width of the bridge is 13.41m (44 ft) with 0.53m (1 ft 9 in.) barriers on each side, making the overall roadway width 12.35m (40.5 ft). The deck has an overhang distance of 1.07m (3.5 ft) from the edge of the exterior girders and is 0.20m (8 in.) thick. The specified compressive strength of the concrete (f'c) is 27.60MPa (4 ksi). It is reinforced with 15.81cm^2 (2.45 in.^{2}) strands stressed to a final force of 3.37x10^{6}N (757 kips) and mild steel for the girders and just mild reinforcement was used in the deck.

Figure 8. Section geometry of the Type IV AASHTO girder.

Instrumentation

To assess the in situ conditions of the California and Utah bridges various test were preformed, including live load and dynamic testing. However these tests only

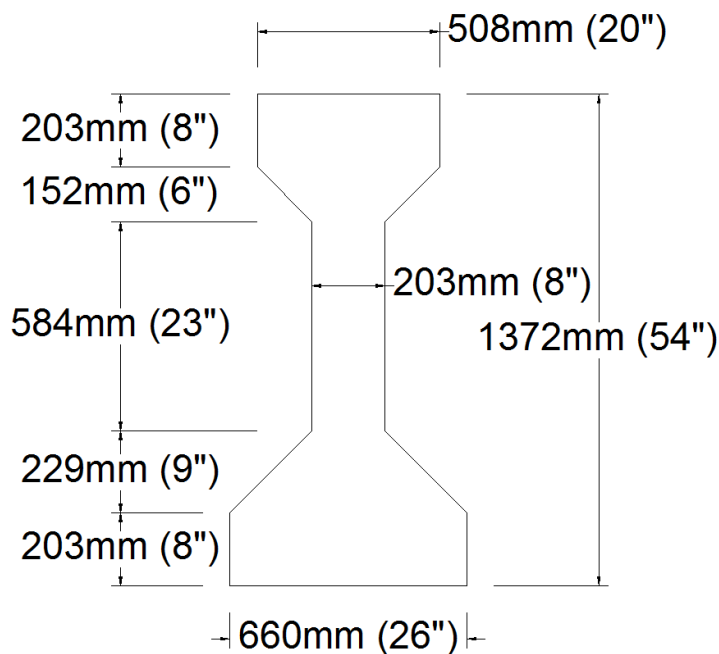determine the state of the bridges in one point in time. In order to have continuous information about the bridges structural health an instrumentation plan was developed in which sensors were placed at strategic locations on the superstructures. These sensors are connected to an onsite data logger that collects readings from the sensors every 15 minutes and sends the information to Utah State University via the internet. This allows the researchers analyze the data without having to travel to the bridges to collect the data. It also gives the opportunity to collect data in the event of a rare and/or catastrophic event, like an earthquake or a collision.

<u>The California Bridge</u>

In order to monitor a complete picture of the bridge's conditions foil strain gauges, velocity transducers, vibrating wire strain gauges, thermocouples and tiltmeters were installed on the superstructure and deck of the bridge. Creating a net of 71 sensors that provide constant information about the structural health of the bridge.

To monitor the changes in temperature throughout the box-girders 44 thermocouples were installed. Twenty of those thermocouples were used to create two deck temperature gradient measuring arrays that quantify the steep changes in temperature along the depth of the deck. This information is crucial to calculate the stresses induced on the superstructure due to temperature changes throughout the day. These arrays are located approximately 2.44m (8 ft) south of the center of the span in the portion of the deck that covers the west cell of the box-girder.

Figures 9 through 16 show the location of the sensors on the bridge. TM tilt-meters, SG strain gauge, TC thermocouple and DTC deck thermocouple. Refer to figure 3 to see the location of the cross-section along the length of the bridge.

Figure 9. Section AA of the California bridge.
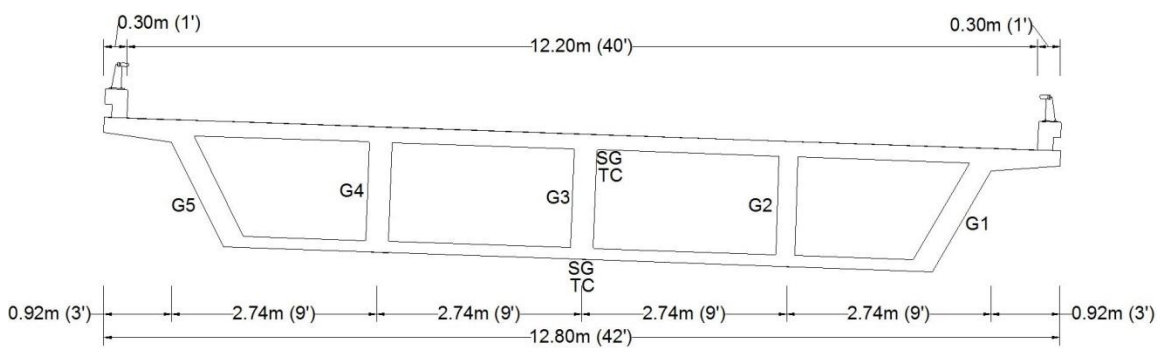
Figure 10. Section BB of the California bridge.
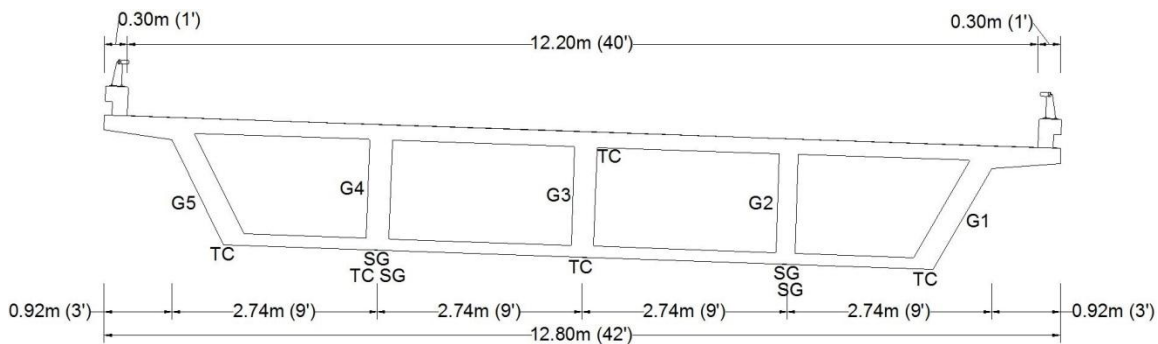
Figure 11. Section CC of the California bridge.
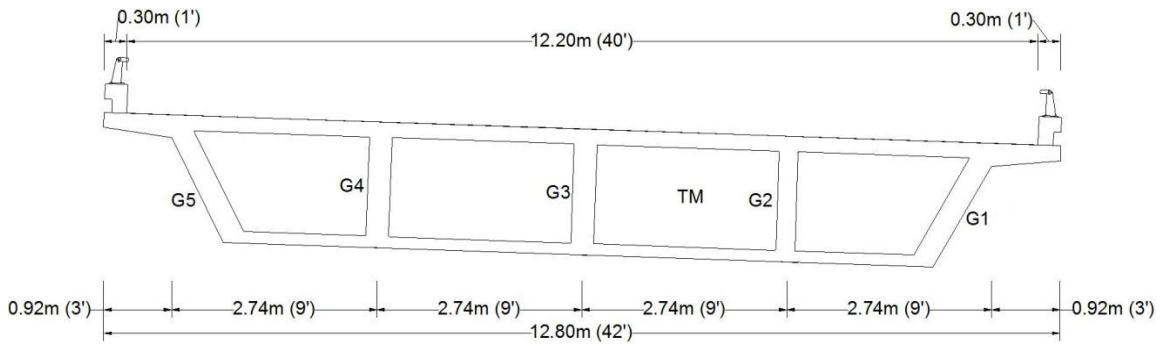
Figure 12. Section DD of the California bridge.
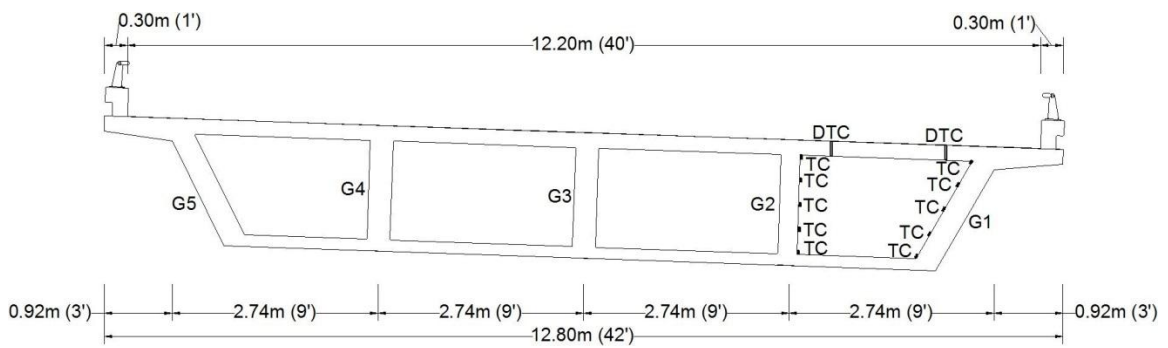
Figure 13. Section E'E' of the California bridge.
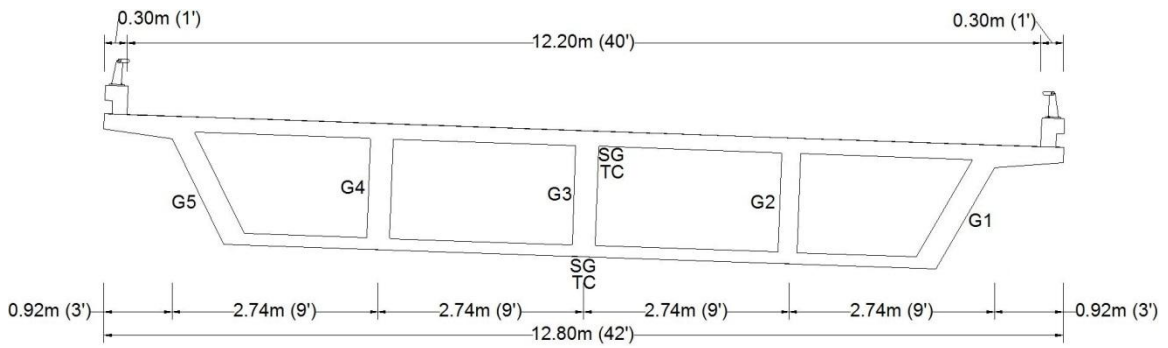
Figure 14. Section EE of the California bridge.
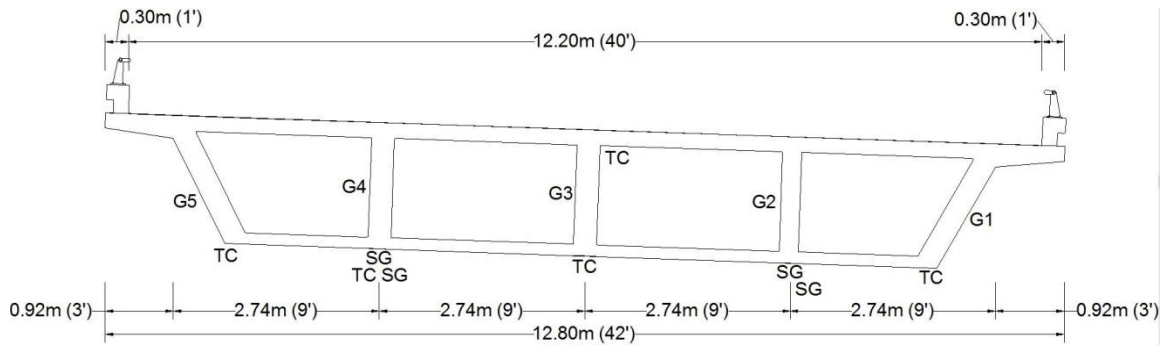
Figure 15. Section FF of the California bridge.
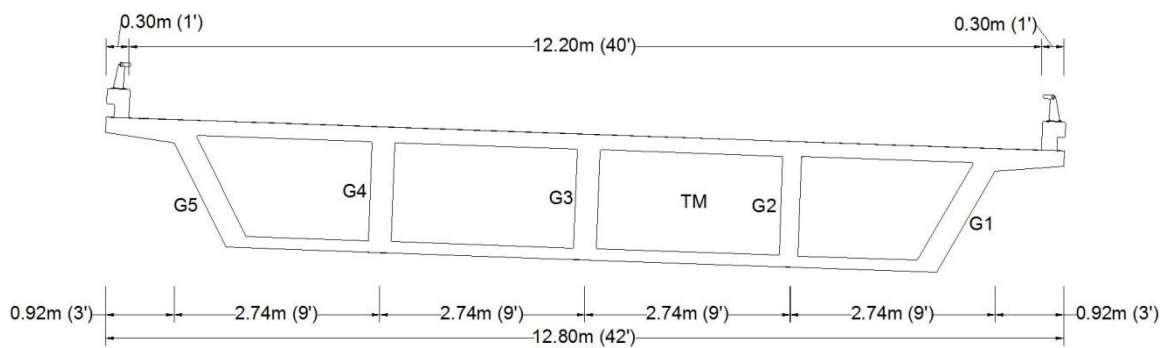
Figure 16. Section GG of the California bridge.

To complete the temperature gradient profile of the whole superstructure, five temperature sensors where located along the depth of girders 1 and 5, on the same cross-section as the deck gradient arrays. Thermocouples where also located on the top and bottom flanges of different girders along the length of the span.

Another important sensor that was installed to monitor the effects of temperature is a tiltmeter, which measures changes in rotation. The California Bridge has three tiltmeters located at the ends and at the midspan.

As part of the instrumentation program four holes where made on the bridge to access the inside of the girders. This allowed instruments to be installed inside of the box-girders and provide for maintenance if necessary.

The Utah Bridge

Foil strain gauges, velocity transducers, vibrating wire strain gauges, thermocouples and tiltmeters were installed on the superstructure and deck of the Utah Bridge in order to monitor changes in the bridge conditions. Creating a total of 46 sensors that constantly provide information about the structural health of the bridge. The deck also has sensors to measure resistivity, moisture content, electrical conductivity and chloride concentration.

To monitor the temperature changes on the superstructure, 31 thermocouples were installed. Ten of those thermocouples were used to create a deck temperature gradient measuring array that quantifies the steep changes in temperature along the depth of the deck. This gradient information is crucial to calculate the stresses induced on the superstructure by the temperature changes throughout the day. This array is located approximately 9.14m (30 ft) from the north end of the bridge in the east side of the deck, between girders 1 and 2.

Six temperature sensors, three on the inside and three on the outside, where located along the depth of girders 1 and 5, and three more along the depth of Girder 3. All the sensors were installed on the same longitudinal cross-section as the deck gradient arrays. Thermocouples where also located on the bottom flange of every girder at 9.75m (32 ft) from the north end of the bridge. The information provided by these thermocouples creates a complete profile of the temperature gradient of the whole superstructure.

Figures 17 through 22 show the location of the sensors on the bridge. TM tilt-meters, SG strain gauge, TC thermocouple and DTC deck thermocouple. Refer to Figure 6 to see the location of the cross-section along the length of the bridge.
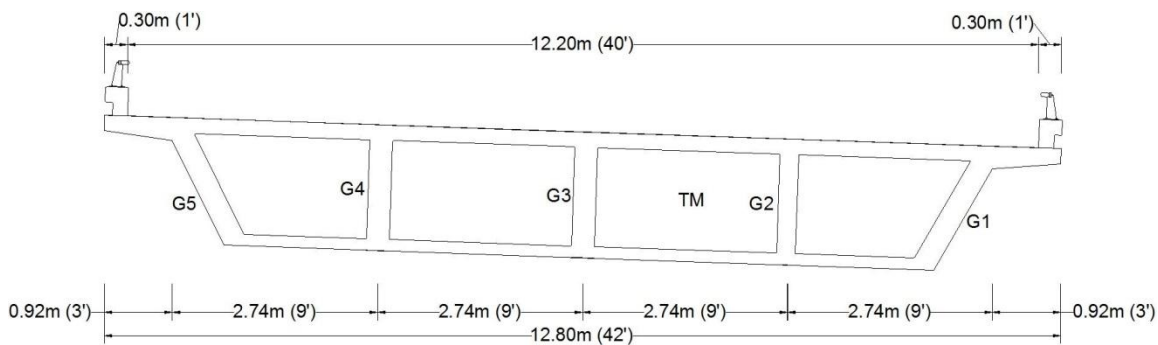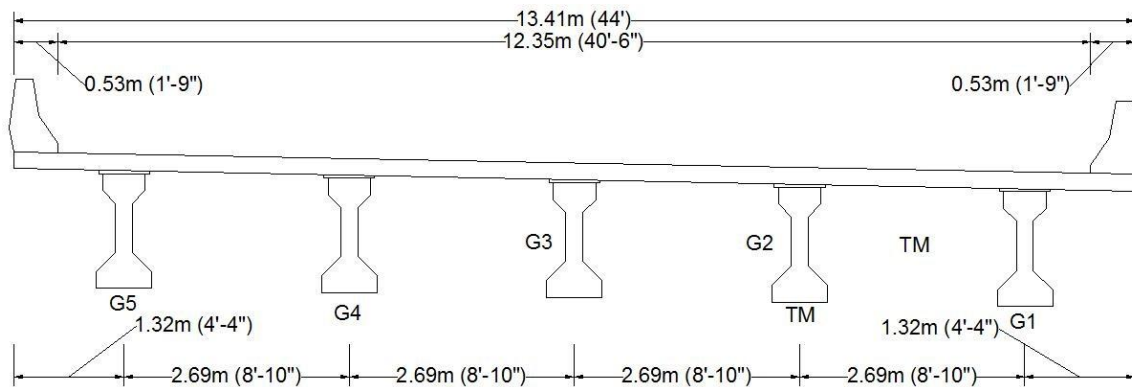

Figure 17. Section AA of the Utah bridge.
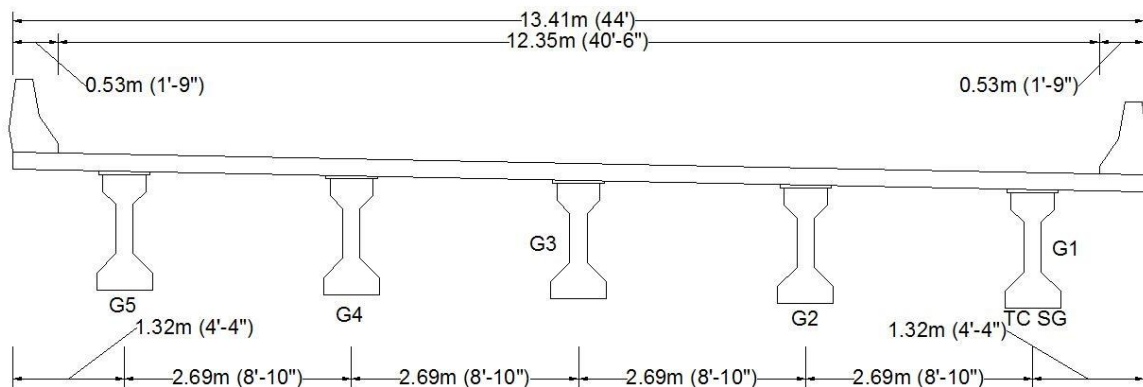

Figure 18. Section BB of the Utah bridge.
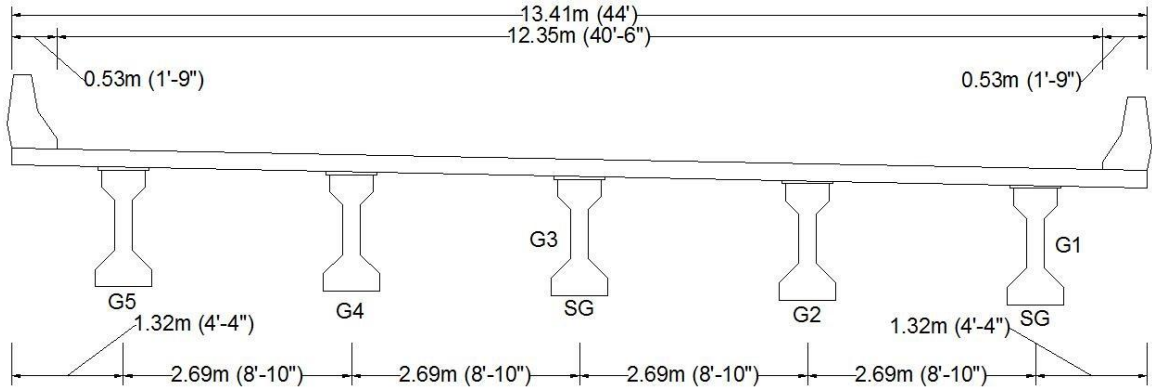
Figure 19. Section CC of the Utah bridge.
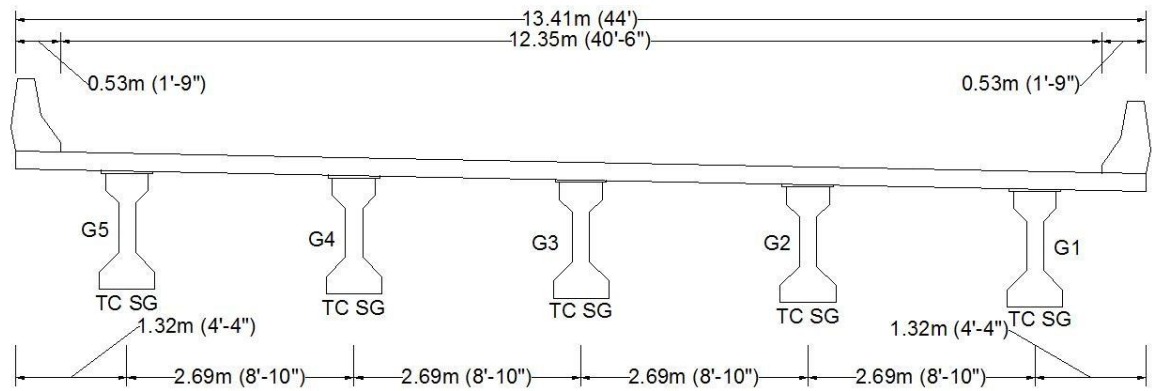
Figure 20. Section DD of the Utah bridge.
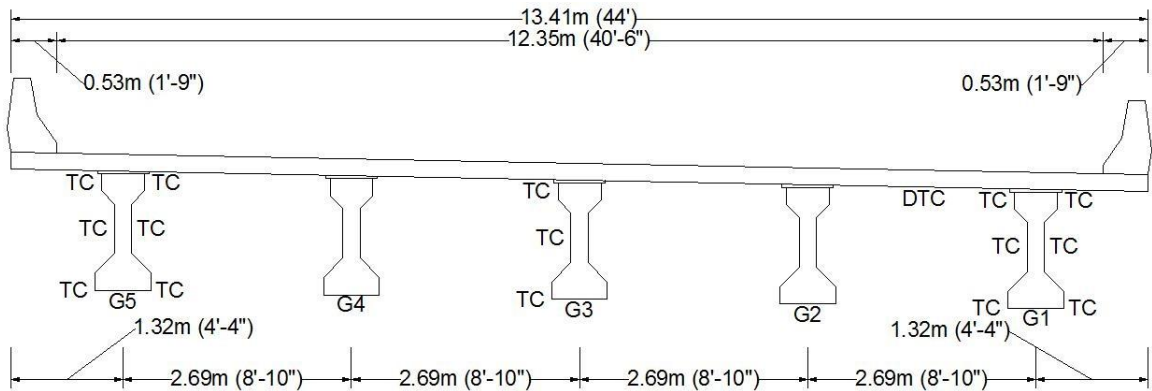
Figure 21. Section EE of the Utah bridge.
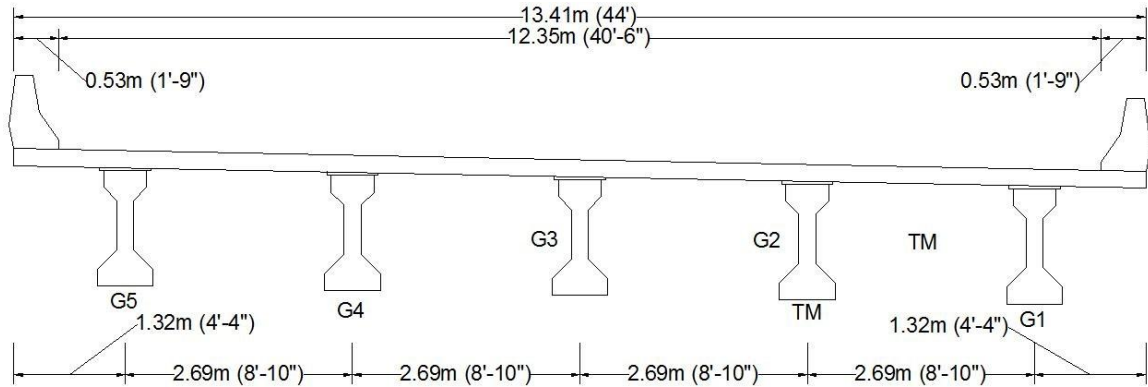
Figure 22. Section FF of the Utah bridge.

Tiltmeters where located at each end of the bridge, one on the abutment and one on the bottom flange of girder 2.

The Utah bridge was provided with instruments to measure in-situ weather conditions like solar radiation, relative humidity, air temperature, rain, wind speed and wind direction. This information was used to quantify the effects of the local weather conditions on the bridge temperature and consequently the structure.

The Utah bridge also has a weight-in-motion (WIM) station nearby which provides information on the weight of the trucks that drive over it. This information can later be related to the strain readings on the girders.

CHAPTER 4

UNIFORM BRIDGE TEMPERATURE

The LRFD Bridge Design Specifications (2010) of the American Association of State Highway and Transportation Officials (AASHTO) defines two methods; Procedure A and Procedure B; to determine the design uniform temperature ranges of bridges. Procedure A divides bridges in steel or aluminum, concrete and wood and the climate zone into moderate and cold. A table gives the temperature range for each combination of bridge type and climate zone. Procedure B determines maximum and minimum design bridge temperatures for concrete girder bridges with concrete decks and steel girder bridges with concrete decks. These design temperatures are given by contour maps for each bridge type. Procedure B yields the larger temperature range for both the Utah and California bridges. The temperature range is defined as the difference between the maximum design temperature ($T_{MaxDesign}$) and the minimum design temperature ($T_{MinDesign}$). Contours maps are used to obtain values for $T_{MaxDesign}$ and $T_{MinDesign}$ for concrete girder bridges with concrete decks and steel girder bridges with concrete decks.

With the contours maps for concrete girder bridges with concrete decks and using linear interpolation as indicated in the commentaries the fallowing design values were obtained: $T_{MaxDesign}$= 44.7 °C (112.5 °F); $T_{MinDesign}$= -1.11 °C (30.0 °F) for the California bridge; and $T_{MaxDesign}$= 40.56 °C (105.0 °F); $T_{MinDesign}$= -23.3 °C (-10.0 °F) for the Utah bridge.

Using the temperature sensors on the bridges the average bridge temperature (ABT) was calculated over time. Subsequently, the maximum ABT of the hottest summer and the minimum ABT of the coldest winter were compared to the $T_{MaxDesign}$ and $T_{MinDesign}$ temperatures obtained using the AASHTO LRFD Bridge Design Specifications (2010), respectively.

Since both the California and the Utah Bridge are oriented in a roughly north-south direction, all the cross sections of the bridges experienced similar sunlight exposure. By using Equation 11, an average bridge temperature was calculated for the cross section. It was assumed the same cross-sectional temperature distribution was experienced along the entire length of the bridge.

Rodriguez (2012) monitored the average bridge temperatures of the California Bridge from May 2011 to June 2012 and from September 2011 to June 2012 for the Utah Bridge. Using the tools and procedures developed by Rodriguez (2012) the average bridge temperature for the California and Utah bridges was continued to be monitored until September 2013 and January 2014 respectively. Covering a period of two years and five months for the California bridge and the Utah bridge.

<center>Measured Data</center>

For the California bridge the maximum ABT occurred on June 2013 with a magnitude of 112.99°F (45°C) and the minimum ABT of 36.9°F (2.72°C) was recorded on January 2013. It's worth noticing that the $T_{MaxDesign}$ was exceeded by 0.49°F (0.28°C). The minimum ABT was not exceeded but got to within 6.9°F

(3.83°C) of the AASHTO $T_{MinDesign}$ (2010). A plot, with the monthly measured maximum and minimum average bridge temperature and the $T_{MaxDesign}$ and $T_{MinDesign}$ temperatures of the AASHTO Bridge Design Specifications (2010), is presented for the California bridge as Figure 23.
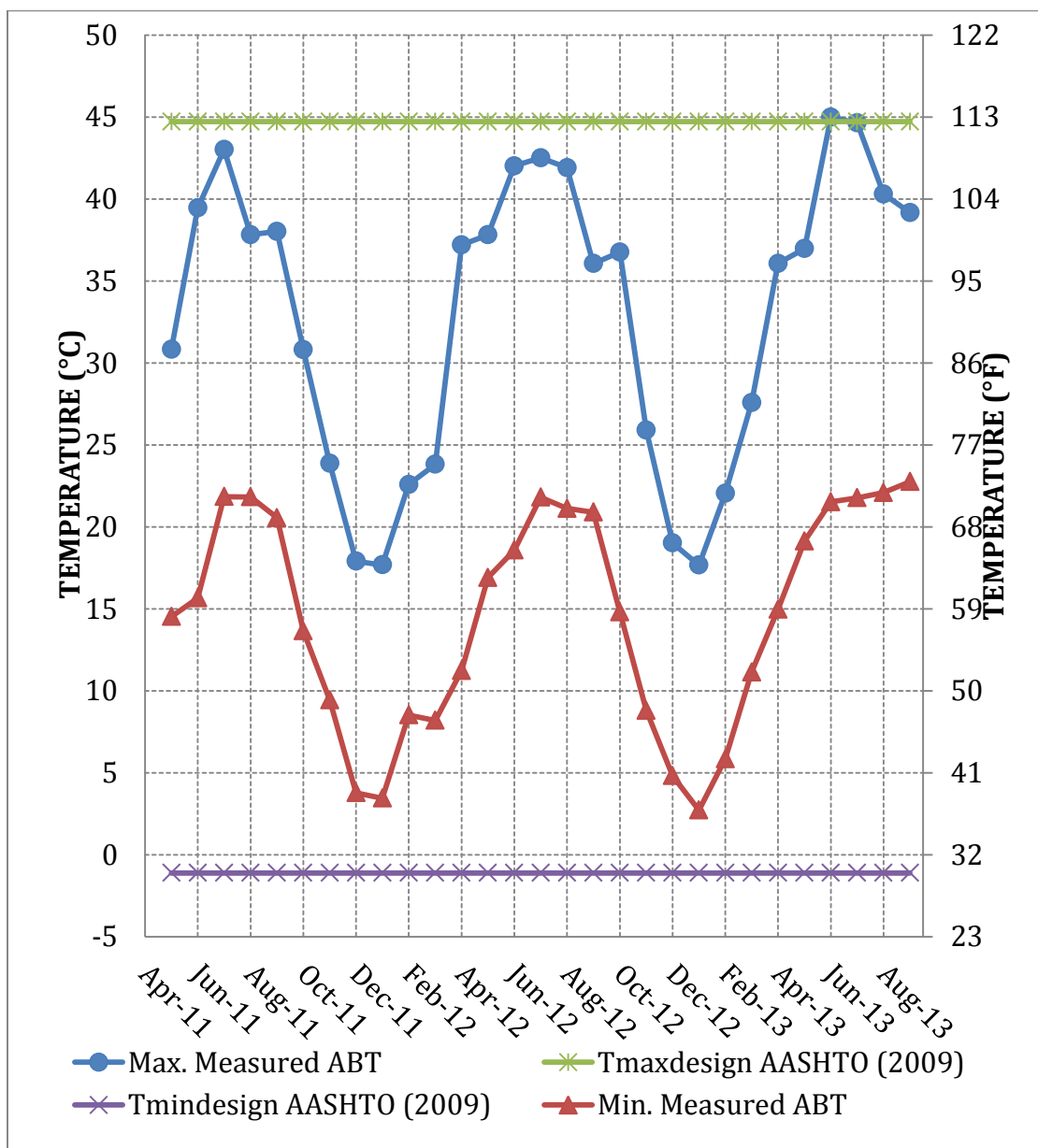
Figure 23. Maximum and minimum average bridge temperature for the California Bridge.

Analyzing the data of the Utah Bridge, the maximum ABT occurred on July 2013 with a magnitude of 106.5°F (41.39°C) and the minimum ABT was recorded as -5.77°F (-21°C) registered on January 2013. The Utah bridge exceeded the $T_{MaxDesign}$ by 1.5°F (0.83°C) and the minimum ABT was conservative by 4.23°F (2.33°C), which was closer to the AASHTO LRFD (2010) limit in comparison to the California bridge. A plot, similar to the one for the California bridge, is presented as Figure 24.
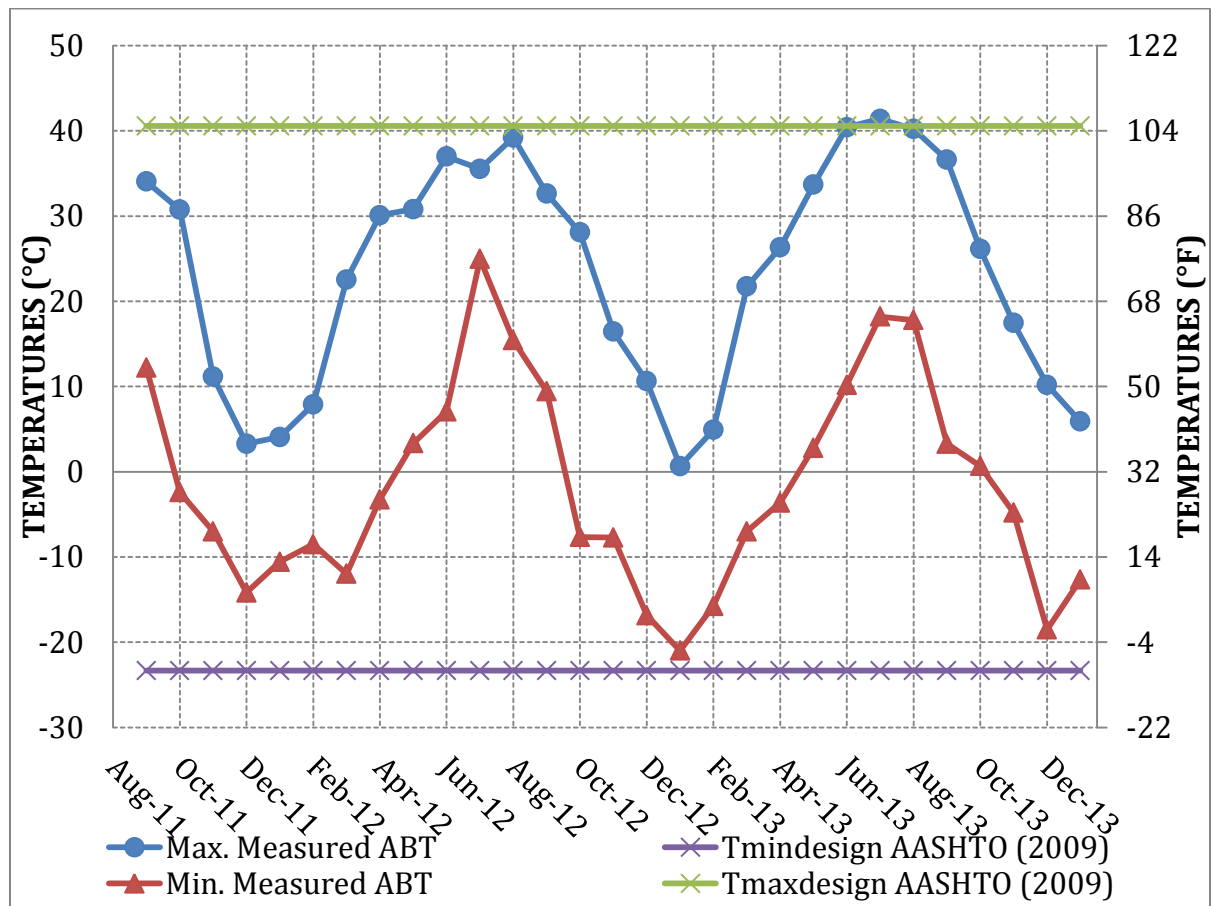
Figure 24. Maximum and minimum average bridge temperature for the Utah Bridge

Even if it wasn't by a significant amount, the fact is that the $T_{MaxDesign}$ was exceeded for both instrumented bridges. This exceedance of the code recommended

values raises the question: if $T_{MaxDesign}$ was exceeded within only two years of exposure to regular weather; what could happen, to both the maximum and minimum ABT, over a longer period of time with exposure to more extreme and even record low and high temperature conditions?

Prediction of Average Bridge Temperature

In order to investigate this question, predictive methods to quantify the average maximum and minimum bridge temperature were developed. To explore the accuracy of existing predictive methods, the measured average bridge temperatures were compared to the Kuppa Method (1991) and the Black and Emerson Method (1976) for calculating the average bridge temperature as a function of the ambient temperature. The Kuppa Method uses one equation for the maximum average bridge temperature and one for the minimum average bridge temperature for all concrete bridges (see Equations 12 and 13). The Black and Emerson Method uses a single equation to determine the minimum average bridge temperature and a related constant to calculate the maximum average bridge temperature based on the minimum ABT (see Equation 14 and Table 1).

Both methods are based on ambient temperature around the bridge. For the Utah Bridge, the ambient data came from the weather station installed on the site as part of the Long Term Bridge Performance Program instrumentation. However, since the California Bridge was not equipped with a weather station, temperature data from the closest weather station to the bridge by the National Oceanic and Atmospheric Administration (NOAA) was used. The weather station is located at the

Sacramento Executive Airport which was approximately 15 miles (24.14 km) from the California bridge.

The results of this comparison are presented in the following plots for both the California and Utah bridges.
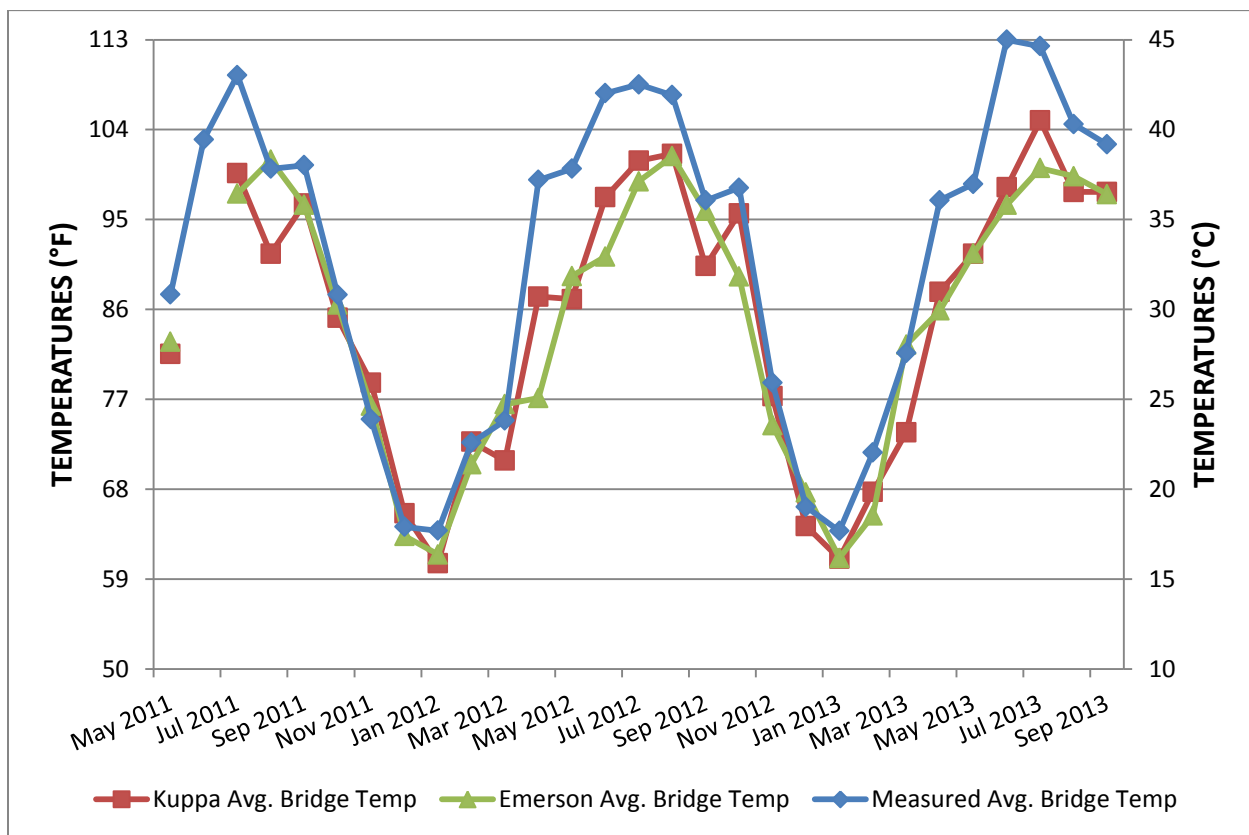
Figure 25. Measured vs. Kuppa vs. Black and Emerson monthly maximum avg. bridge temperature for the California bridge.
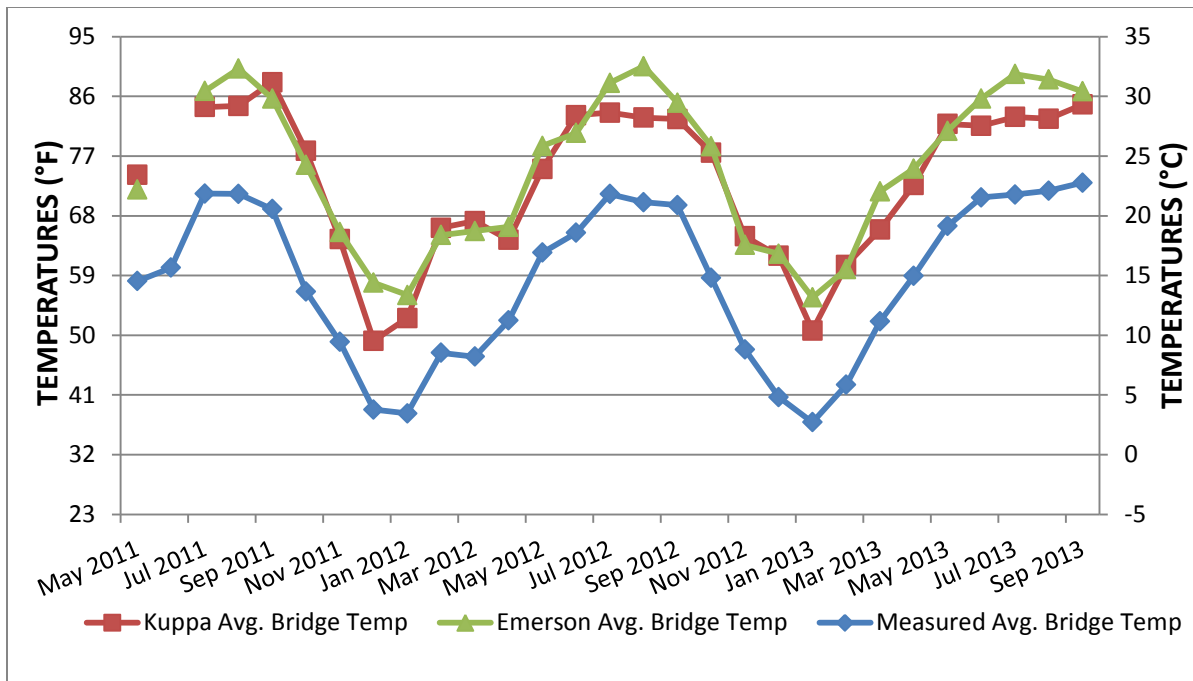
Figure 26. Measured vs. Kuppa vs. Black and Emerson monthly minimum avg. bridge temperature for the California bridge.
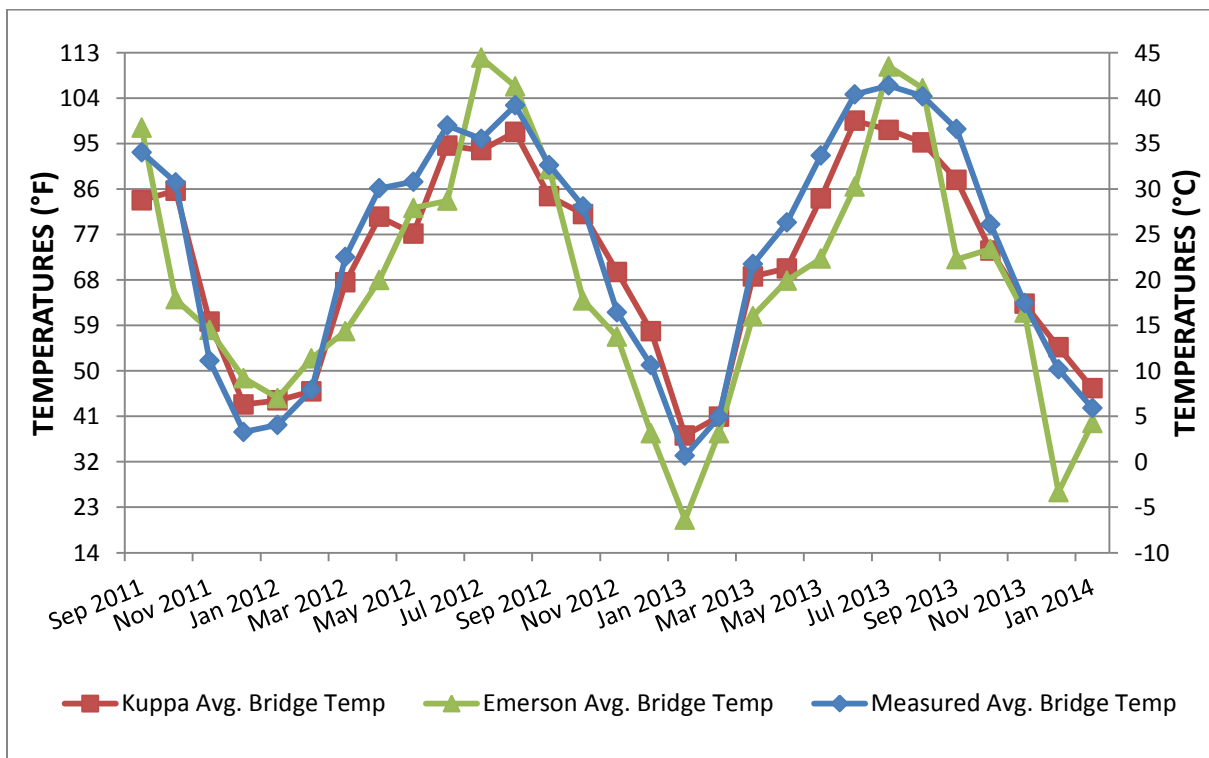
Figure 27. Measured vs. Kuppa vs. Black and Emerson monthly maximum avg. bridge temperature for the Utah bridge.
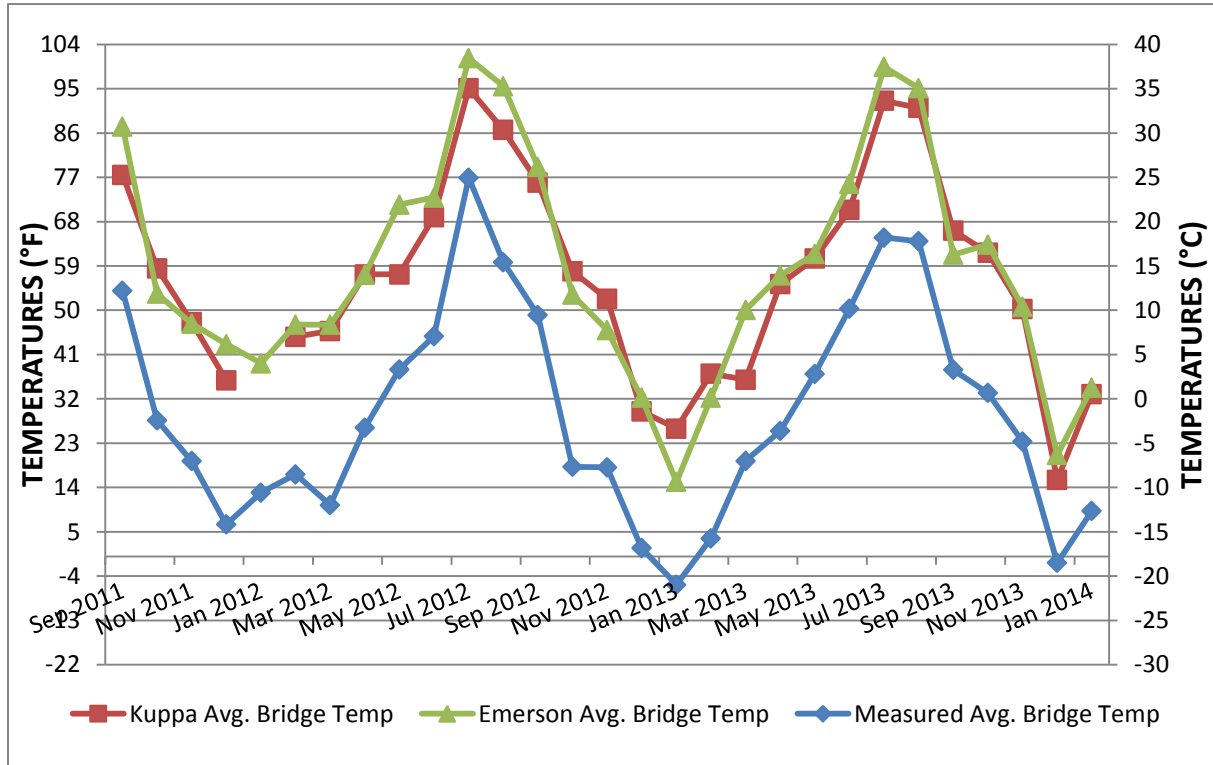
Figure 28. Measured vs. Kuppa vs. Black and Emerson monthly minimum avg. bridge temperature for the Utah bridge.

A comparison of these plots for both bridges showed that the Kuppa and the Black and Emerson Methods do a reasonable job of predicting the maximum average bridge temperature. However, when it comes to the minimum bridge temperature, the Kuppa and Black and Emerson Methods consistently underestimate the temperature by an average of 15.45°F (8.58°C) and 17.35°F (9.64°C) for the California Bridge and 27.65°F (15.36°C) and 30.31°F (16.84°C) for the Utah Bridge, respectively. This Results in hotter minimum average bridge temperatures in comparison to the actual measured minimum average bridge temperature.

As a result, a better predictive method for quantifying the average bridge temperature was formulated. Two set of equations were evaluated, the first set just takes into account the maximum air temperature of the hottest day and the previous day for the predictive tools for the maximum average bridge temperature; and the minimum air temperature of the coldest day and the previous day for the minimum average bridge temperature. The second set, which proved to be more accurate overall, was named ERL Method. ERL stands for Edyson Rojas Lopez. The ERL Method uses an average of the maximum air temperature of the hottest day and the previous day and an average of the minimum air temperature of that day and the previous day to calculate the maximum average bridge temperature. The minimum average bridge temperature is calculated using an average of the minimum air temperature of the coldest day and the previous day and an average of the maximum air temperature of that day and the previous day.

After calibrating the equations of the ERL method, it was observed that the equation for the maximum average bridge temperature for both bridges was the same. However, for the equation of the minimum average bridge temperature the constant in the equation for the California and Utah bridges was different. Indicating that there are factors, outside air temperature, that possibly affects box girder and I girder bridges differently.

One factor that is believed to mostly contribute to the difference in the equations of the minimum average bridge temperature is the bridge type. One reason for this could be that at night and during sunrise when the minimum average bridge temperature occurs, the effect of direct sun radiation on the bridge is not

important. The lack of sun radiation combined with the big exposed surface of the Utah bridge resulted in the average bridge temperature being lower. As for the California bridge, the intense sun radiation during the day heated up the air inside the box-girders of the bridge. Since this air is enclosed, during the night it keeps the California bridge warmer.

In order to obtain a single equation to satisfy both bridges, a new constant was found for the equation of minimum air temperature creating the ERL unified equation for the average minimum bridge temperature. The equations of the ERL method to calculate average maximum and minimum air temperature are presented below.

Maximum average bridge temperature of concrete bridges

$$T_{AvgMax} = \frac{T_{MaxAir1}+T_{MaxAir2}}{2}\,1.32 - \frac{T_{MinAirMax1}+T_{MinAirMax2}}{2}\,0.20 - 12.68\,(°F)$$
Equation 18

$$T_{AvgMax} = \frac{T_{MaxAir1}+T_{MaxAir2}}{2}\,1.32 - \frac{T_{MinAirMax1}+T_{MinAirMax2}}{2}\,0.20 - 4.91\ \ (°C)$$
Equation 19

Average minimum bridge temperature for concrete girder bridges (Utah Bridge)

$$T_{AvgMin} = \frac{T_{MaxAirMin1}+T_{MaxAirMin2}}{2}\,0.44 + \frac{T_{MinAir1}+T_{MinAir2}}{2}\,0.67 - 14.71\ \ (°F)$$
Equation 20

$$T_{AvgMin} = \frac{T_{MaxAirMin1}+T_{MaxAirMin2}}{2}\,0.44 + \frac{T_{MinAir1}+T_{MinAir2}}{2}\,0.67 - 6.22\ \ \ (°C)$$
Equation 21

Average minimum bridge temperature for concrete box-girder bridges (California Bridge)

$$T_{AvgMin} = \frac{T_{MaxAirMin1}+T_{MaxAirMin2}}{2}\,0.44 + \frac{T_{MinAir1}+T_{MinAir2}}{2}\,0.67 - 2.56 \quad (°F)$$
Equation 22

$$T_{AvgMin} = \frac{T_{MaxAirMin1}+T_{MaxAirMin2}}{2}\,0.44 + \frac{T_{MinAir1}+T_{MinAir2}}{2}\,0.67 + 0.53 \quad (°C)$$
Equation 23

Unified equation for the average minimum bridge temperature of concrete bridges

$$T_{AvgMin} = \frac{T_{MaxAirMin1}+T_{MaxAirMin2}}{2}\,0.44 + \frac{T_{MinAir1}+T_{MinAir2}}{2}\,0.67 - 8.64 \quad (°F)$$
Equation 24

$$T_{AvgMin} = \frac{T_{MaxAirMin1}+T_{MaxAirMin2}}{2}\,0.44 + \frac{T_{MinAir1}+T_{MinAir2}}{2}\,0.67 - 2.84 \quad (°C)$$
Equation 25

where

T_{AvgMax} – Maximum average bridge temperature.

T_{AvgMin} – Minimum average bridge temperature.

$T_{MaxAir1}$ – Maximum air temperature of the hottest day.

$T_{MaxAir2}$ – Maximum air temperature of the day before the hottest day.

$T_{MinAirMax1}$ – Minimum air temperature of the hottest day.

$T_{MinAirMax2}$ – Minimum air temperature of the day before the hottest day.

$T_{MinAir1}$ – Minimum air temperature of the coldest day.

$T_{MinAir2}$ – Minimum air temperature of the day before the coldest day.

T$_{MaxAirMin1}$ – Maximum air temperature of the coldest day.

T$_{MaxAirMin2}$ – Maximum air temperature of the day before the coldest day.

Now that new equations to predict the average bridge temperature were developed, they were compared to the average measured bridge temperatures and other equations already established, i. e., the Kuppa (1991) and Black and Emerson (1976) Methods. Plots comparing the different methods with the measured values are presented below.

Figure 29. Comparison of maximum measured and predicted average bridge temperatures (California bridge).

Figure 29 shows that the Kuppa and Black and Emerson equations are good predicting the maximum average bridge temperatures during the winter months. In

the summer when the maximum average bridge temperature is critical the Kuppa and Emerson equations predict cooler temperatures than the actual measured average bridge temperate. The average bridge temperature predicted by the ERL method follows closer the trend of the measured average bridge temperature through the year.
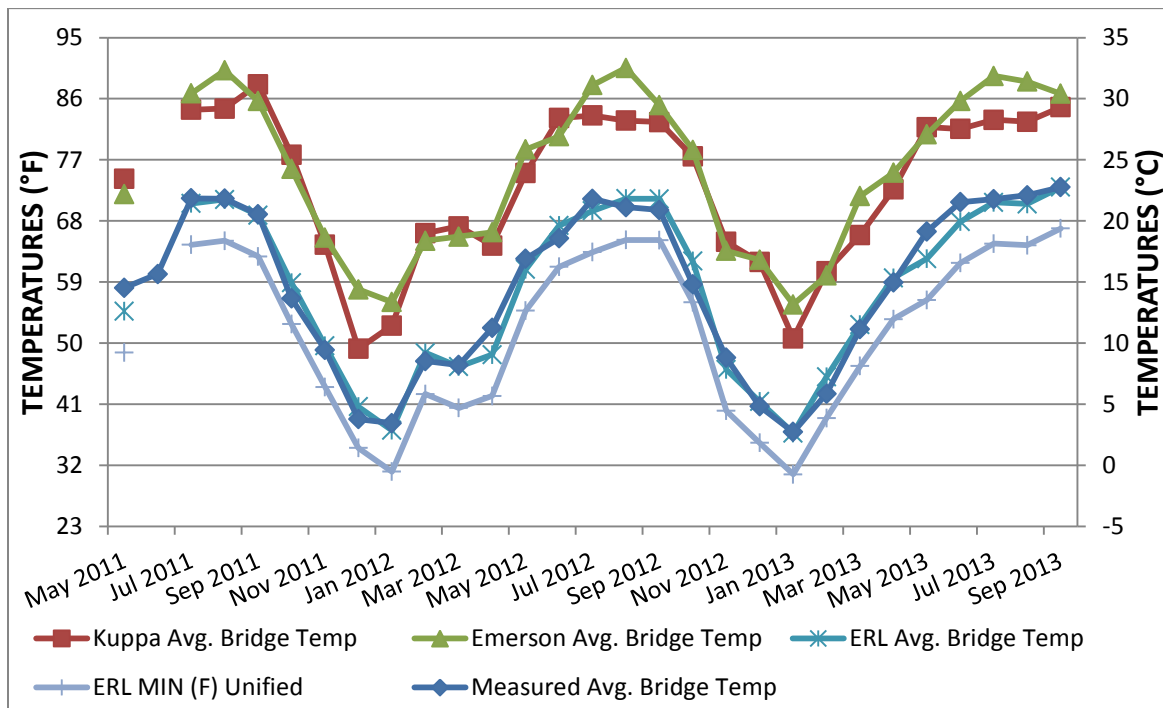
Figure 30. Comparison of minimum measured and predicted average bridge temperatures (California bridge).

Even though the Kuppa and Black and Emerson Methods curves have similar shape to the measured data, for every month of the year both methods predict warmer temperatures. Resulting in an un-conservative design. The ERL method specific for concrete box-girder bridges matched almost perfectly the shape and magnitude of the measured data. The unified version of the ERL equation for the minimum average bridge temperature yields conservative results. But the difference

between the ERL unified predictions and the measured data is smaller than the difference between the Kuppa and Black and Emerson and the measured data.
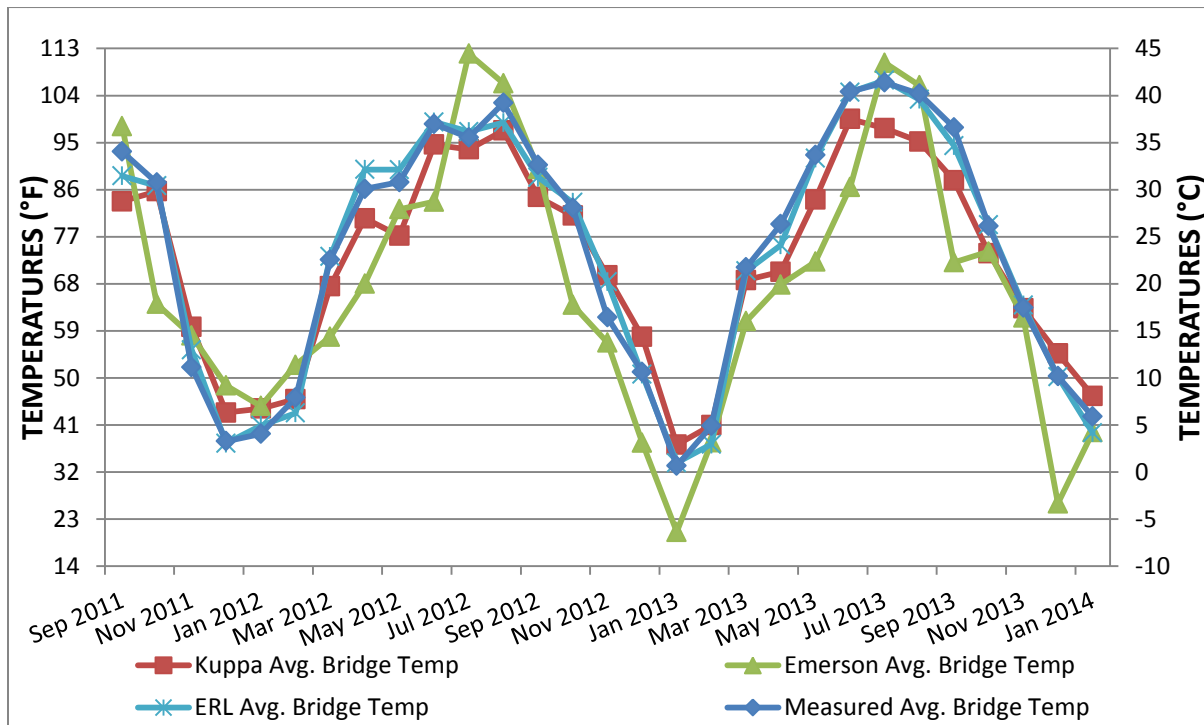
Figure 31. Comparison of maximum measured and predicted average bridge temperatures (Utah bridge).

Every method does a good job in estimating the magnitude of the maximum average bridge temperature for the Utah bridge. The Black and Emerson Method is the one that matches the less the shape of the measured data curve. The Kuppa and the ERL Methods follow closely the measured data curve, but the ERL method yields more accurate predictions specially during the summer months.
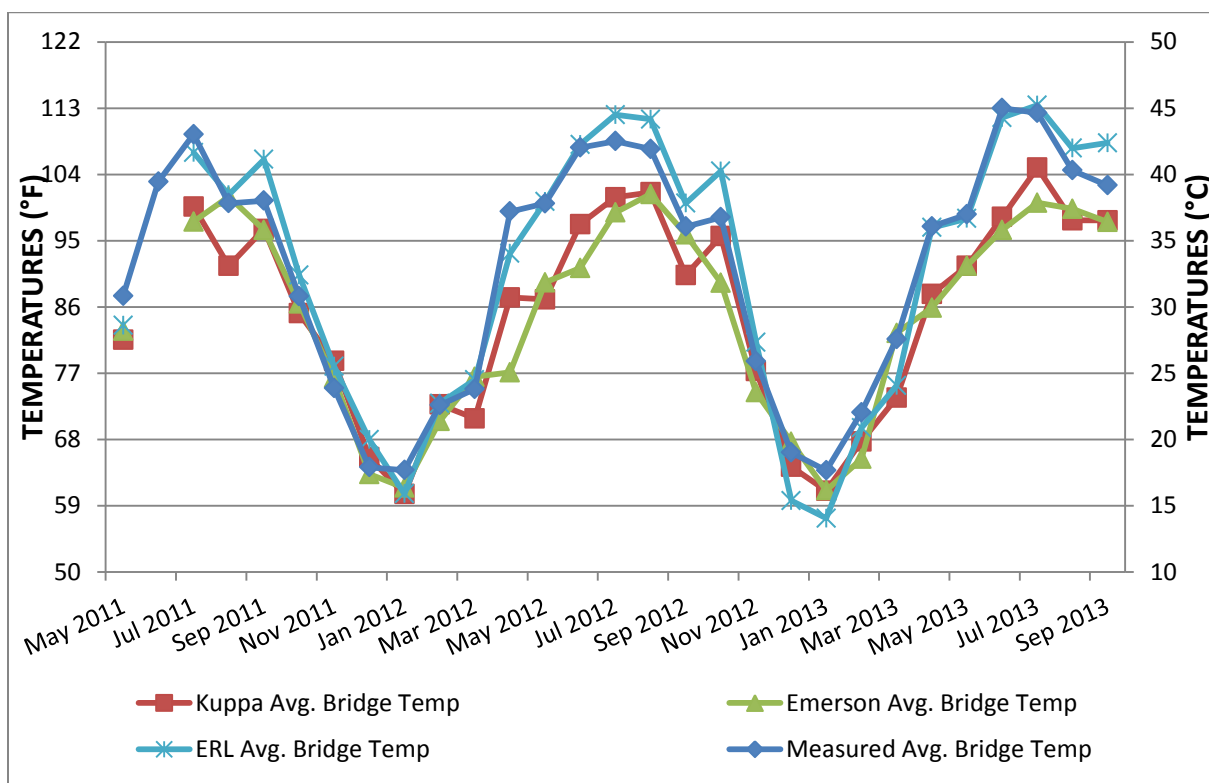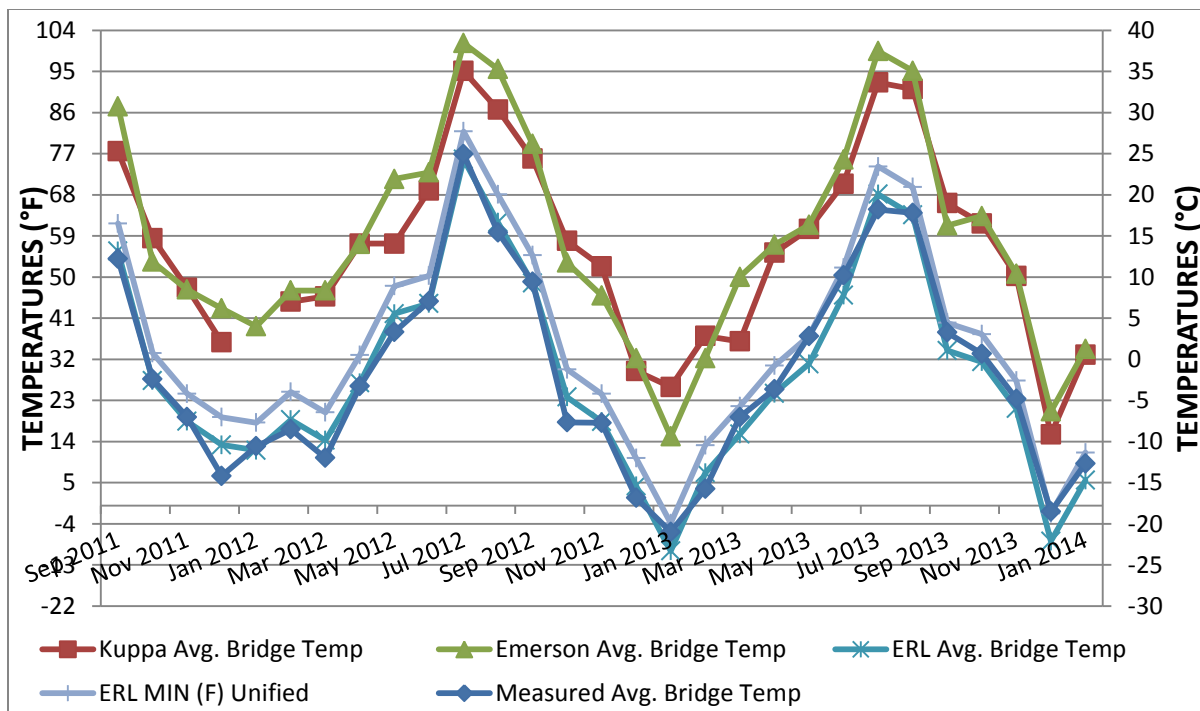
Figure 32. Comparison of minimum measured and predicted average bridge temperatures (Utah bridge).

Figure 32 shows that for the Utah bridge minimum average bridge temperature every method produced a curve with similar shape to the measured data. The Kuppa and Black and Emerson Methods are un-conservative, predicting warmer temperature than the measured data. The ERL unified equation predicted slightly warmer temperatures but closer to the measured values than the Kuppa and Black and Emerson equations. The ERL equation specific for concrete girder bridges matches almost perfectly the measured average bridge temperature curve.

For both bridges it is easily noticeable that the ERL method does a better job at predicting the average bridge temperatures. In the plots of the maximum average bridge temperature is especially more accurate during the summer, when it is more important, than the Kuppa and Black and Emerson methods. Using the equation

corresponding to each bridge type, the ERL method produces great results for the average minimum bridge temperatures. When the ERL unified equation is used on the Utah bridge the results are in general a little warmer that the measure average minimum bridge temperature. On the contrary, on the California bridge the equation produces lower temperature than the measured average minimum bridge temperature; and the error is bigger than on the Utah bridge.

To provide quantified statistical evidence of the measured and predicted data, the R-squared (R^2) and the mean squared error (MSE) where calculated for each prediction method with respect to the measured average bridge temperatures.

$$R^2 = \left(\frac{\sum_{i=1}^{n}(x_i - \bar{x})(y_i - \bar{y})}{\sqrt{\sum_{i=1}^{n}(x_i - \bar{x})^2 \ \sum_{i=1}^{n}(y_i - \bar{y})^2}} \right)^2 \qquad \text{Equation 26}$$

$$MSE = \frac{\sum_{i=1}^{n}(x_i - y_i)^2}{n} \qquad \text{Equation 27}$$

where

n Total number of months.

x_i Measured average bridge temperature for a particular month.

y_i Predicted average bridge temperature for a particular month.

$\bar{x} = \frac{\sum_{i=1}^{n} x_i}{n}$

$\bar{y} = \frac{\sum_{i=1}^{n} y_i}{n}$

Table 2. R² and MSE for the California bridge.

California Bridge				
Method	Avg. Max. Bridge Temp.		Avg. Min. Bridge Temp.	
	R^2	MSE	R^2	MSE
Kuppa Avg. Bridge Temp	0.9517	49.675	0.9283	235.238
Emerson Avg. Bridge Temp	0.8774	70.771	0.9715	297.015
ERL Avg. Bridge Temp	0.9617	13.946	0.9753	3.634
ERL Unified Avg. Bridge Temp	-	-	0.9753	42.7497

Table 3. R² and MSE for the Utah bridge.

Utah Bridge				
Method	Avg. Max. Bridge Temp.		Avg. Min. Bridge Temp.	
	R^2	MSE	R^2	MSE
Kuppa Avg. Bridge Temp	0.9698	37.74	0.9362	742.45
Emerson Avg. Bridge Temp	0.7955	167.66	0.9648	874.25
ERL Avg. Bridge Temp	0.9885	6.40	0.9767	11.07
ERL Unified Avg. Bridge Temp	-	-	0.9767	45.74

For both the California and Utah bridges, the R^2 and the minimum squared error, present better results for the ERL method in comparison with the Kuppa and the Black and Emerson methods. Concluding that, the ERL equations are a better method for predicting the average bridge temperature of concrete bridges.

Long-Term Prediction of Average Temperature Ranges

With the derived equations that were shown to be more accurate, They can be used to determined how the bridges would have and have been behaving through time. The ambient temperature database of the National Oceanic and Atmospheric Administration (NOAA) was consulted to obtain as much data as possible to model the behavior of the average bridge temperature of the bridge for a significant amount of time.

The weather station selected for the California Bridge is located at the Sacramento Executive Airport approximately 24.14 km (15 miles) north of the bridge. The station provided data from July 1931 to December 2012, but with information missing from November 1940, December 1940 and July 1948 to December 1972. Resulting in a model of the monthly variations of the maximum and minimum average bridge temperature for a period of 56 years and 9 months.

For the Utah Bridge the weather station selected was located the Hill Air Force Base approximately 38.62 km (24 miles) south of the bridge. The station provided data from October 1941 to December 2012, but with information missing from March 1946 to May 1946, January 1971 to December 1972, January 2000 to December 2004. Resulting in a model of the monthly variations of the maximum and minimum average bridge temperature for a period of 64 years.

For both Bridges three predictive models were compared to obtain the monthly average bridge temperatures namely the Kuppa, Black and Emerson and ERL methods. The results of each predictive equation are presented in plots with maximum and minimum limits that match the ASSHTO LRFD Bridge design specifications for the $T_{MaxDesign}$ and $T_{MinDesign}$ of each bride. $T_{MaxDesign}$= 112.5°F; $T_{MinDesign}$= 30.0°F for the California bridge; and $T_{MaxDesign}$= 105.0°F; $T_{MinDesign}$= -10.0°F for the Utah bridge.

Figure 33. Yearly predicted maximum average bridge temperature for the California bridge.

Figure 33 shows that the maximum average bridge temperature predicted by the ERL method exceeds the AASHTO limit on multiple occasions from 1931 to 2012. The Black and Emerson Method also exceeds the AASHTO limit on 1939. The Kuppa method does not exceeds the AASHTO limit on any year.

Figure 34. Monthly predicted maximum average bridge temperature for the California bridge (1932-1933).

Figure 34 shows a two years section of figure 33, from 1932 to 1933. The AASHTO limit is exceeded by the ERL method on both years, reaching a maximum on 1933. For this particular two year period neither the Kuppa nor the Black and Emerson Method exceeds the AASHTO limit.

Figure 35. Yearly predicted minimum average bridge temperature for the California bridge.

Figure 35 shows the predictions of the minimum average bridge temperatures for the California Bridge. From 1931 to 2012 the AASHTO limit for the average bridge temperature is exceeded on various occasions by the ERL and ERL unified methods. The Kuppa and the Black and Emerson Methods did not exceed the AASHTO limit.

Figure 36. Monthly predicted minimum average bridge temperature for the California bridge (1932-1933).

Figure 36 shows a two years section of figure 35 from 1932 to 1933. The ERL and ERL unified methods exceeded the AASHTO limit. The Kuppa and the Black and Emerson Methods did not exceed the AASHTO limit.

The $T_{MaxDesign}$ established by the ASSHTO for the California bridge was exceeded on 28 years by the predictions of the ERL Method. The $T_{MinDesign}$ was exceeded on 5 years by the ERL Unified method and on 3 years by both the ERL Unified and ERL for box-girder bridges.
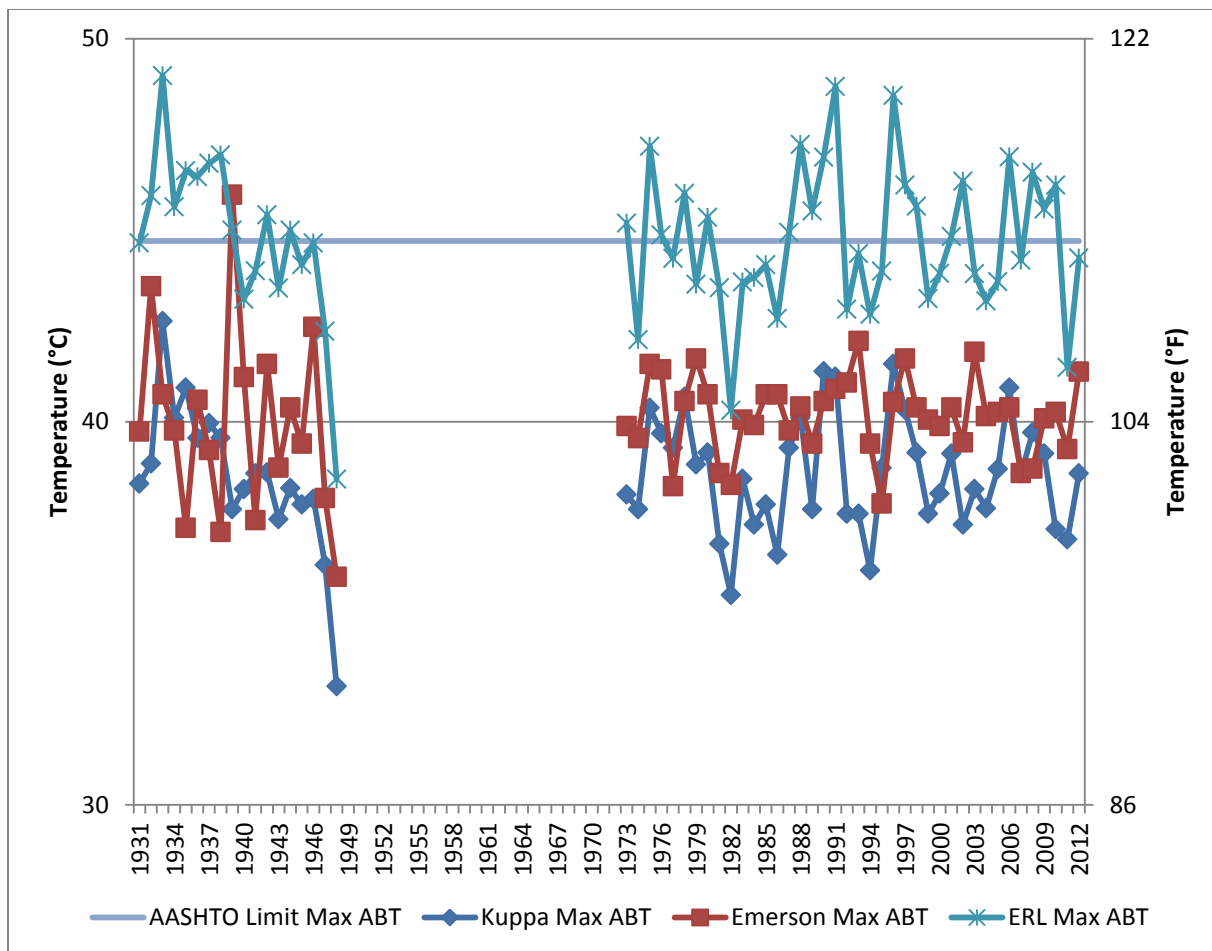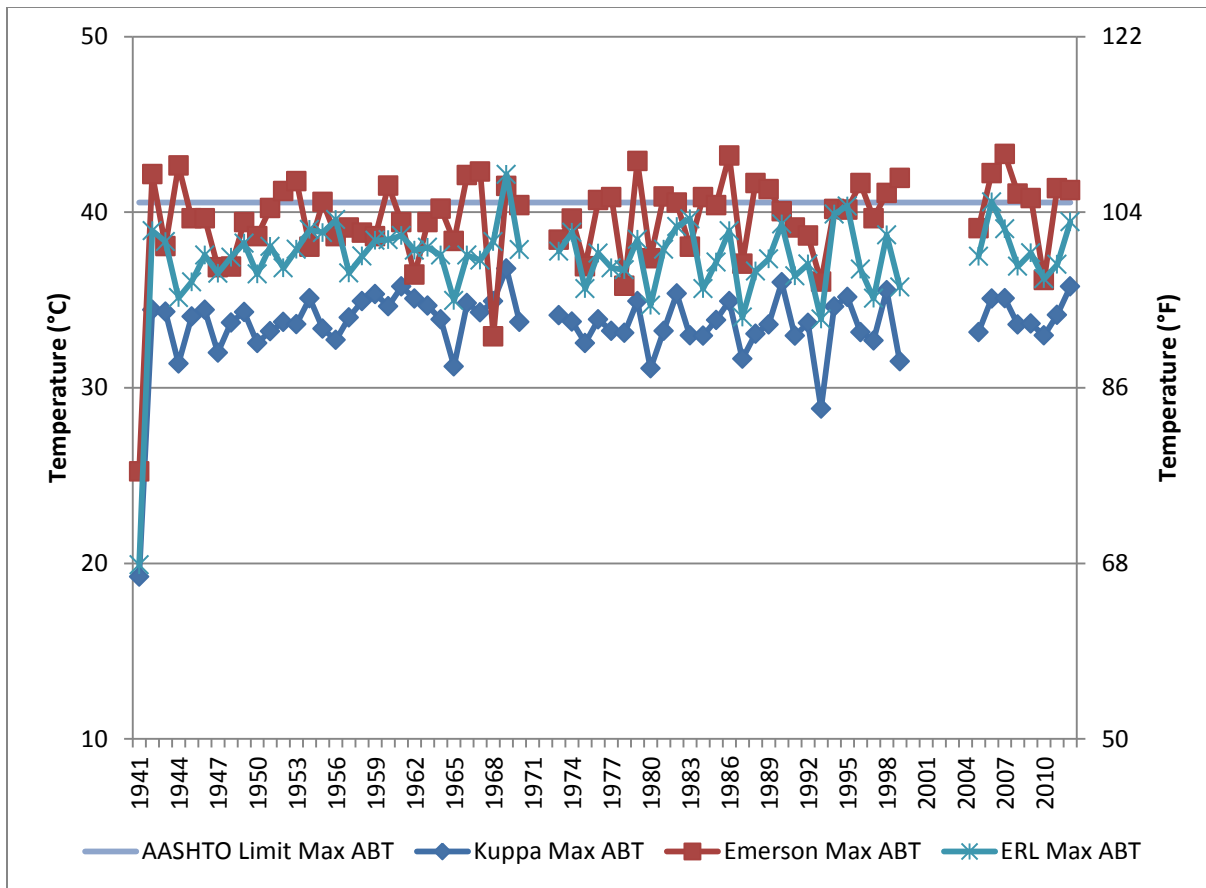
Figure 37. Yearly predicted maximum average bridge temperature for the Utah bridge.

Figure 37 shows the predictions of the maximum average bridge temperature for the Utah bridge from 1941 to 2012. The ERL and the Black and Emerson Methods exceed the AASHTO limit on multiple occasions, while the Kuppa Method never exceeded the AASHTO limit.
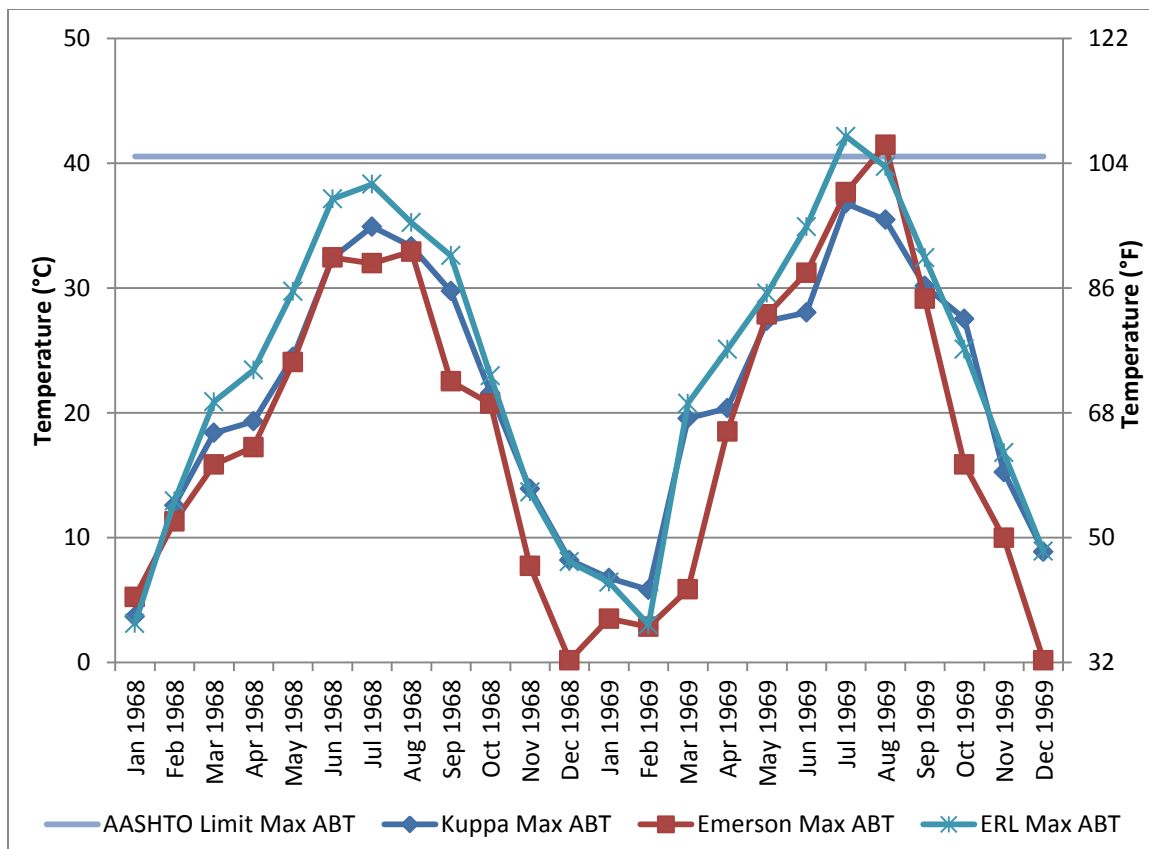
Figure 38. Monthly predicted maximum average bridge temperature for the Utah bridge (1968-1969).

Figure 38 shows a two years section of Figure 37 from 1968 to 1969. The AASHTO limit on the average bridge temperature is exceeded on 1969 by the Black and Emerson and the ERL Methods. The Kuppa Method did not exceed the AASHTO limit.
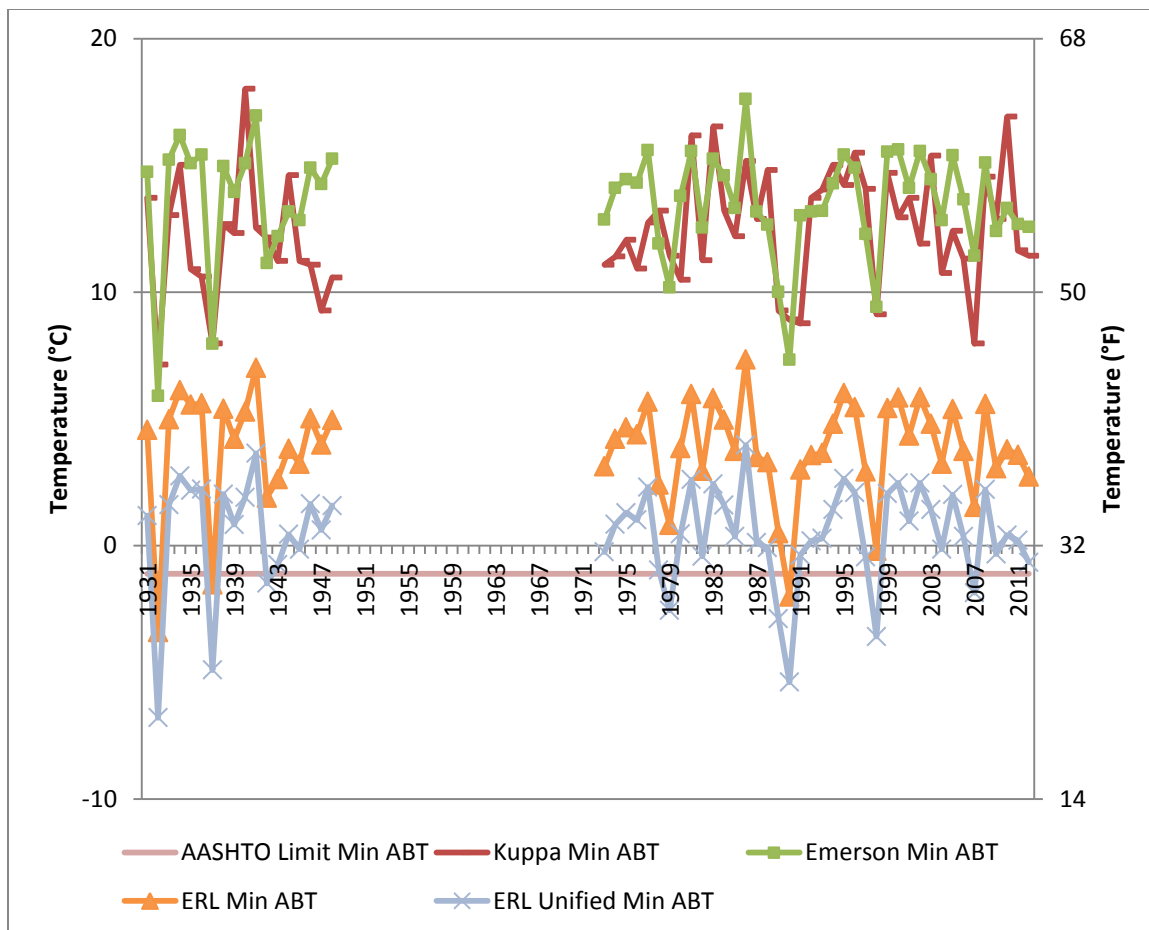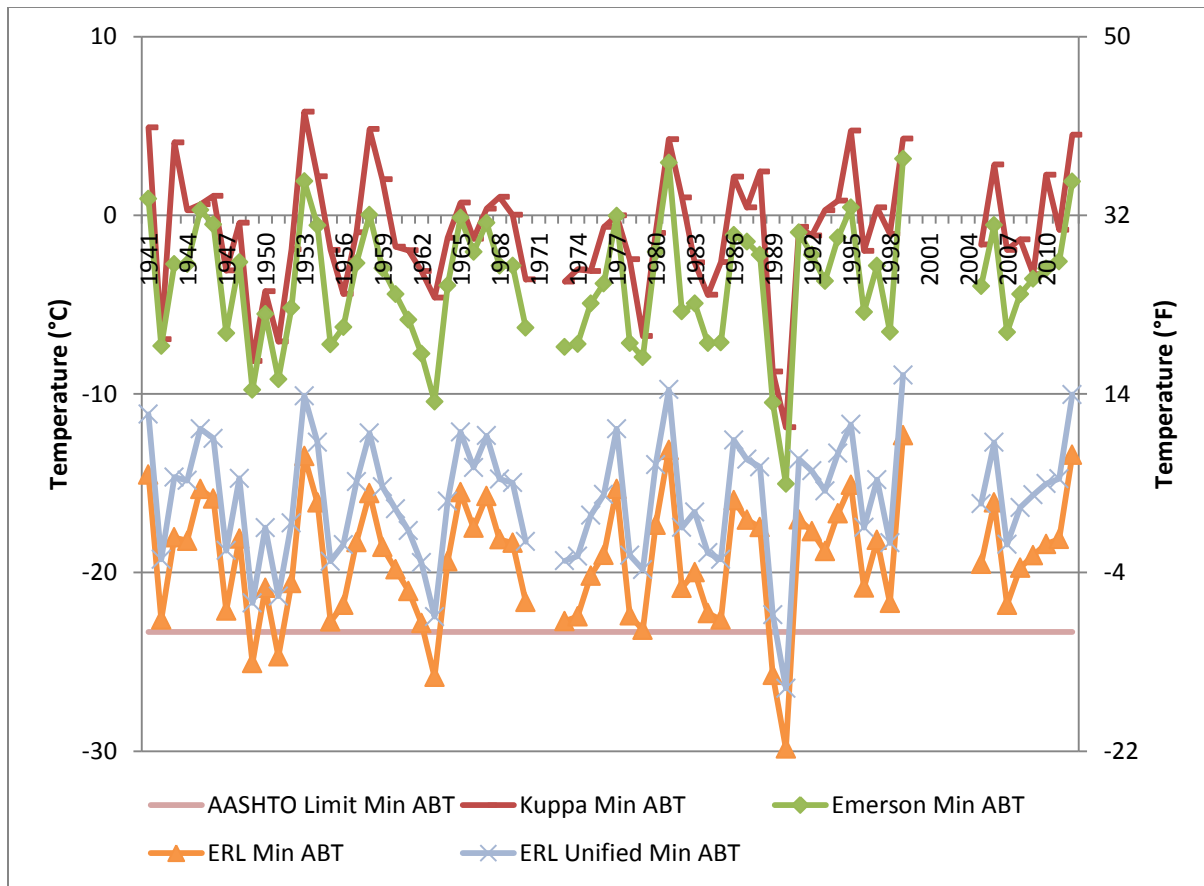
Figure 39. Yearly predicted minimum average bridge temperature for the Utah bridge.

Figure 39 shows the predictions of the minimum average bridge temperatures for the Utah bridge from 1941 to 2012. The Kuppa and the Black and Emerson Methods never exceeded the AASHTO limit. The ERL and ERL unified methods exceeded the limit on various occasions.

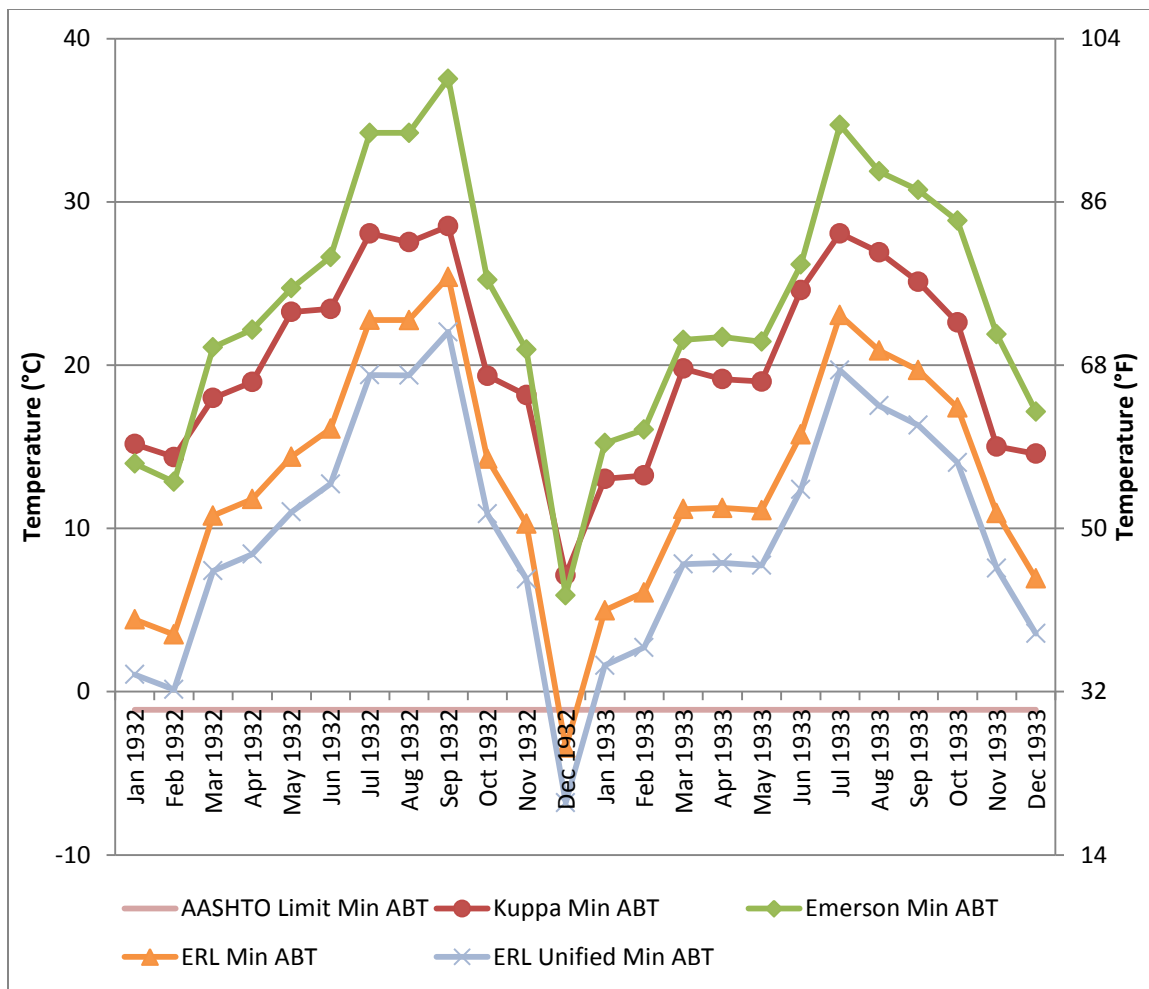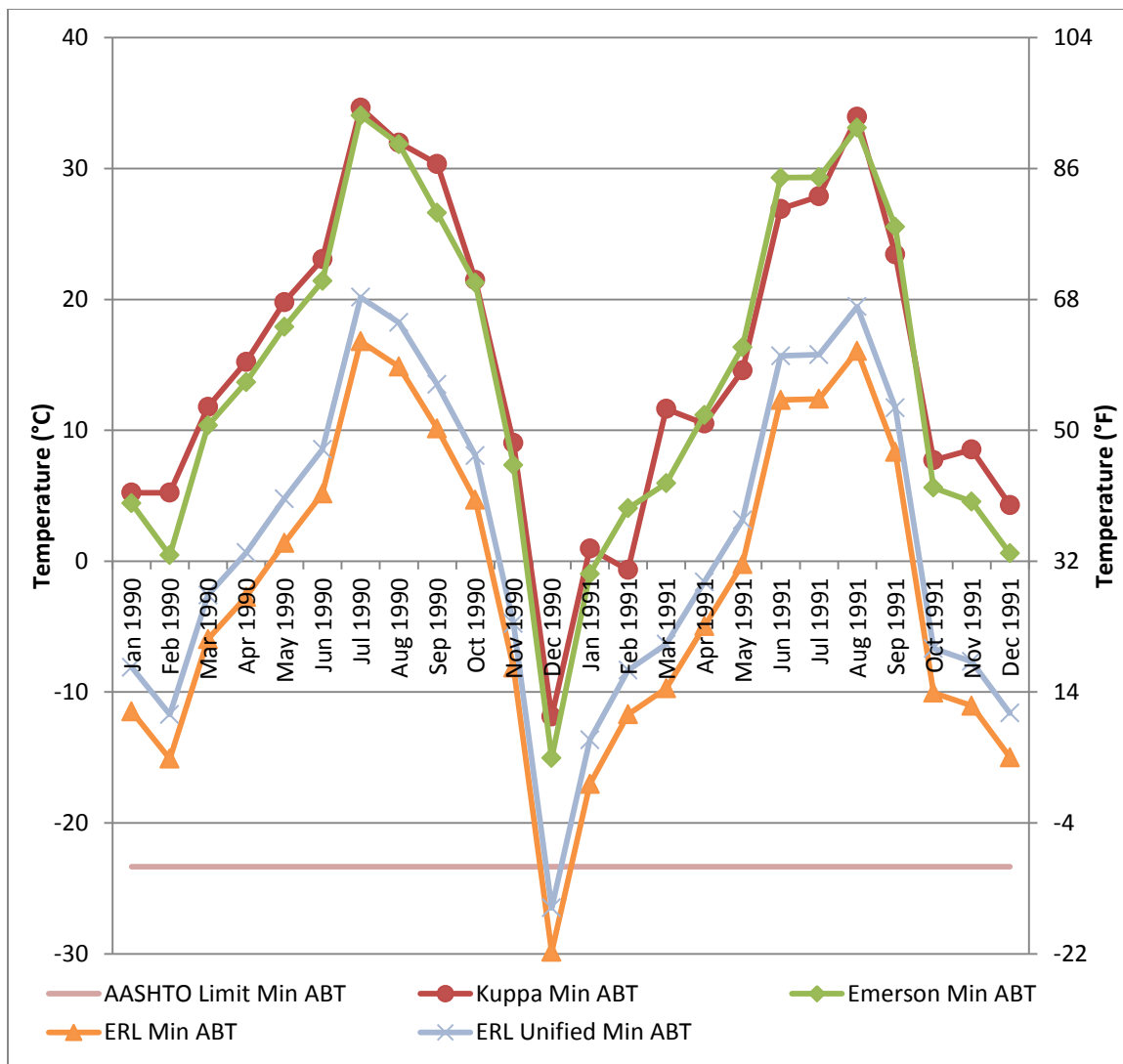Figure 40. Monthly predicted minimum average bridge temperature for the Utah bridge (1990-1991).

Figure 40 shows a two year section of Figure 39, from 1990 to 1991. During this period the minimum predicted average bridge temperature was reached. The ERL and the ERL unified methods exceeded the AASHTO limit, but this was not the case for the Kuppa and the Black and Emerson methods.

The $T_{MaxDesign}$ established by the ASSHTO for the Utah bridge was exceeded on two years by the predictions of the ERL method, but on multiple occasions by the

Black and Emerson Method. The $T_{MinDesign}$ was exceeded on 5 years by the ERL Method for girder bridges.

The tables presented below show a summary of the maximum and minimum values reached by the three models for both bridges.

Table 4. Summary of the maximum predicted average bridge temperature for the California bridge.

Summary of the California Max Avg. Bridge Temp			
Method	MONTH	Max Avg. Bridge Temp. °F (°C)	AASHTO °F (°C)
Kuppa ABT	Aug 1933	108.73 (42.63)	112.50 (44.72)
Emerson ABT	Jul 1939	114.67 (45.93)	112.50 (44.72)
ERL ABT	Aug 1933	120.26 (49.03)	112.50 (44.72)

Table 5. Summary of the minimum predicted average bridge temperature for the California bridge.

Summary of the California Min Avg. Bridge Temp			
Method	MONTH	Min Avg. Bridge Temp. °F (°C)	AASHTO °F (°C)
Kuppa ABT	Dec 1932	44.84 (7.13)	30.00 (-1.11)
Emerson ABT	Dec 1932	42.62 (5.90)	30.00 (-1.11)
ERL ABT	Dec 1932	25.84 (-3.42)	30.00 (-1.11)
ERL Unified ABT	Dec 1932	19.76 (-6.80)	30.00 (-1.11)

Table 6. Summary of the maximum predicted average bridge temperature for the Utah bridge.

Summary of the Utah Max Avg. Bridge Temp			
Method	MONTH	Max Avg. Bridge Temp. °F (°C)	AASHTO °F (°C)
Kuppa ABT	Jul 1969	98.22 (36.79)	105.00 (40.56)
Emerson ABT	Jul 2007	109.95 (43.31)	105.00 (40.56)
ERL ABT	Jul 1969	107.87 (42.15)	105.00 (40.56)

Table 7. Summary of the minimum predicted average bridge temperature for the Utah bridge.

Summary of the Utah Min Avg. Bridge Temp			
Method	MONTH	Min Avg. Bridge Temp. °F (°C)	AASHTO °F (°C)
Kuppa ABT	Dec 1990	10.63 (-11.87)	-10.00 (-23.33)
Emerson ABT	Dec 1990	4.91 (-15.05)	-10.00 (-23.33)
ERL ABT	Dec 1990	-21.75 (-29.86)	-10.00 (-23.33)
ERL Unified ABT	Dec 1990	-15.67 (-26.48)	-10.00 (-23.33)

From the data presented above it can be concluded that the maximum and minimum average bridge temperatures were exceeded for both the California and the Utah bridge on multiple occasions and therefore the contour maps established in the ASSHTO LRFD Bridge design specifications to determine $T_{MaxDesign}$ and $T_{MinDesign}$ of concrete bridges should be revised.

CHAPTER 5

TEMPERATURE GRADIENT

To determine the design temperature gradient to be applied to a bridge, the LRFD Bridge Design Specifications (2010) of the American Association of State Highway and Transportation Officials (AASHTO) divides the map of the United States into four regions. For each region a T_1 and T_2 value is provided, which defines the design positive temperature gradient. These values are presented without differentiating between concrete and steel bridges; or the absence or presence of an asphalt overlay. The T_1 and T_2 values for the design negative temperature gradient are obtain by multiplying the values for the positive temperature gradient by -0.30 for plain concrete decks, and -0.20 for decks with an asphalt overlay.

The difference in design gradients for concrete and steel bridges comes with the shape of the temperature gradient. For concrete bridges T_1 is applied at the top of the cross-section and decreases linearly to T_2 over the first 101.6 mm (4 in.). From T_2 the temperature gradient decreases linearly to zero over a distance A. The distance A depends on whether it is a concrete or a steel bridge. For steel bridges A is defined as 305 mm (12 in.), and there is a value t that should be taken as the depth of the concrete deck. For concrete structures A is a function of the depth of the section, having a value of 305 mm (12 in.) for superstructures that are 406 mm (16 in.) or deeper.

For the bottom of the cross-section, a T_3 value can be applied that decreases linearly to zero over 203 mm (8 in.). The LRFD Bridge Design Specifications (2010) specifies that T3 should be 0 °C (0 °F), unless a site-specific study determines a

more appropriate value, but it should never be greater than 2.78 °C (5 °F). Figure 41 is presented in page 3-104 of the AASHTO LRFD Specifications (2010) and illustrates the positive design temperature gradient.
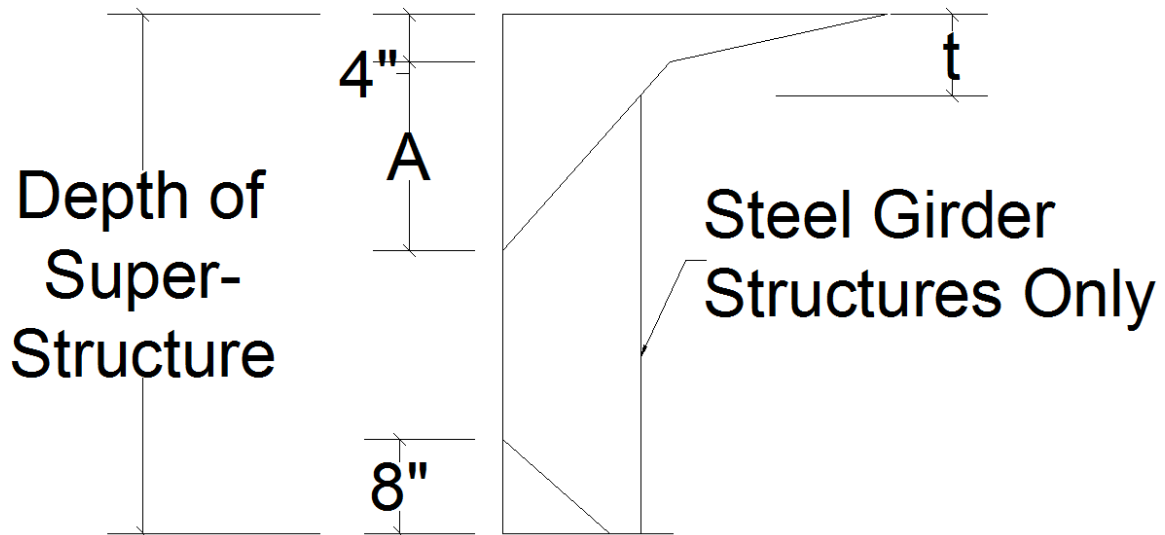
Figure 41. Positive design temperature gradient defined in the AASHTO LRFD Bridge Design Specifications (2010).

The California and the Utah Bridge are both located in Region 1 according to the AASHTO LRFD Bridge Design Specifications (2010) making T_1= 30 °C (54 °F) and T_2= 7.78 °C (14 °F). The superstructure of the California bridge is 1.68 m (66 in.) in depth and the Utah bridge is 1.57 m (62 in.), making A equals to 305 mm (12 in.) for both bridges. Figures 42 and 43 show the positive and negative design temperature gradients of the AASHTO LRFD Bridge Design Specifications (2010) respectively, applied over the height of the cross-section of the California bridge.
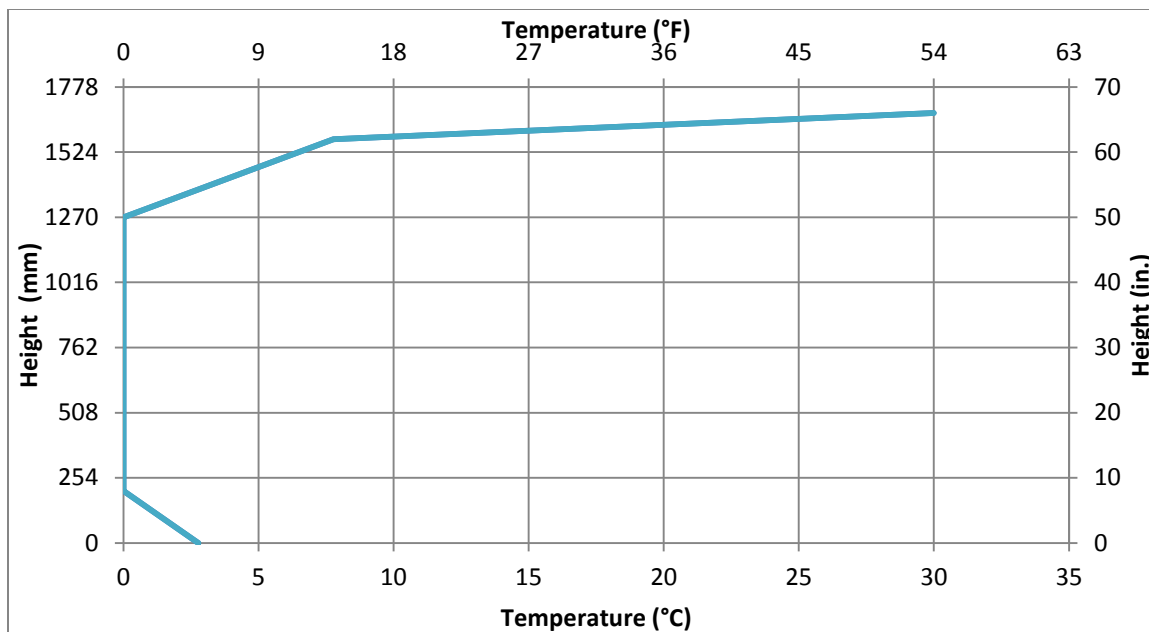
Figure 42. Positive design gradient of the AASHTO Specifications (2010).
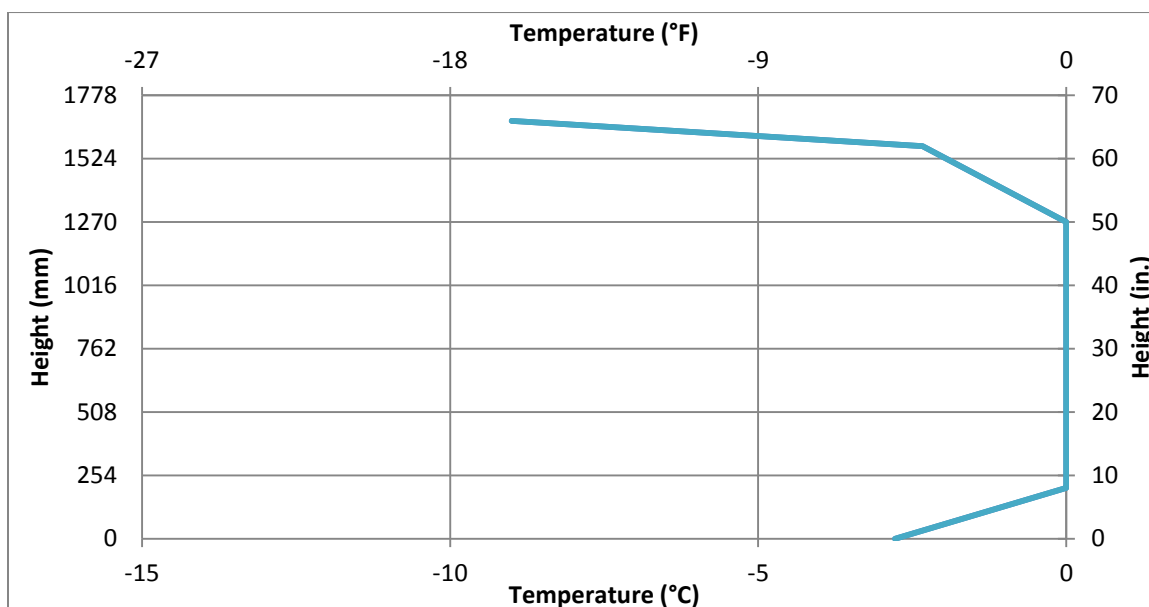
Figure 43. Negative design gradient of the AASHTO Specifications (2010).

Another temperature gradient often utilized by designer was proposed by Priestley (1978) which was used in the New Zealand Design Code. The positive temperature gradient starts with a temperature T at the top of the cross section. The

value of T is dependent on the presence of asphalt overlay and drops to zero at a depth of 1200 mm (47.2 in.) following a 5th order curve. The value for T is 32 °C (57.6 °F) for a bridge without an asphalt overlay and 16.76°C (30.17 °F) when there is a 76.2 mm (3 in.) overlay present. At the bottom of the cross section, a gradient of 1.5 °C (2.7 °F) is applied and decreases linearly to zero at a height of 200 mm (8 in.). Priestley (1978) did not propose a negative temperature gradient. Figure 44 shows the Priestley (1978) positive gradient with and without a 76.2 mm (3 in.) asphalt overlay applied over the height of the cross-section of the Utah Bridge.

Figure 44. Positive design gradient proposed by Priestley (1978).

Measured Temperature Gradients

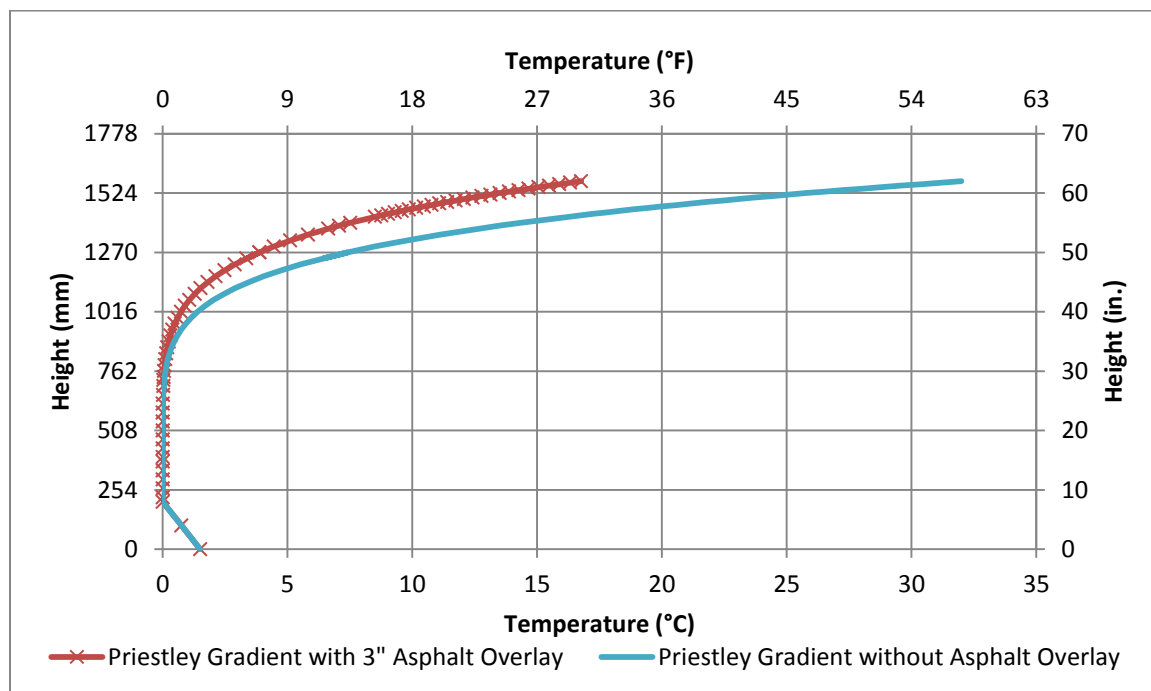If changes in the Bridge temperature were uniform throughout the entire cross-section, only axial deformation would develop. Flexural deformation, stresses, and moments develop due to differences in concrete temperature over the cross-section. For this study, the positive temperature gradient was defined as the measured sensor temperature at any location minus the minimum measurement. The negative temperature gradient similarly was defined as the measured temperature readings from the sensors minus the maximum measured temperature.

Sensors along the cross-sectional depth of the California and the Utah bridge were selected to form a temperature profile of the cross section from which the temperature gradient was extracted using the definition on the previous paragraph. To form the temperature profile of the California bridge 16 thermocouples were used; 10 in the deck, 5 along the web and 1 at the bottom of girder 1. For the Utah Bridge, 10 thermocouples in the deck, 3 along the web, and 1 at the bottom of Girder 3 were used to form the temperature profile; adding up to a total of 14 thermocouples.

For both bridges, temperature measurements along the cross-section were monitored every 15 minutes. Maximum positive and negative temperature gradients were obtained monthly based on the maximum the temperature gradient at the top of the cross section.

<u>The California Bridge</u>

The maximum positive temperature gradient measured on the California bridge occurred on June 2013. The temperature difference at the top of the cross-section was 25.22 °C (45.40 °F) and 5.82 °C (10.48 °F) at the bottom. The positive gradient was zero at 1194 mm (47 in.) from the top, which is similar to the 1200 mm (47.24 in.) proposed by Priestley (1978) and the 1220 mm (48.03 in.) found based on field measurements by Roberts-Wollman et al. (2002). However, the measured distance from the top to where the gradient is zero was very different to the 406.4 mm (16 in.) established in the AASHTO LRFD Specifications (2010).
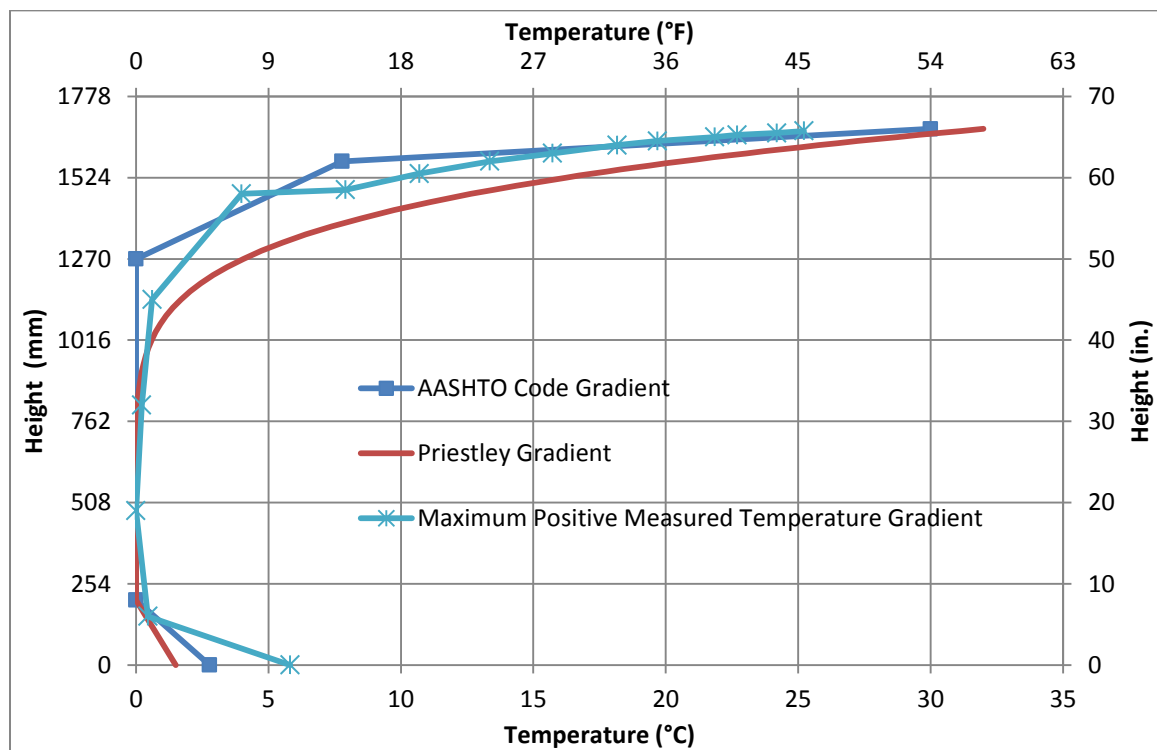

Figure 45. Maximum positive temperature gradient in June 2013 measured in the California bridge compared to AASHTO (2010) and Priestley (1978).

Figure 45 shows the maximum positive temperature gradient recorded in comparison to the AASHTO LRFD Specifications (2010) and the Priestley Method (1978). The measured value at the top, 25.22 °C (45.40 °F), was lower than the AASHTO Specifications (2010) 30 °C (54 °F) and the Priestley Method (1978) 32 °C (57.6 °F). However, the measured bottom value, 5.82 °C (10.48 °F), was larger than both design gradients, 2.78 °C (5 °F) defined in AASHTO LRFD Specifications (2010) and 1.5 °C (2.7 °F) established in the Priestley Method (1978).

The shape of the measured positive temperature gradient was best described by the AASHTO LRFD Specifications (2010) having an R^2 of 0.95 and a Mean Square Error (MSE) of 22, in comparison to the R^2 of 0.94 and a Mean Square Error (MSE) of 113 of the Priestley Method (1978). A temperature gradient defined with the measured values at the top and bottom of the cross section and following a 7th order curve to the point where the gradient is zero, 1194 mm (47 in.) below the top, was determine to be an almost exact fit to the measured gradient with a R^2 of 0.99 and a MSE of 3. A 5th order curve following the same principle yielded a R^2 of 0.97 and a MSE of 19. Figure 46 shows the comparison between the measured values and the values obtained by the 7th and 5th order curves.

For the California Bridge, the maximum negative temperature gradient was recorded in July 2013. The temperature at the top of the cross section was -9.87 °C (-17.77 °F) and -9.98 °C (-17.96 °F) at the bottom. The temperature gradient was zero at a depth of 533.4 mm (21 in.), which is close to the 610 mm (24.02 in.) measured by Roberts-Wollman et al. (2002) and somewhat similar to the 406.4 mm

(16 in.) established in the AASHTO LRFD Specifications (2010). Priestley (1978) did not define a negative temperature gradient.
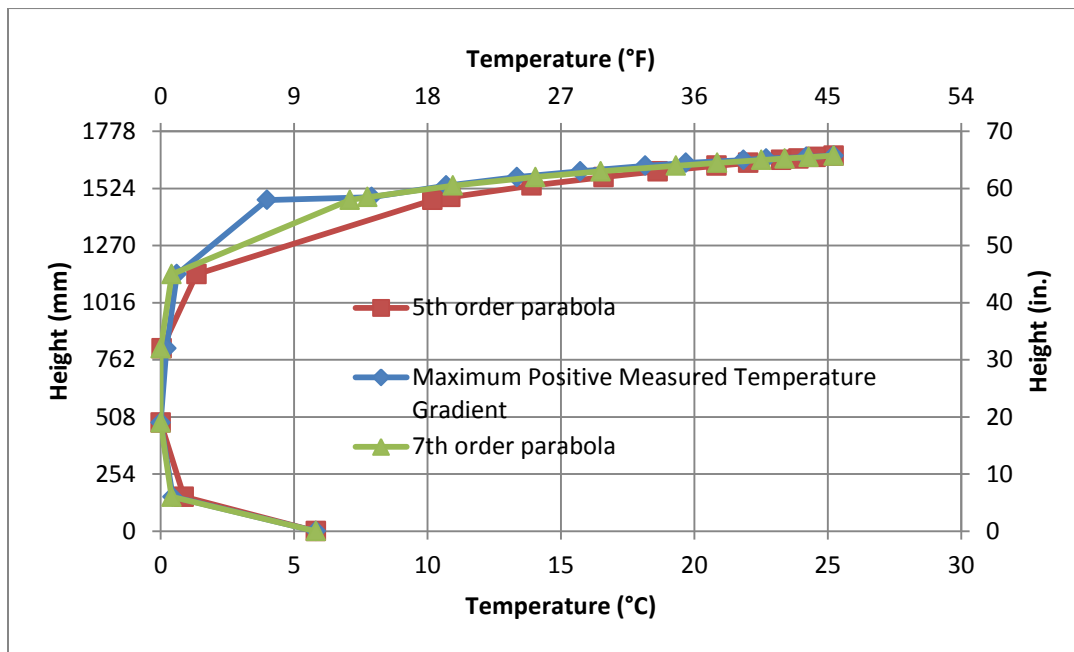

Figure 46. Maximum positive measured gradient in June 2013 in comparison to a 5th and 7th order curve.
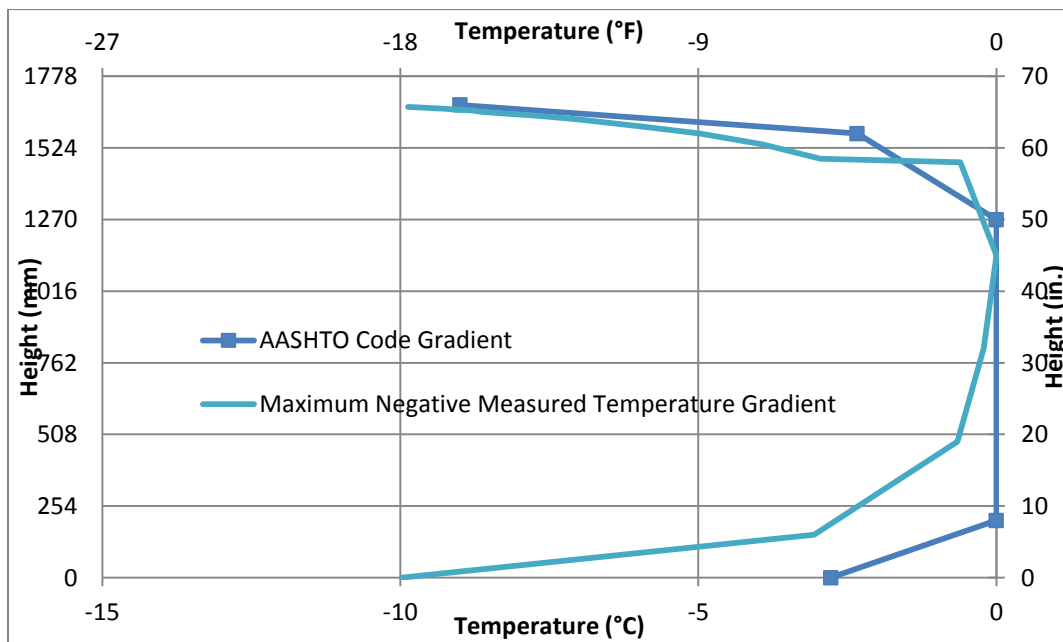

Figure 47. Maximum negative temperature gradient in July 2013 measured in the California bridge compared to the AASHTO Specifications (2010).

Figure 47 shows the maximum negative temperature gradient in comparison to the gradient specified in the AASHTO LRFD Specifications (2010). The upper value, -9.87 °C (-17.77 °F), was 15% above the -8.58 °C (-15.45 °F) established in the AASHTO LRFD Specifications (2010). The value at the bottom of the cross-section, -9.98 °C (-17.96 °F), was 259% greater than the -2.78 °C (-5.00 °F) established in the AASHTO LRFD Specifications (2010).

An R^2 of 0.77 and a MSE of 17 were found for the AASHTO LRFD Specifications (2010) when comparing it to the shape of the maximum measured negative temperature gradient. The best fit was found to be a temperature gradient defined with the measured values at the top and bottom of the cross-section and following a 5th order curve to the point where the gradient is zero, 533.4 mm (21 in.) below the top, having a R^2 of 0.95 and a MSE of 3. Figure 48 shows the comparison between the measured values and the values obtained with the 5th order curve.

Figure 48. Maximum Negative Measured Gradient in July 2013 in comparison to a 5th order curve.

The Utah Bridge

The maximum positive temperature gradient measured on the Utah bridge occurred in June 2012. The measured temperature at the top of the cross-section was 13.75 °C (24.75 °F) and the bottom temperature was 9.16 °C (16.48 °F). The gradient was zero at a depth of 1473 mm (58 in.) from the top of the cross-section. This value was different from the 1200 mm (47.24 in.) proposed by Priestley (1978), the 1220 mm (48.03 in.) for the box-girder bridge measured by Roberts-Wollman et al. (2002), and the 406.4 mm (16 in.) established in the AASHTO LRFD Specifications (2010). The difference between the box-girder California bridge and the I-girder Utah bridge it is possibly due to the particular thermal dynamic interaction of each bridge geometry with the environment.

Figure 49. Maximum positive temperature gradient in June 2012 measured in the Utah bridge compared to AASHTO (2010) and Priestley (1978).

Figure 49 shows the maximum positive temperature gradient recorded in comparison to the AASHTO LRFD Specifications (2010) and the Priestley Method (1978) with and without the 76.2 mm (3 in.) asphalt overlay. The maximum recorded temperature value at the top, 13.75 °C (24.75 °F), is relatively close to the Priestley Method (1978) with asphalt overlay 16.76 °C (30.17 °F); suggesting that the asphalt overlay plays a part as an insulator. The AASHTO LRFD Specifications (2010), 30 °C (54 °F), and the Priestley Method (1978) without asphalt overlay, 32 °C (57.6 °F), are 118% and 137% above the measured value respectively. The measured value at the bottom, 9.16 °C (16.48 °F), was larger than the 2.78 °C (5 °F) defined in AASHTO LRFD Specifications (2010) and 1.5 °C (2.7 °F) established in the Priestley Method (1978) for a bridge with and without asphalt overlay.

Between the Priestley (1978) and AASHTO LRFD Specifications (2010), the shape of the measured positive temperature gradient was best described by the Priestley Method (1978) with the 76.2 mm (3 in.) asphalt overlay with a R^2 of 0.84 and a MSE of 20.70. The AASHTO LRFD Specifications (2010) had a R^2 of 0.74 and a MSE of 207.27 and the Priestley Method (1978) without asphalt overlay had a R^2 of 0.82 and a MSE of 447.58. Suggesting that the asphalt overlay is an important factor in predicting the maximum positive temperature gradient. A temperature gradient defined with the measured values at the top and bottom of the cross-section and following a 5th order curve to the point where the gradient is zero, 1473 mm (58 in.) below the top, was determined to be a nearly perfect fit with a R^2 of 1.00 and a MSE of 0.46.
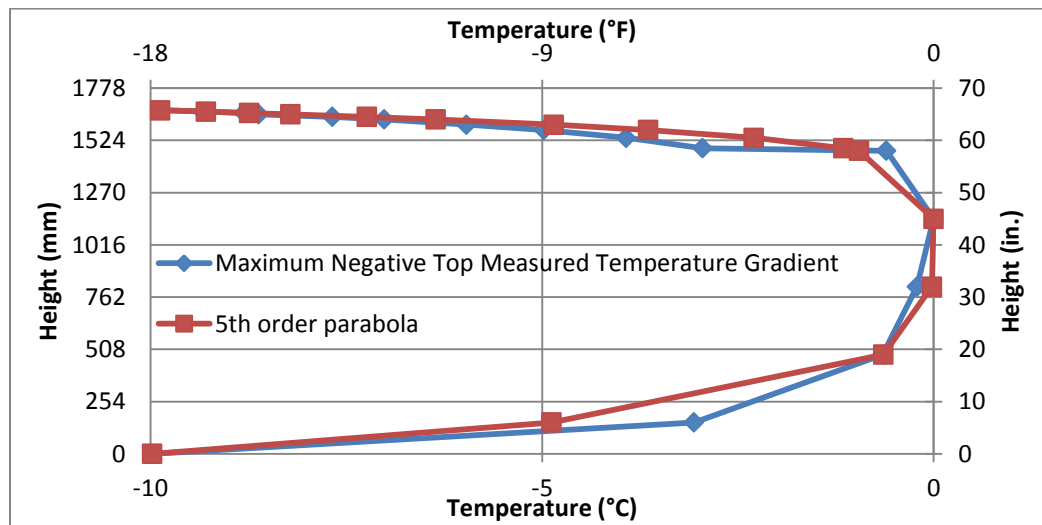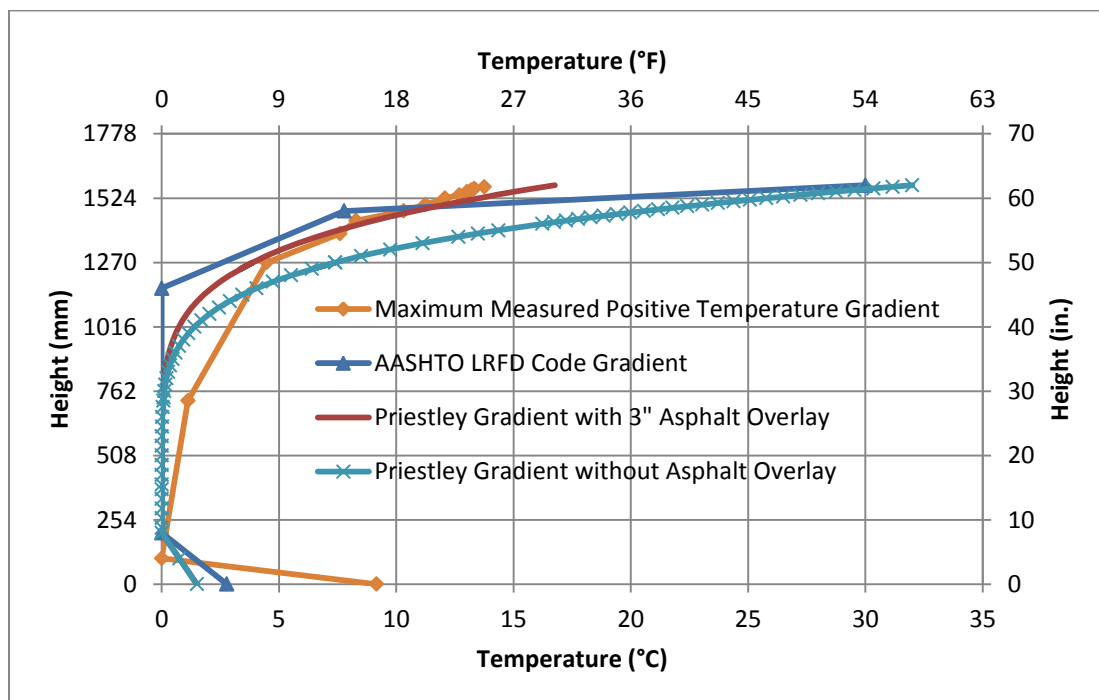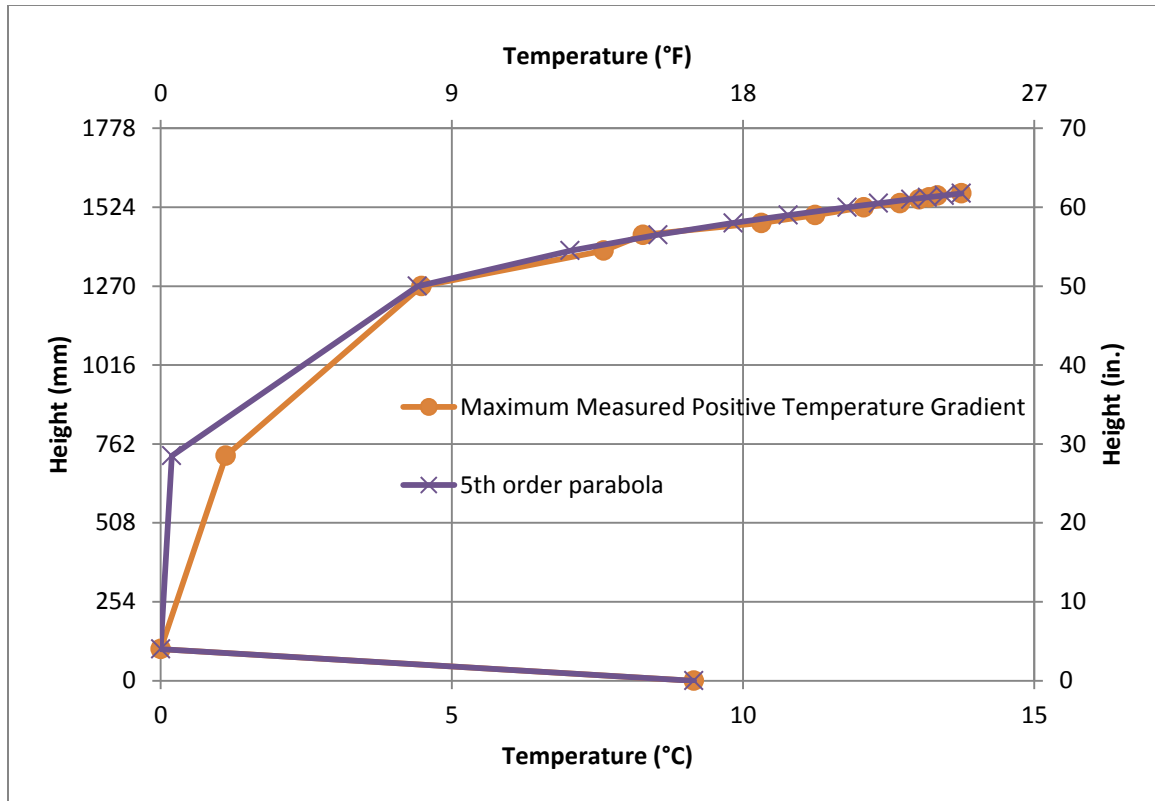
Figure 50. Maximum positive measured gradient in June 2012 in comparison to a 5th order curve.

The maximum negative temperature gradient for the Utah Bridge was recorded in September 2011. The temperature at the top of the cross-section was -6.10 °C (-10.99 °F) and -6.79 °C (-12.22 °F) at the bottom. The temperature gradient was zero at 305 mm (12 in.) from the top of the cross-section, which is similar to the 406.4 mm (16 in.) established in the AASHTO LRFD Specifications (2010) and very different to the 610 mm (24.02 in.) measured by Roberts-Wollman et al. (2002). Priestley (1978) did not define a negative temperature gradient.
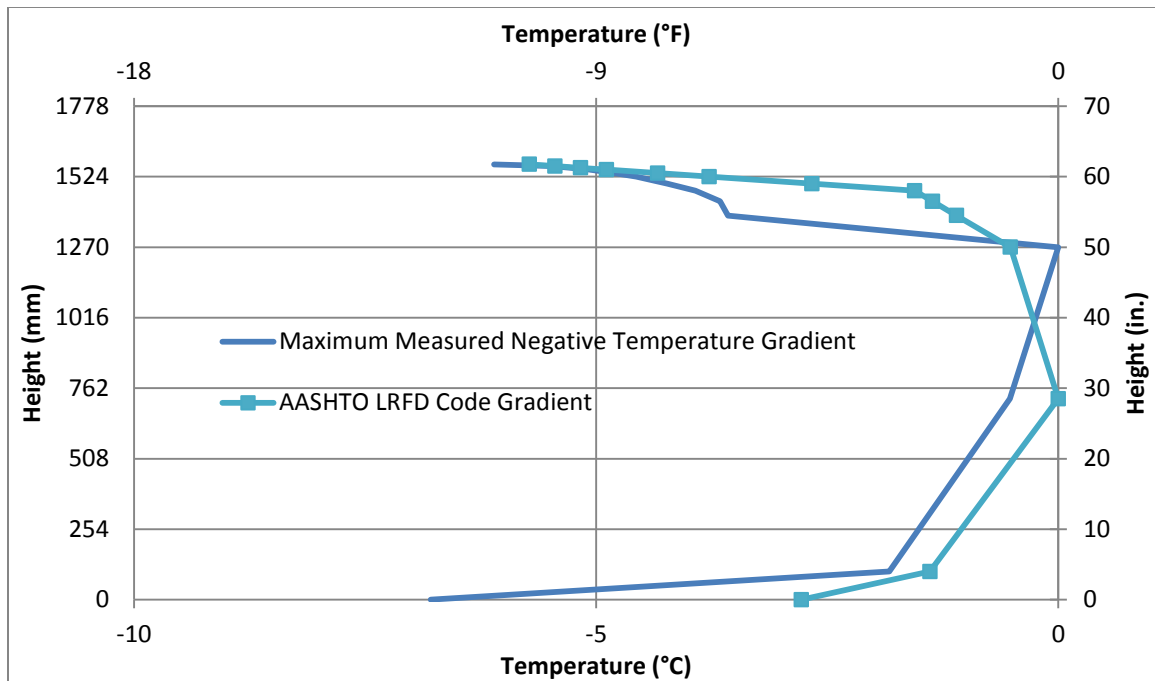
Figure 51. Maximum negative temperature gradient in September 2011 measured in the Utah bridge compared to the AASHTO Specifications (2010).

Figure 51 shows the maximum negative temperature gradient in comparison to the gradient defined in the AASHTO LRFD Specifications (2010). The temperature at the top of the deck, -6.10 °C (-10.99 °F), was a slightly above the -6.00 °C (-10.8 °F) established in the AASHTO LRFD Specifications (2010). The bottom girder value, -6.79 °C (-12.22 °F), was well above the -2.78 °C (-5.00 °F) defined in the AASHTO LRFD Specifications (2010).

Comparing the shape of the maximum measured negative temperature gradient with the AASHTO LRFD Specifications (2010) yielded a R^2 of 0.63 and a MSE of 8.64. Neither a 5th nor a 7th order curve, were a good fit to describe the shape of maximum measured negative temperature gradient. The 5th order curve had a R^2

of 0.53 and a MSE of 12.17, and the 7th order curve yielded a R² of 0.51 and a MSE of 15.19.

Figure 52. Maximum Negative Measured Gradient in September 2011 in comparison to a 5th and 7th order curve.

In general a 5th order curve proved to be the best way to describe the shape of the temperature gradient.

<u>Stresses Due to Temperature Gradients</u>

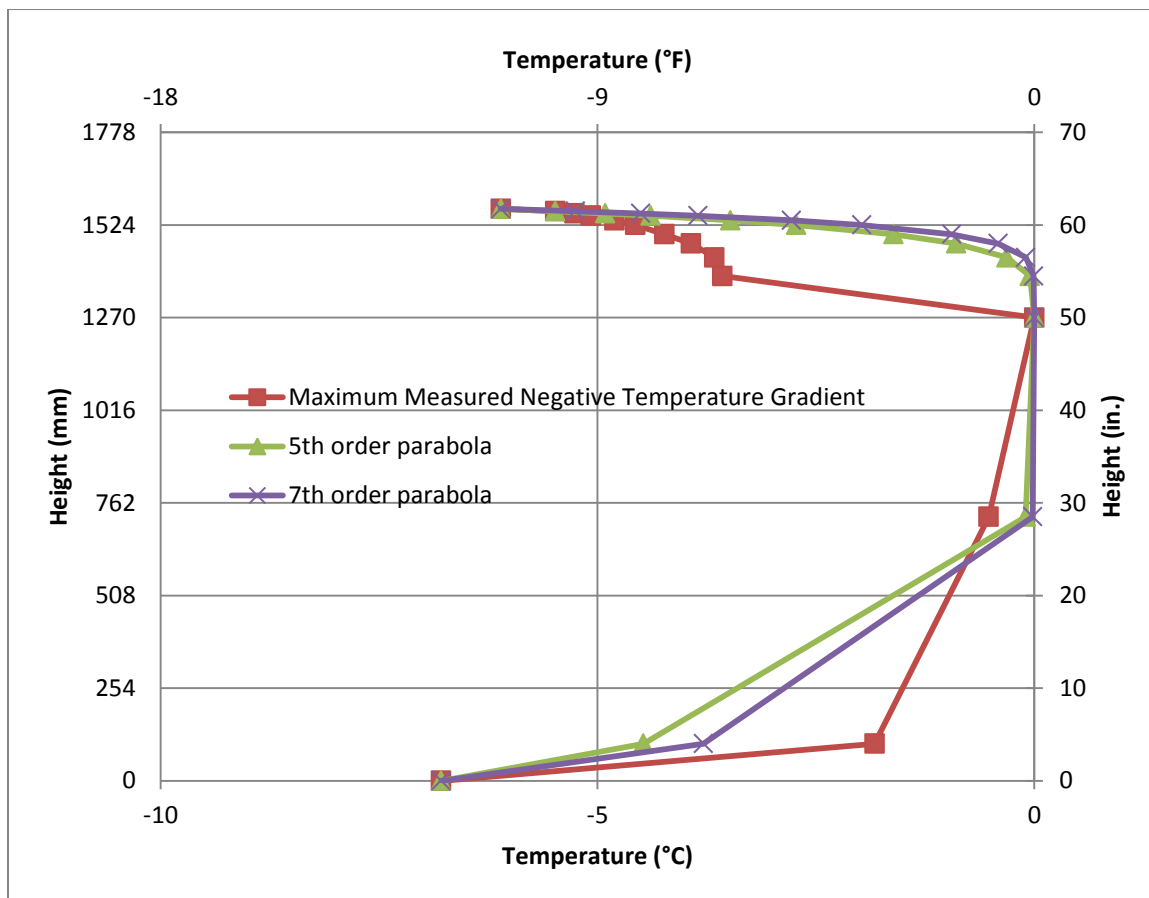The most important effect of a nonlinear temperature gradient is the development of stresses in the cross section of the bridge. In general, the stresses can be divided into two categories. Self-equilibrating stresses are produced on an unrestrained bridge girder due to the nonlinearity of the temperature gradient. Continuity stresses develop due to the restriction of movement of the supports on indeterminate structures.

To calculate the stresses due to a temperature gradient on a bridge, first the bridge is considered simply supported and self-equilibrating stresses are calculated. Subsequently, the stresses caused by any internal moments produced by the restrictions of rotation and movement of middle supports and fixed supports at the ends, are added to the self-equilibrating stresses. These last stresses are the continuity stresses.

<u>Self-equilibrating Stresses</u>

If the cross-section of a bridge is divided into layers and a different temperature is applied to each one; each layer would try to deform proportionally to the temperature applied developing a free strain (ε_{fn}) as defined in Equation 28.

$$\varepsilon_{fn} = T_n \alpha_n \qquad \text{Equation 28}$$

where T_n is the temperature and α_n is the coefficient of thermal expansion of a particular nth layer. In the California and Utah bridges the entire super structure is

made of concrete, therefore a constant coefficient of thermal expansion of 10.1×10^{-6} /°C (5.6×10^{-6} /°F) was used.

If the temperature varies linearly along the depth of a statically determinate, simply-supported bridge the different layers would deform freely proportionally to their temperature and no stresses would develop. However, when the shape of the temperature gradient is nonlinear the deformation of one layer is restrained by the adjacent layers producing self-equilibrating stresses. Another way of looking at this phenomenon is that a nonlinear temperature gradient would produce a nonlinear free strain distribution on the cross-section and, since plane sections must remain plane the self-equilibrating stresses produce a stain distribution that makes the real strain on the statically determinate simply supported bridge linear. This is illustrated in Figure 53.
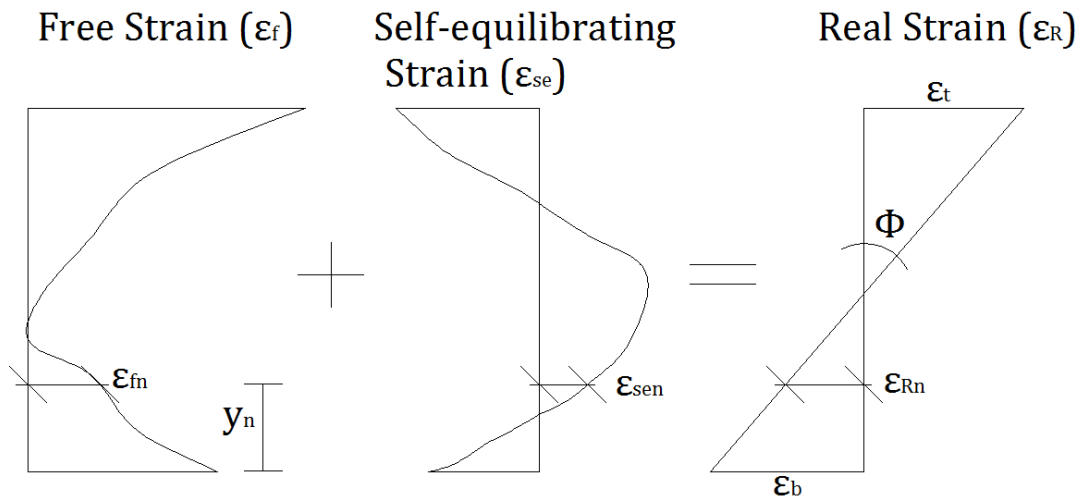

Figure 53. Strain on a statically determinate bridge subjected to nonlinear temperature distribution.

The procedure used to calculate the self-equilibrating stresses is as follows:

$$\begin{Bmatrix} \varepsilon_b \\ \varepsilon_t \end{Bmatrix} = \begin{bmatrix} \sum_{n=1}^{n}\left[\left(1-\frac{y_n}{h}\right)A_n\right] & \sum_{n=1}^{n}\left[\frac{y_n}{h}A_n\right] \\ \sum_{n=1}^{n}\left[\left(1-\frac{y_n}{h}\right)A_n y_n\right] & \sum_{n=1}^{n}\left[\frac{y_n}{h}A_n y_n\right] \end{bmatrix}^{-1} \begin{Bmatrix} \sum_{n=1}^{n}A_n\varepsilon_{fn} \\ \sum_{n=1}^{n}A_n y_n\varepsilon_{fn} \end{Bmatrix} \qquad \text{Equation 29}$$

$$\varepsilon_{Rn} = \left(1-\frac{y_n}{h}\right)\varepsilon_b + \frac{y_n}{h}\varepsilon_t \qquad\qquad \text{Equation 30}$$

$$\varepsilon_{sen} = \varepsilon_{Rn} - \varepsilon_{fn} \qquad\qquad \text{Equation 31}$$

$$\sigma_{sen} = \varepsilon_{sen}E \qquad\qquad \text{Equation 32}$$

where

ε_b = Real strain at the bottom of the cross-section.

ε_t = Real strain at the top of the cross-section.

y_n = Distance from the bottom to the centroid of the nth layer.

A_n = Area of the nth layer.

h = Height of the cross-section.

ε_{fn} = Free strain at an nth layer.

ε_{Rn} = Real strain at an nth layer.

ε_{sen} = Strain due to self-equilibrating stresses at an nth layer.

σ_{sen} = Self-equilibrating stress at an nth layer.

The deflection at the midspan of the simply supported bridge can be determined using the following equations.

$$\Phi = \frac{\varepsilon_t - \varepsilon_b}{h} \qquad\qquad \text{Equation 33}$$

$$\Delta = \frac{\Phi L^2}{8} \qquad\qquad \text{Equation 34}$$

where

Φ = Rotation.

Δ = Deflection at midspan of simply supported bridge.

L = Length of the bridge.

Continuity Stresses

To obtain the total stresses that act on the cross section of a continuous bridge, the self-equilibrating stresses, which affect every cross section, need to be added to the continuity stresses that vary along the length of the bridge and are developed due to redundant supports.

To start the analysis of the continuity stresses, the flexural deformation that the self-equilibrating stresses would produce if the bridge was simply supported should be calculated.
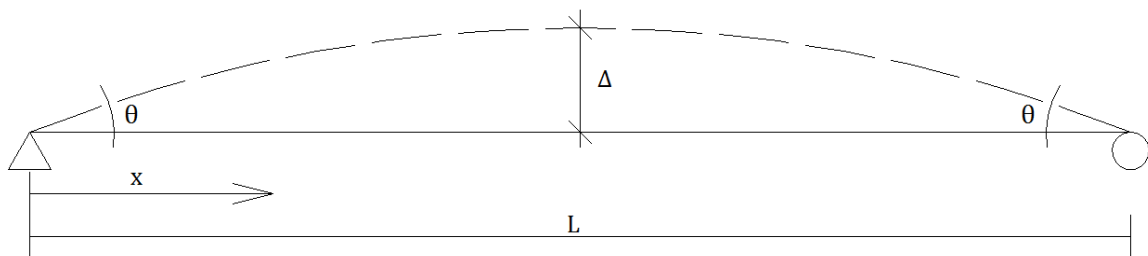

Figure 54. Deformed shape of a simply supported bridge subjected to a nonlinear temperature gradient.

Figure 54 shows the deformed shape that a bridge would adopt if it was simply supported. The deflection at midspan is defined using Equation 34. After

applying a nonlinear temperature gradient to a simply-supported bridge the deflection is zero at the supports and has a known value Δ at midspan. The deflection at any point along the length of the bridge can be defined using the equation of a circle.

$$\Delta_{(x)} = \sqrt{r^2 - (x - a)^2} + b$$

where

$$a = \frac{L}{2}$$

$$r = \frac{L^2}{8\Delta} + \frac{\Delta}{2}$$

$$b = \frac{\Delta}{2} - \frac{L^2}{8\Delta}$$

L = Length of the bridge.

x = Distances from left support.

Δ = Deflection at midspan caused by self-equilibrating stresses.

The slope at every point can be obtained by differentiating Δ with respect to x. The slope at the supports is calculated by evaluating θ(x) at x=0.

$$\theta_{(x)} = \frac{d\Delta_{(x)}}{dx} = -(x - a)(r^2 - (x - a)^2)^{-1/2} \qquad \text{Equation 35}$$

$$\theta = \frac{d\Delta_{(0)}}{dx} = \frac{a}{\sqrt{r^2 - a^2}} \qquad \text{Equation 36}$$

After this point, since the continuity stresses depend on the support condition of each bridge, an individual analysis is required for every case.

California Bridge

The California bridge is a two span structure with fixed support conditions due to the integral abutments as shown in Figure 55.
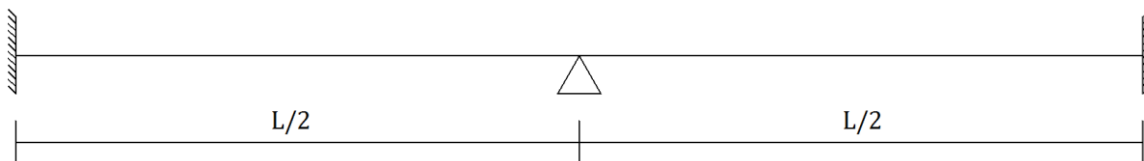
Figure 55. Support conditions of the California bridge.

To go from the simply supported structure shown in Figure 54 to the two spans fixed-fixed conditions on the California bridge, a load at midspan and moments at the ends have to be applied such that the deflection at midspan and the rotation at the supports are zero. This is illustrated in Figure 56 and Equations 37 and 38.

Figure 56. External forces required to meet the support conditions of the California bridge.

$$\theta = 0 = \frac{ML}{2EI} + \frac{PL^2}{16EI} \qquad \text{Equation 37}$$

$$\Delta = 0 = \frac{ML^2}{16EI} + \frac{PL^3}{48EI} \qquad \text{Equation 38}$$

Once the external forces are obtained, the internal moments were calculated at midspan and the supports. The continuity stresses at both locations were calculated using Equation 39 and then added to the self-equilibrating stresses to obtain the total stresses at both locations according to Equation 40.
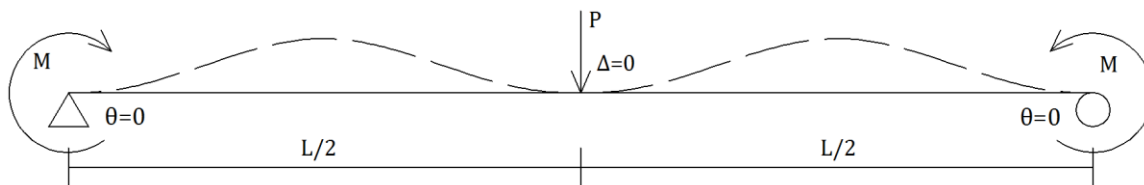
$$\sigma_{cn} = \frac{M(y_c - y_n)}{I} \qquad \text{Equation 39}$$

$$\sigma_{Tn} = \sigma_{sen} + \sigma_{cn} \qquad \text{Equation 40}$$

M = Internal moment at examined cross section.

σ_{cn} = Continuity stress at the nth layer of the examined cross section.

y_c = Distance from the bottom to the centroid of the cross section.

I = Moment of inertia of the cross section.

y_n = Distance from the bottom to the centroid of the nth layer.

σ_{Tn} = Total stress at the nth layer of the examined cross section.

Utah Bridge

The structural model of the Utah Bridge, both supports with integral abutments, consists of a fixed-fixed single span as shown in Figure 57.
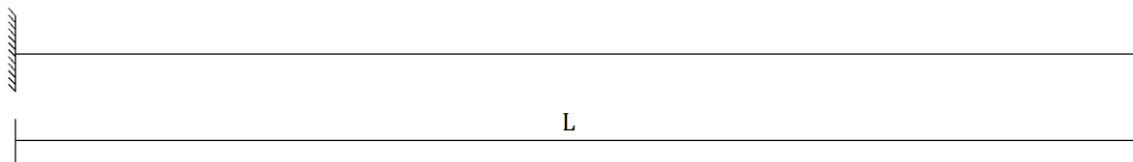

Figure 57. Support conditions of the Utah bridge.

Moments at the supports have to be applied to simply supported bridge of Figure 54 such that the slope at the ends is zero. This is illustrated in Figure 58 and Equation 41.
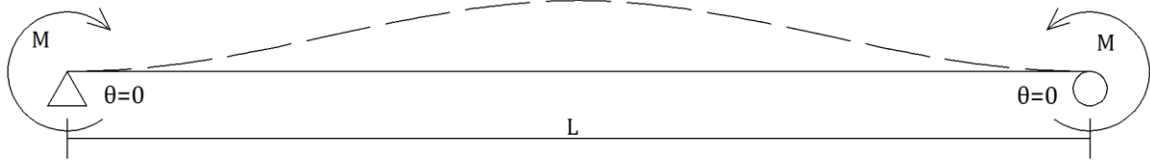
Figure 58. External forces required to meet the support conditions of the Utah Bridge.

$$\theta = 0 = \frac{ML}{2EI} \qquad \text{Equation 41}$$

For the Utah Bridge the external moment produces a constant internal moment along the length of the bridge, therefore the continuity and total stresses are equal on every cross section. Equations 39 and 40 are used to determine the continuity and total stresses, respectively.

<u>Stresses due to Measured Temperature Gradient</u>

Applying the general procedure described in the previous section for a temperature gradient measured in a bridge is possible to determine the magnitude of the flexural stresses causes by temperature. Using the measured maximum positive and negative temperature gradients for the California and the Utah Bridge the stresses were calculated.

The tensional resistance of concrete is defined in accordance to the AASHTO LRFD Specifications (2010) as $0.8f_r$. The formula for f_r is defined in Equation 42,

where f'$_c$ is in ksi. The concrete compressive strength, f'$_c$, for the California bridge was 24.13 MPa (3.5 ksi) and 27.58 MPa (4 ksi) for the Utah bridge.

$$f_r = 0.24\sqrt{f'_c} \qquad\qquad \text{Equation 42}$$

Substituting the f$_r$ formula into the 0.8f$_r$ results in $0.192\sqrt{f'_c}$, which is the tension limit established in the AASHTO LFRD Bridge Design Specifications (2010) for components with bonded prestressing at the service limit state after applying the loads and the prestressing forces. The effects of temperature gradient for the service load case are reduced by a factor γ_{TG}, that is defined as 0.50 when live load is considered. Although positive and negative design gradients are define in the AASHTO LFRD Bridge Design Specifications (2010), it is common practice to neglect the effects of temperature in the design. The limit, $0.192\sqrt{f'_c}$, for the California Bridge was 2.48 MPa (0.36 ksi) and 2.65 MPa (0.384 ksi) for the Utah Bridge.

<u>The California Bridge</u>

The self-equilibrating stresses are constant for any longitudinal location, and the continuity stresses are higher at the midspan and the supports. Therefore, the stresses on the California Bridge were calculated at midspan and the supports for both the maximum positive and maximum negative temperature gradients. The barriers were neglected to calculate the moment of inertia, which was 1.35 m^4 (156 ft^4).

Figure 59 shows the calculated self-equilibrating stresses for the maximum positive measured temperature gradient. The maximum stresses for this case were

1.93 MPa (0.28 ksi) in tension at 1143 mm (45 in.) from the bottom, and 3.10 MPa

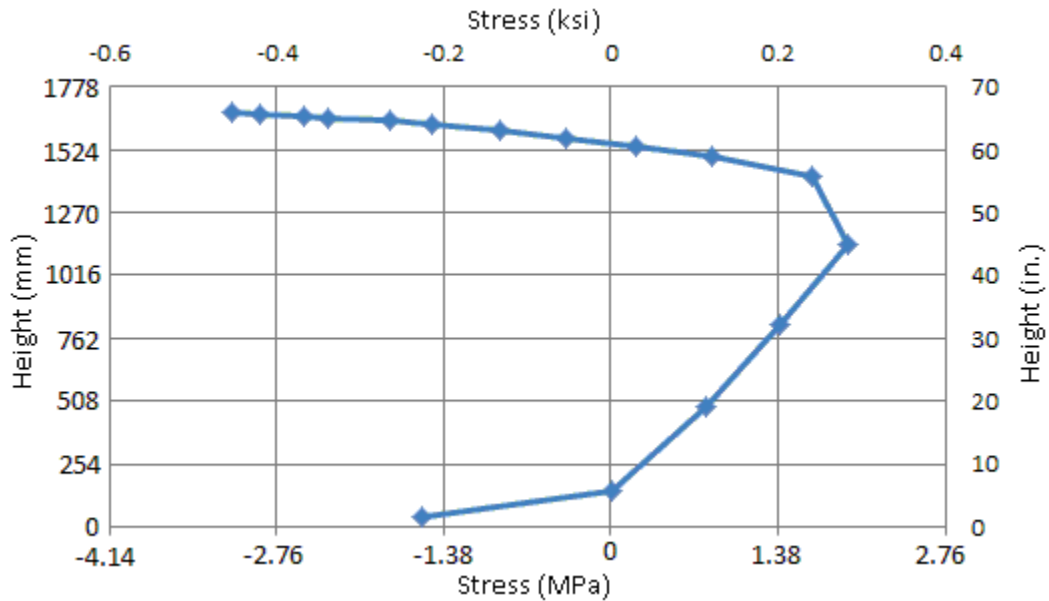(0.45 ksi) in compression at the top of the cross section.

Figure 59. Self-equilibrating stresses for the maximum positive temperature gradient on the California bridge.
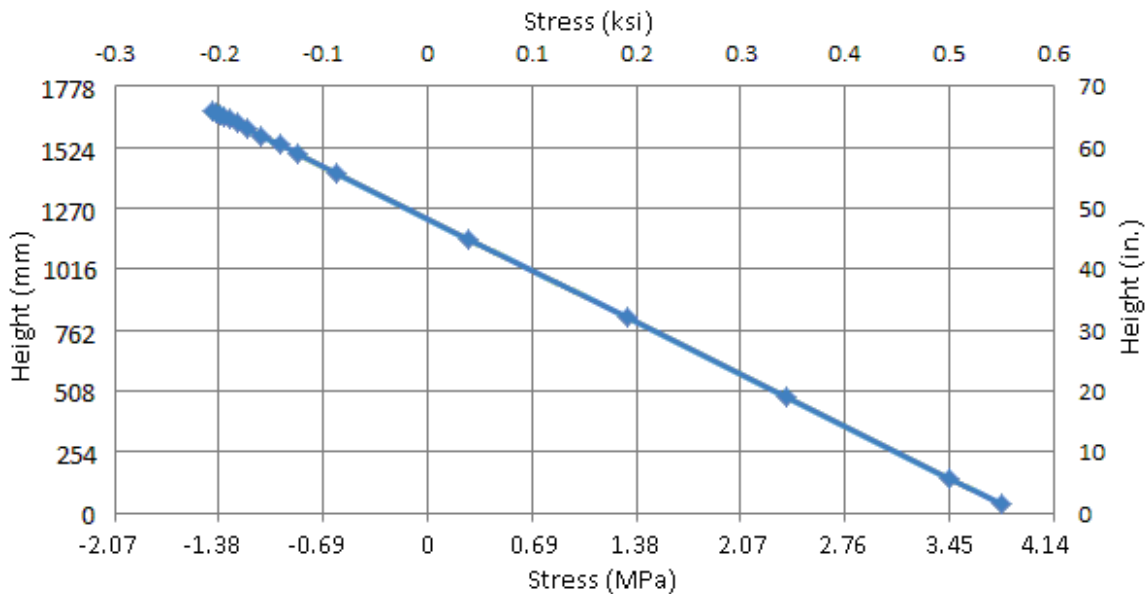

Figure 60. Continuity stresses at midspan for the maximum positive temperature gradient on the California bridge.

The continuity stresses at midspan for the maximum positive temperature gradient, caused by the fixed ends and the support in the middle of the bridge, are shown in Figure 60. Theses stresses varied linearly from 1.45 MPa (0.21 ksi) in compression at the top to 3.80 MPa (0.55 ksi) in tension at the bottom.

Figure 61. Total stresses at midspan for the maximum positive temperature gradient on the California bridge.

Combining the self-equilibrating stresses with the continuity stresses at midspan yielded the total stresses at midspan caused by the maximum positive measured temperature gradient, shown in Figure 61. The maximum values were 4.55 MPa (0.66 ksi) in compression at the top and 3.45 MPa (0.50 ksi) in tension at 146 mm (5.75 in.) from the bottom. The maximum tension stress was 0.97 MPa (0.14 ksi) or 39% greater than the 2.48 MPa (0.36 ksi) limit established by the AASHTO LRFD Specifications (2010).

Figure 62 shows the continuity stresses at the end supports for the maximum positive measured temperature gradient. The maximum compressive stress at the

top of the deck was 0.34 MPa (0.05 ksi) and the maximum tension at the bottom was 0.97 MPa (0.14 ksi).

Figure 62. Continuity stresses at supports for the maximum positive temperature gradient on the California bridge.

The total stresses at the end supports for the maximum positive temperature gradient are shown in Figure 63. The maximum compressive stress was 3.52 MPa (0.51 ksi) at the top of the cross section and the maximum tensile stress was 2 MPa (0.29 ksi) at 1143 mm (45 in.) from the bottom.
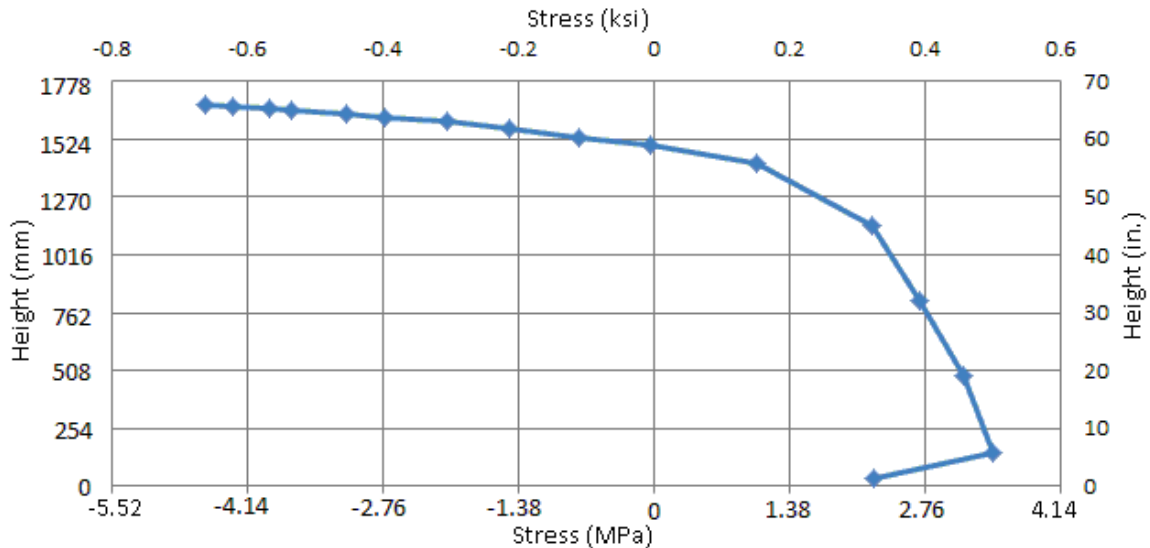

Figure 63. Total stresses at supports for the maximum positive temperature gradient on the California bridge.

Figure 64. Self-equilibrating stresses for the maximum negative temperature gradient on the California bridge.

Figure 64 shows the self-equilibrating stresses for the maximum negative temperature gradient on the California bridge. The tensile stresses at the top and bottom of the cross-section were almost the same, 1.52 MPa (0.22 ksi) at the top and 1.45 MPa (0.21 ksi) at the bottom. The maximum compressive stress was 0.97 MPa (0.14 ksi), which occurred at 1143 mm (45 in.) from the bottom.

Due to the depth of the superstructure, the high moment of inertia of the cross-section, and the low magnitude of the moments develop by the interaction of the temperature gradient with the support conditions; the continuity stresses tend to be small. The maximum continuity stresses at midspan for the maximum negative temperature gradient on the California bridge were 0.028 MPa (0.004 ksi) in compression at the top and 0.076 MPa (0.011 ksi) in tension at the bottom. Figure 65 shows the linear variation of these continuity stresses.
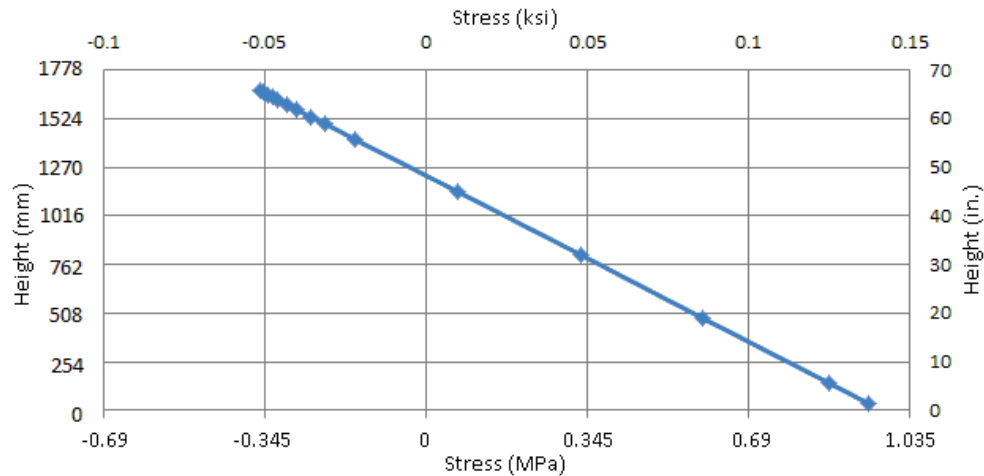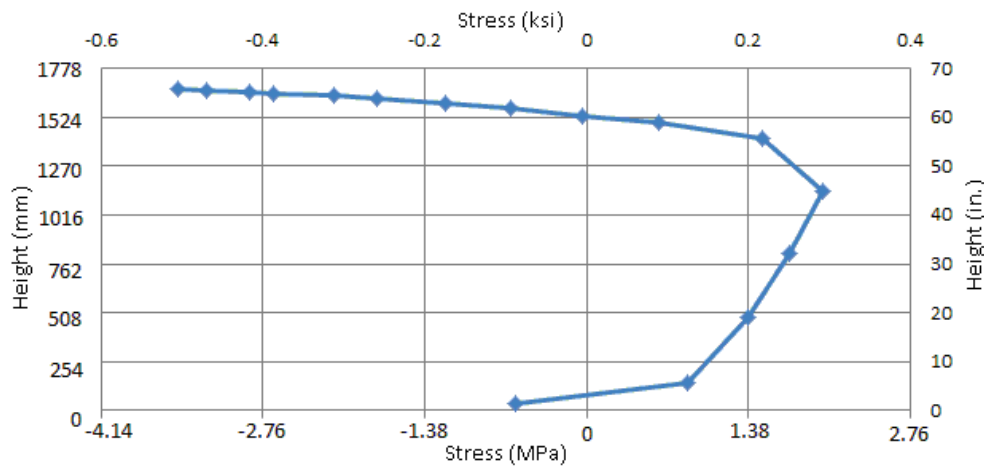
Figure 65. Continuity stresses at midspan for the maximum negative temperature gradient on the California bridge.

The total stresses at midspan due to the maximum negative temperature gradient on the California bridge are presented in Figure 66. Tensile stresses were developed at the top and bottom of 1.45 MPa (0.21 ksi) and 1.52 MPa (0.22 ksi), respectively. The maximum compressive stress was 0.97 MPa (0.14 ksi) at 1143 mm (45 in.) from the bottom.

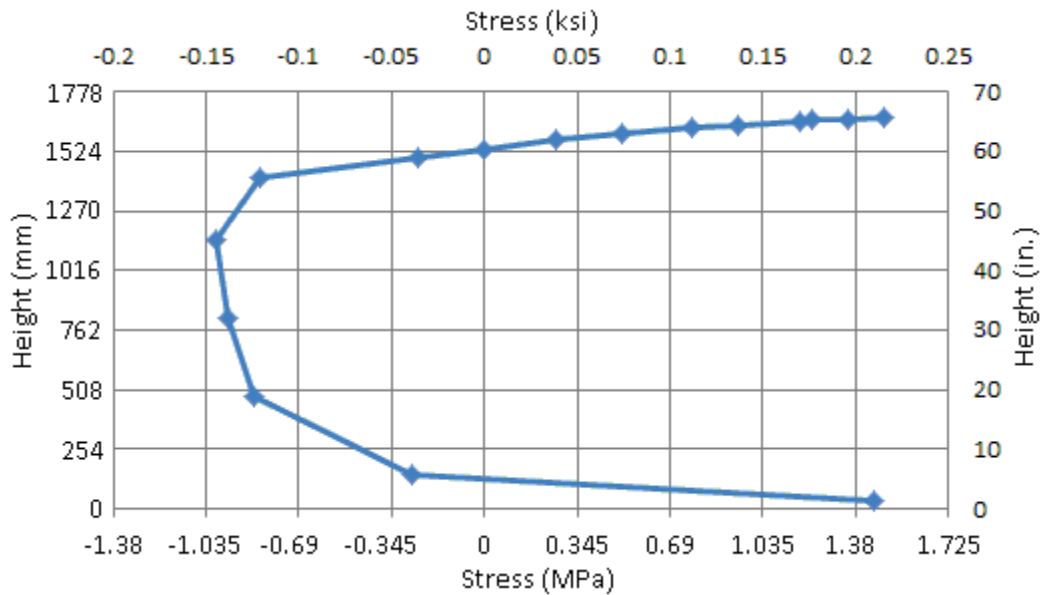Figure 66. Total stresses at midspan for the maximum negative temperature gradient on the California bridge.
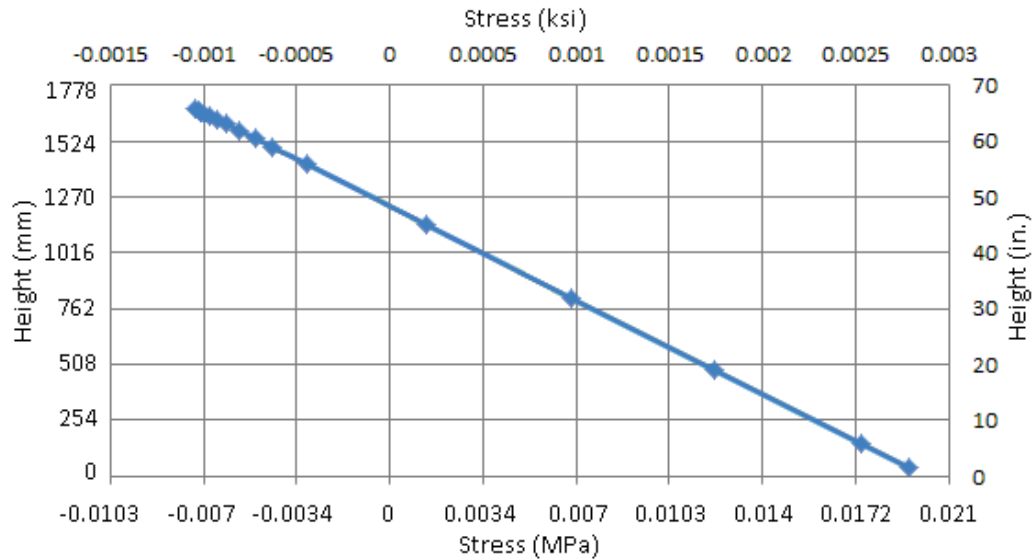
Figure 67. Continuity stresses at supports for the maximum negative temperature gradient on the California bridge.

Figure 67 shows the linearly changing continuity stresses at the supports due to the maximum negative temperature gradient. The top of the cross-section developed a compressive stress of 0.007 MPa (0.001 ksi) and the bottom experienced a tensile stress of 0.019 MPa (0.0028 ksi).
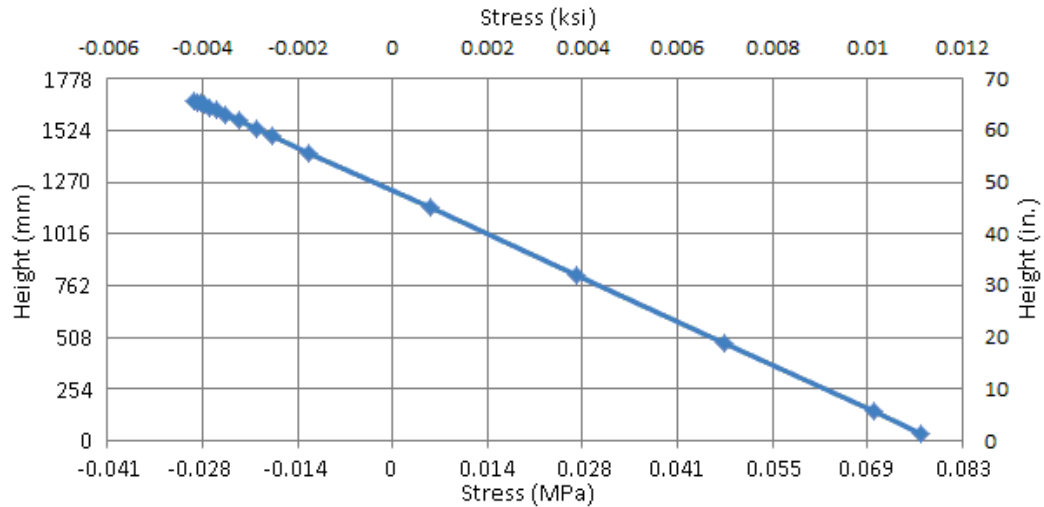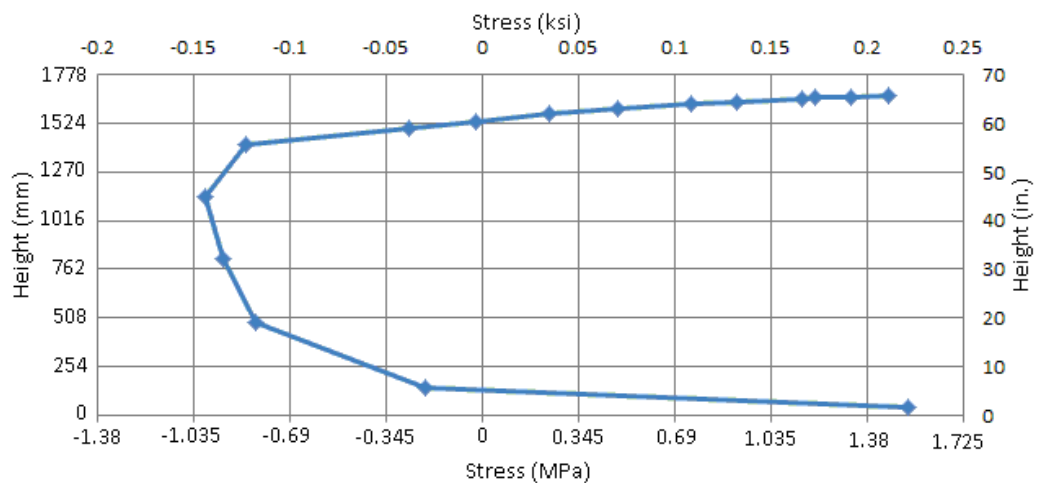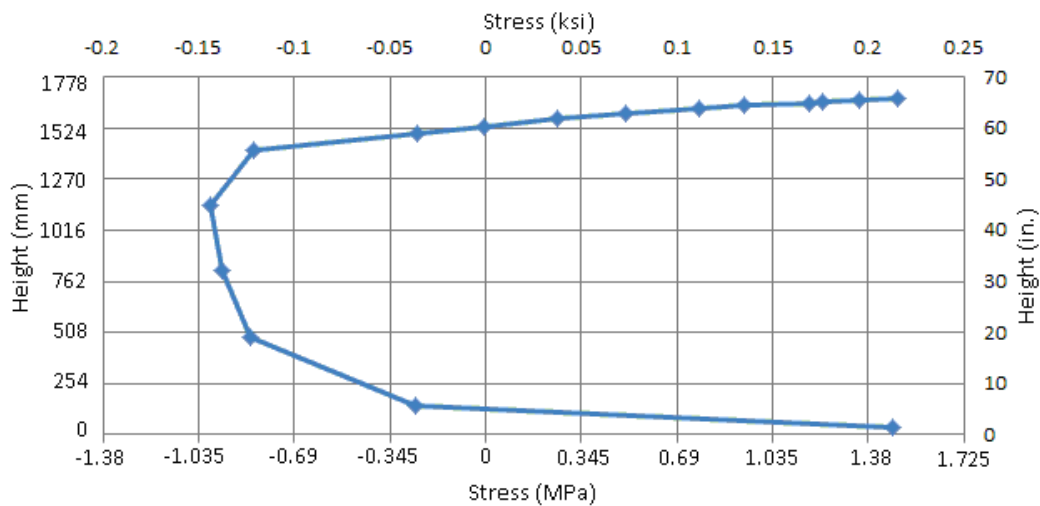

Figure 68. Total stresses at supports for the maximum negative temperature gradient on the California bridge.

The total stresses at the supports, due to the maximum negative temperature gradient, were 1.52 MPa (0.22 ksi) at the top and 1.45 MPa (0.21 ksi) at the bottom in tension. The maximum compressive stress was 0.97 MPa (0.14 ksi) at 1143 mm (45 in.) from the bottom. The distribution of the total stresses along the depth of the cross-section is shown in Figure 68.

The Utah Bridge

For the Utah bridge, stresses were calculated for the maximum positive and maximum negative measured temperature gradients. Since the Utah bridge is a single span structure the continuity stresses are only caused by the restriction of movement due to the integral abutments at the end supports. Therefore, the stresses developed due to a particular temperature gradient are constant along the length of the bridge. However, a factor that may affect the magnitude of the continuity stresses is the increase in moment of inertia and shift of the centroid due to the presence of New Jersey barriers. The moment of inertia of the Utah bridge without the Jersey Barriers was calculated to be 1.56 m^4 (181 ft^4) and 2.03 m^4 (236 ft^4) including the additional stiffness due to the Jersey Barriers, which represents a 30% increase in moment of inertia. Continuity and total stresses were calculated with and without New Jersey barriers for the two maximum measured temperature gradients.

The self-equilibrating stresses for the maximum positive measured temperature gradient are presented in Figure 69. The maximum tensile stress was 0.76 MPa (0.11 ksi) at 1177 mm (46.34 in.) from the bottom of the cross section. The

stress at the top was 0.97 MPa (0.14 ksi) and 2.69 MPa (0.39 ksi) at the bottom, both

in compression.

Figure 69. Self-equilibrating stresses for the maximum positive temperature
gradient on the Utah bridge.

Ignoring the effects of the barriers, the maximum continuity stresses for the

maximum positive temperature gradient were 0.90 MPa (0.13 ksi) in compression

and 2 MPa (0.29 ksi) in tension. Figure 70 shows the linear distribution of the

continuity stresses due to the integral abutment restraint.

Figure 70. Continuity stresses for the maximum positive temperature gradient on the Utah bridge without barriers.

The total stresses for the maximum positive temperature gradient without barriers are presented in Figure 71. The maximum tensile stress was 1.8 MPa (0.26 ksi) at 176.3 mm (6.94 in.) from the bottom. The maximum compression stress occurred at the top with a value of 1.86 MPa (0.27 ksi).

Figure 71. Total stresses for the maximum positive temperature gradient on the Utah bridge without barriers.

Taking into account the barriers, the continuity stress at the top for the maximum positive temperature gradient was 0.76 MPa (0.11 ksi) in compression. At the bottom the tensile stress was 2.21 MPa (0.32 ksi). Figure 72 shows the distribution of these stresses.

Figure 72. Continuity stresses for the maximum positive temperature gradient on the Utah bridge with barriers.

Figure 73. Total stresses for the maximum positive temperature gradient on the Utah bridge with barriers.

Figure 73 shows the total stresses for the maximum positive temperature gradient on the Utah bridge, taking into account the effects of the barriers. The maximum tensile stress occurred at 176.3 mm (6.94 in.) from the bottom with a value of 1.93 MPa (0.28 ksi). The maximum compressive stress was 1.72 MPa (0.25 ksi) at the top of the cross-section. The effect of the New Jersey barriers made the stress profile 8% more tensile.

The self-equilibrating stresses for the maximum negative temperature gradient are presented in Figure 74. The stress at the top was 1.72 MPa (0.10 ksi) and 1.45 MPa (0.21 ksi) at the bottom of the cross section, both in tension. The maximum compressive stress was 0.76 MPa (0.11 ksi) at 1177 mm (46.34 in.) from the bottom of the cross section.
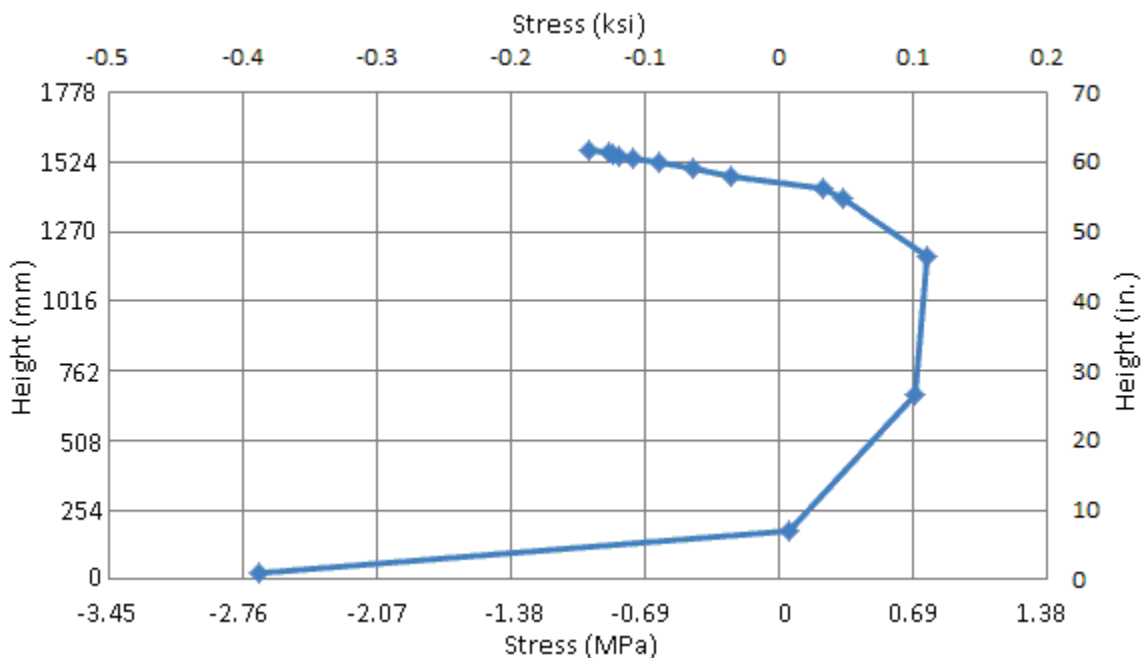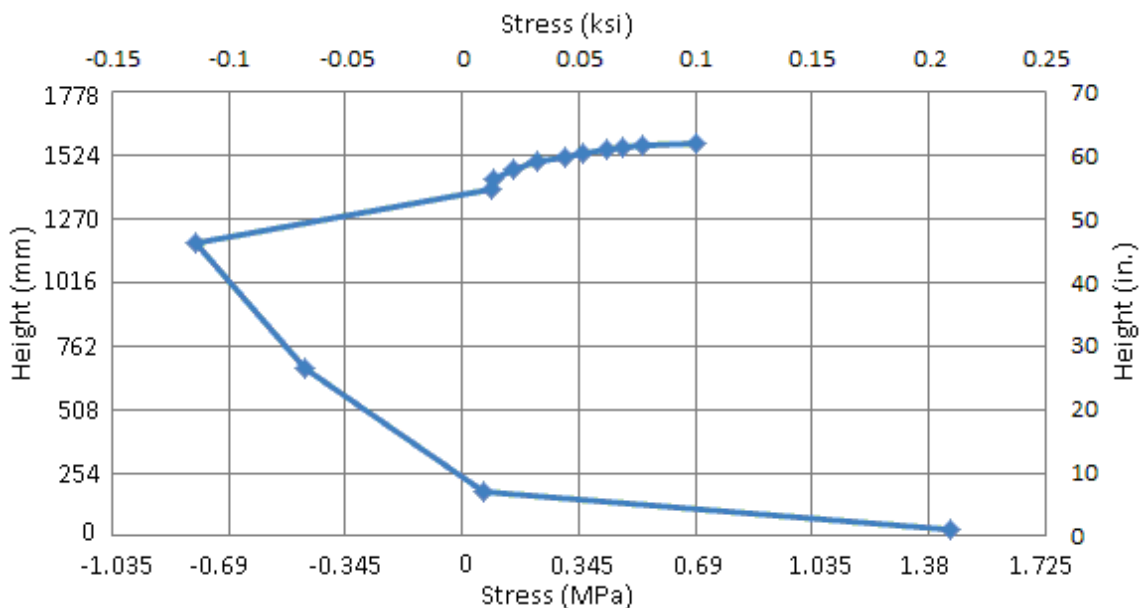

Figure 74. Self-equilibrating stresses for the maximum negative temperature gradient on the Utah bridge.

Ignoring the effects of the barriers, the maximum continuity stresses for the maximum measured negative temperature gradient were 0.21 MPa (0.03 ksi) in tension and 0.41 MPa (0.06 ksi) in compression. Figure 75 shows the linear distribution on the continuity stresses.
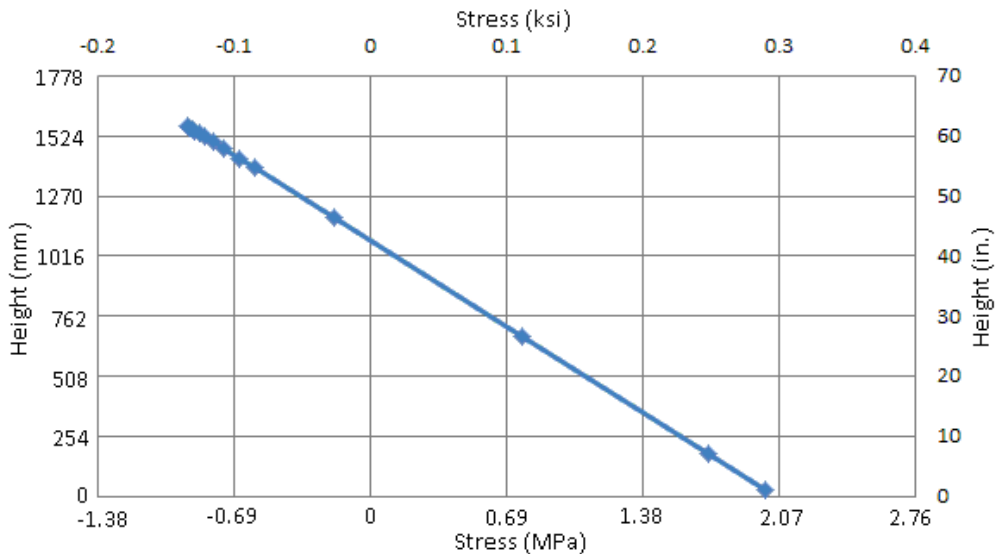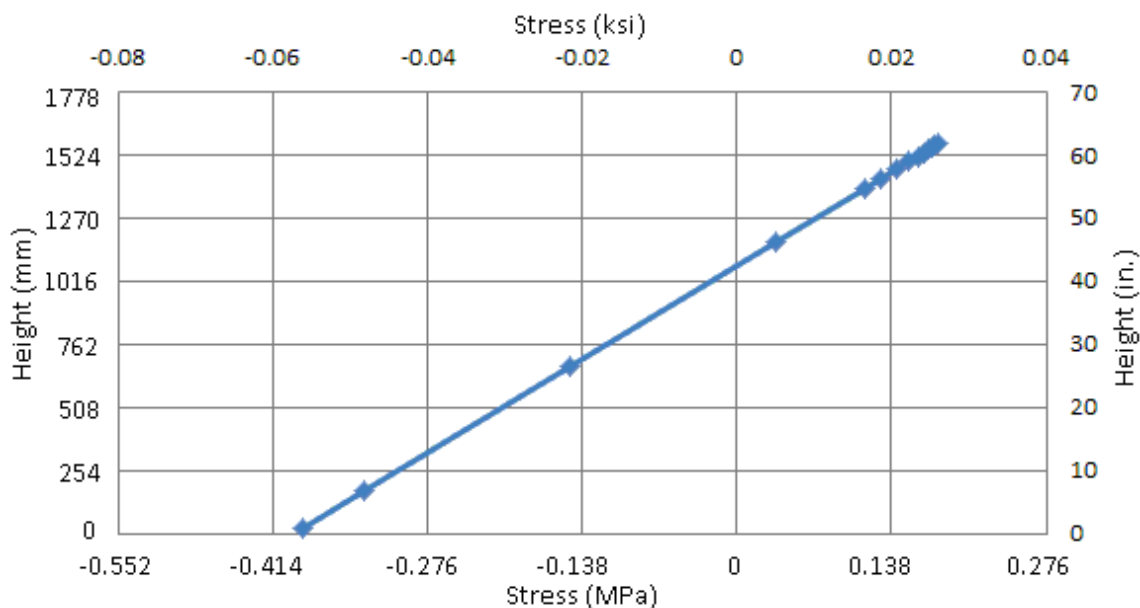

Figure 75. Continuity stresses for the maximum negative temperature gradient on the Utah bridge without barriers.

The total stresses for the maximum measured negative temperature gradient without barriers are presented in Figure 76. The maximum tensile occurred at the bottom of the cross-section with a value of 1.03 MPa (0.15 ksi). The maximum compressive stress was 0.76 MPa (0.11 ksi) at 1177 mm (46.34 in.) from the bottom.
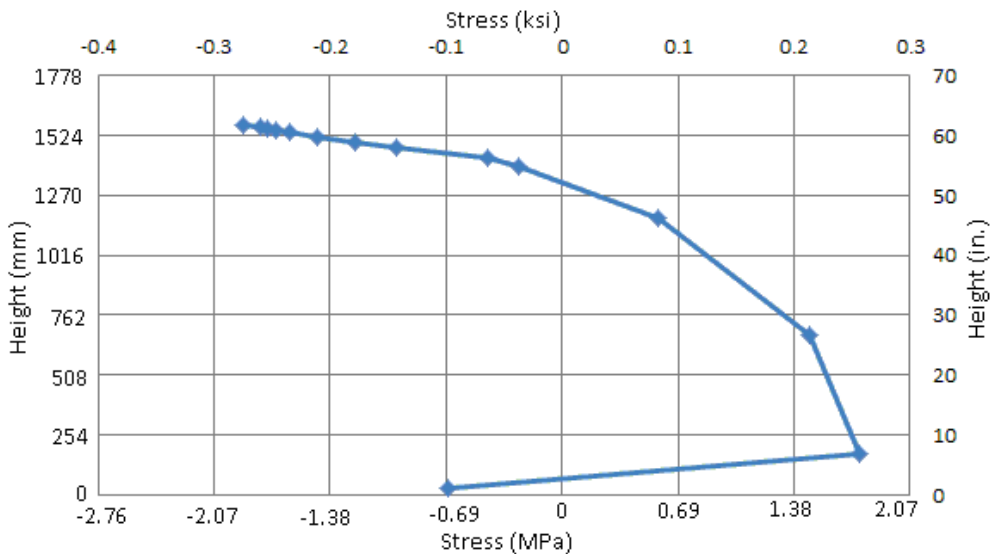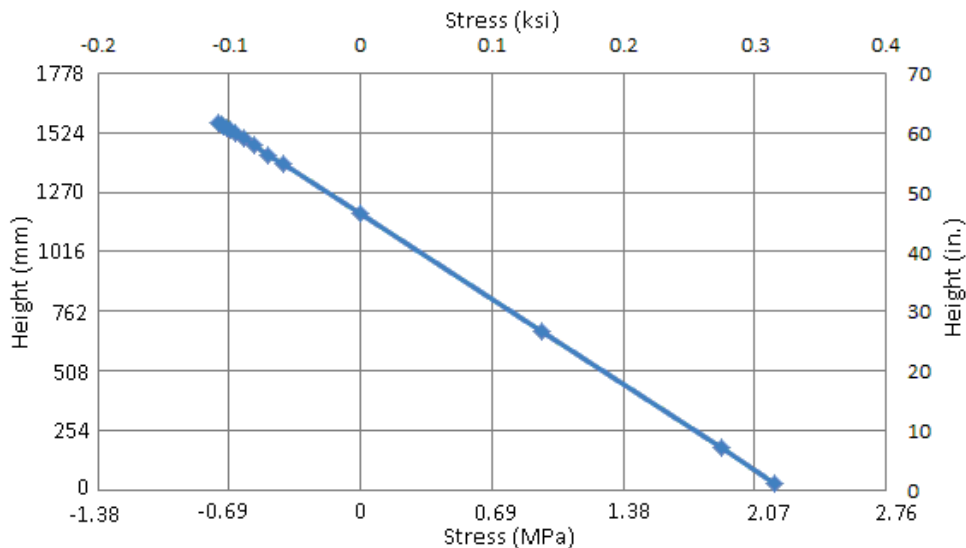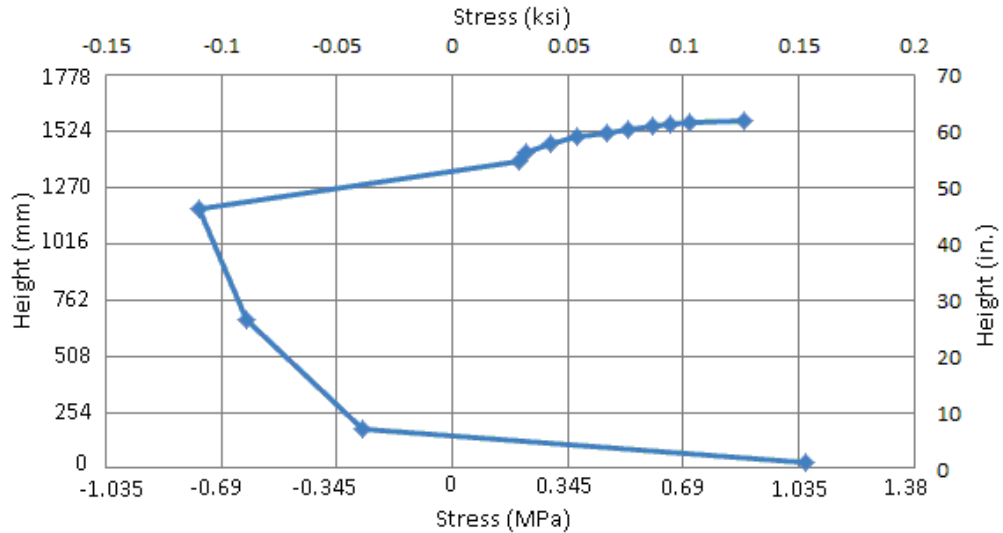
Figure 76. Total stresses for the maximum negative temperature gradient on the Utah bridge without barriers.

Taking into account the barriers, the continuity stress at the top for the maximum negative temperature gradient was 0.14 MPa (0.02 ksi) in tension. At the bottom, the compressive stress was 0.41 MPa (0.06 ksi). Figure 77 shows the distribution of these stresses.
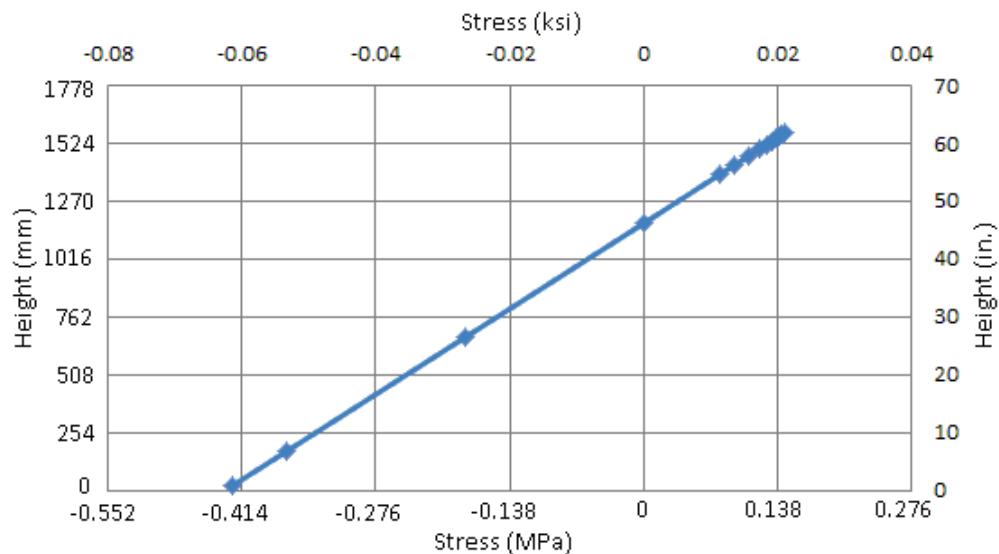
Figure 77. Continuity stresses for the maximum negative temperature gradient on the Utah bridge with barriers.
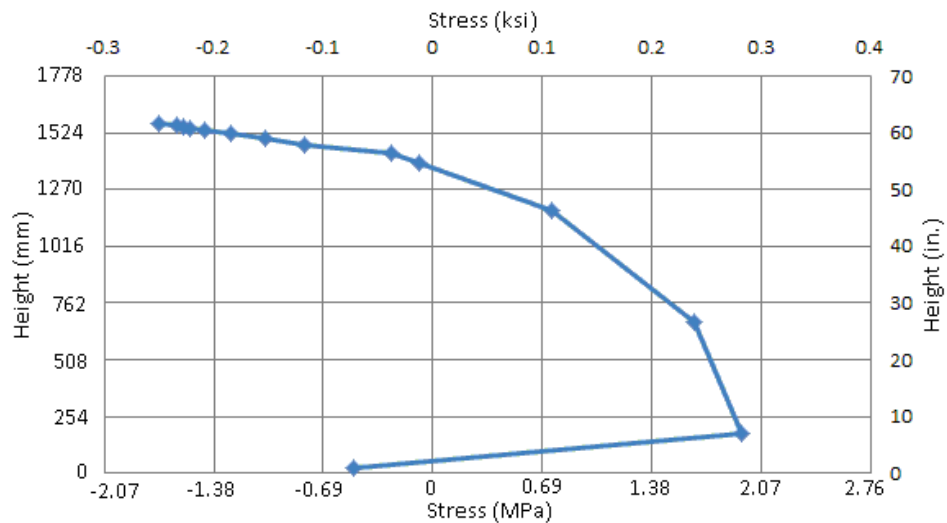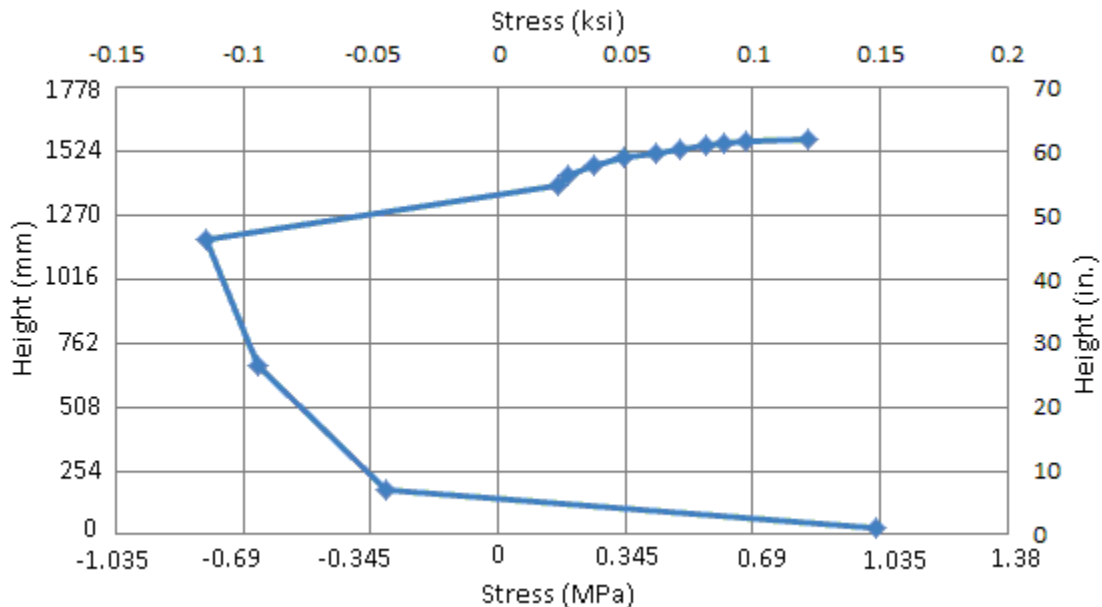
Figure 78. Total stresses for the maximum negative temperature gradient on the Utah bridge with barriers.

Figure 78 shows the total stresses for the maximum negative temperature gradient on the Utah bridge, taking into account the effects of the barriers. The maximum compressive stress occurred at 1177 mm (46.34 in.) from the bottom with a value of 0.76 MPa (0.11 ksi). The maximum tensile stress was 1.03 MPa (0.15 ksi) at the bottom of the cross-section. The presence of the New Jersey barriers didn't make a difference in the maximum stresses due to the maximum negative measured temperature gradient.

The maximum tensile stress 1.93 MPa (0.28 ksi) occurred with the maximum positive measured temperature gradient and taking into account the effects of the New Jersey barriers. The stress was 73% of the limit established in the AASHTO LFRD Bridge Design Specifications (2010), that for the Utah Bridge was 2.65 MPa (0.384 ksi). Although the limit was not exceeded the temperature induced stresses

were close by themselves and only a limited amount of data was available. The presence of other loads in combination with a more extreme temperature gradient could easily exceed the limit established in the AASHTO LFRD Bridge Design Specifications (2010).

The higher moment of inertia due to the Jersey Barriers increases the moment in Equation 41. However, the moment of inertia is dividing the moment in Equation 39 which cancels the increased moment from Equation 41. The presence of the Jersey Barriers shifts up the location of the centroid, making the continuity stresses, and consequently the total stresses, more tensile according to Equation 39. The centroid is located at 1081 mm (42.55 in.) from the bottom when the Jersey Barriers are not considered, and 1175 mm (46.28 in.) when they are. This makes the continuity stresses, and consequently the total stresses, 8% more tensile.

CHAPTER 6

SUMMARY AND CONCLUSIONS

Summary

This research investigated the effects of temperature changes in concrete bridges. Two bridges were monitored one south of Sacramento, California and the other close to Perry, Utah.

Built in 1975, the California bridge consists of two equal length, continuous spans of 39.32 m (129 ft). At midspan the bridge is supported by a reinforced concrete column and at the ends with reinforced concrete, open ended hinged diaphragm abutments. The thickness of the deck is 0.20 m (8 in.). The superstructure consists of post-tensioned, cast-in-place, concrete box-girders with four cells. The overall width of the bridge is 12.80 m (42 ft) with a 0.30 m (1 ft) barrier on each side, making the overall roadway width 12.20 m (40 ft). To monitor the changes in temperature throughout the box-girders, 44 thermocouples were installed throughout the height of the cross-section. Twenty of those thermocouples were used to create two deck temperature gradient measuring arrays that monitored the steep changes in temperature concrete along the depth of the deck.

Built in 1976, the Utah bridge consists of a single bridge 24.90m (81 ft 8 in.) long span. The ends were supported with reinforced concrete integral abutments. The superstructure consists of five, AASHTO type IV, pre-stressed concrete girders. The overall width of the bridge is 13.41 m (44 ft) with 0.53m (1 ft 9 in.) barriers on each side, making the overall roadway width 12.35 m (40.5 ft). The deck is 0.20m (8

in.) thick with the surface covered with a 76 mm (3 in.) asphalt overlay. To monitor the temperature changes on the superstructure, 31 thermocouples were installed. Ten of those thermocouples were used to create a deck temperature gradient measuring array that measured the steep changes in temperature along the depth of the deck.

The uniform bridge temperature was monitored at a 15 minute interval for both bridges and compared to the design uniform temperatures recommended in the AASHTO LRFD Bridge Design Specifications (2010). Rodriguez (2012) monitored the average bridge temperatures of the California bridge from May 2011 to June 2012 and from September 2011 to June 2012 for the Utah bridge. Using the tools and procedures developed by Rodriguez (2012) the average bridge temperature for the California and Utah bridges was monitored continuously until September 2013. Covering a period of two years and five months for the California Bridge and two years and one month for the Utah Bridge.

The measured values for the maximum and minimum average bridge temperature gradient were compared to the predictions obtained using the Kuppa Method (1991) and the Black and Emerson Method (1976). Also, a new method, called ERL, was developed which estimates the average bridge temperature based on the ambient temperature close to the bridge location. Mean square error (MSE) and R^2 were used to statistically compare the predictions of each method with the measured values. Using ambient temperature data from the National Oceanic and Atmospheric Administration (NOAA) and the equations of the Kuppa Method (1991), the Black and Emerson Method (1976), and the ERL Method, the estimated

uniform bridge temperatures were calculated for a period of 56 years and 9 months for the California bridge and 64 years for the Utah bridge. The results were compared to the design uniform temperatures established in the AASHTO LRFD Bridge Design Specifications (2010).

The change in temperature throughout the depth of the cross-section was also monitored using the thermocouples on the bridges. Maximum positive and maximum negative temperature gradients were measured for both bridges and compared to the gradient recommended by the AASHTO LRFD Bridge Design Specifications (2010) and the Priestley (1978). For this study, the positive temperature gradient was defined as the measured sensor temperature at any location minus the minimum measurement. The negative temperature gradient similarly was defined as the measured temperature readings from the sensors minus the maximum measured temperature.

Using the measured maximum positive and maximum negative temperature gradients, self-equilibrating, continuity and total stresses were calculated for the Utah and California bridges. The flexural temperature induced stresses were compared to the tension limit established in the AASHTO LFRD Specifications (2010) for components with bonded pre-stressing for the service limit state.

Conclusions

The thermal behavior of both bridges was monitored and compared to the established code design parameters. Based on the findings, the following conclusions were established.

1. The maximum measured average bridge temperature for the California Bridge occurred during June of 2013 with a magnitude of 112.99°F (45°C) exceeding the AASHTO LRFD Bridge Design Specifications (2010) by 0.49°F (0.28°C). For the Utah bridge, the maximum measured average bridge temperature occurred during July 2013 with a magnitude of 106.5°F (41.39°C) exceeding the AASHTO LRFD Bridge Design Specifications (2010) by 1.5°F (0.83°C).

2. The ERL Method more accurately predicted the maximum and minimum average bridge temperatures for both bridges in comparison to the Kuppa (1991) and the Black and Emerson (1976) Methods. For the California bridge, the ERL Method had a R^2 of 0.9617 and a MSE of 13.946 for the maximum average bridge temperature and a R^2 of 0.9753 and MSE of 3.634 for the minimum average bridge temperature. For the Utah bridge, the ERL Method had a R^2 of 0.9877 and a MSE of 7.02 for the maximum average bridge temperature and a R^2 of 0.9786 and a MSE of 10.31 for the minimum average bridge temperature.

3. The long-term predictions of the ERL Method for the maximum and minimum average bridge temperature on the California bridge were 49 °C (120.26 °F) and -3.42 °C (25.84 °F) respectively, in contrast with the

44.7 °C (112.5 °F) and -1.11 °C (30 °F) established in the AASHTO LRFD Bridge Design Specifications (2010). For the Utah bridge the maximum and minimum average bridge temperatures were 42.15 °C (107.87 °F) and -29.9 °C (-21.75 °F) respectively, while the AASHTO LRFD Bridge Design Specifications (2010) established 40.6 °C (105 °F) and -23.3 °C (-10 °F).

4. The maximum measured negative temperature gradient on both bridges exceeded the values established in the AASHTO LRFD Specifications (2010). For the Utah bridge, the maximum measured positive temperature gradient was best described by the Priestley Method (1978) with the 76.2 mm (3 in.) asphalt overlay, suggesting that the asphalt overlay plays an important part as an insulator on the temperature gradient. In general, the shape of the maximum positive and negative temperature gradients was best described by a 5th order curve.

5. The maximum tension stress produced only by temperature gradient on the California bridge was 3.45 MPa (0.50 ksi) or 39% greater than the 2.48 MPa (0.36 ksi) limit established by the AASHTO LRFD Bridge Design Specifications (2010). The maximum tensile stress on the Utah bridge due to temperature gradient was 1.93 MPa (0.28 ksi). This represents 73% of the 2.65 MPa (0.384 ksi) limit established in the AASHTO LFRD Bridge Design Specifications (2010), for the Utah bridge. Although the limit was not exceeded for the Utah bridge, the temperature induced stresses were close to the cracking stress by themselves, without taking into account

dead, live and other loads. Only a limited amount of data was available, over a longer period of time higher stresses could develop. The presence of other loads in combination with a more extreme temperature gradient could easily exceed the limit established in the AASHTO LFRD Bridge Design Specifications (2010).

It is worth noticing that the California and Utah bridges were built in 1975 and 1976, respectively, and comply with the design specifications of the time.

BIBLIOGRAPHY

American Association of State Highway and Transportation Officials (AASHTO). (1989). *Standard Specifications for Highway Bridges,* 15th Ed., Washington, D.C.: American Association of State Highway and Transportation Officials (AASHTO).

American Association of State Highway and Transportation Officials (AASHTO). (1994). *AASHTO LRFD Bridge Design Specifications.* Washington, D.C.: American Association of State Highway and Transportation Officials (AASHTO).

American Association of State Highway and Transportation Officials (AASHTO). (1998). *Guide Specifications for Design and Construction of Segmental Concrete Bridges, Proposed 2nd Ed.,* Washington, D.C.: American Association of State Highway and Transportation Officials (AASHTO).

American Association of State Highway and Transportation Officials (AASHTO). (1999). *Guide Specifications for Design and Construction of Segmental Concrete Bridges,* 2nd Ed., Washington, D.C.: American Association of State Highway and Transportation Officials (AASHTO).

American Association of State Highway and Transportation Officials (AASHTO). (2010). *LRFD Bridge Design Specifications.* Washington, D.C.: American Association of State Highway and Transportation Officials (AASHTO).

California Department of Transportation - Division of Maintenance. (2006). *24 0287R/L Lambert Road Under Crossing As-Built Drawings.* Los Angeles, CA: California Department of Transportation (Caltrans).

Corres Peiretti, H., Ezeberry Parrotta, J. I., Berecibar Oregui, A., Perez Caldentey, A., and Ariñez Fernandez, F. (2012). Experimental Study of Thermal Actions on a Solid Slab Concrete Deck Bridge: Validation by Measured Displacements and Comparison with Eurocode 1 Specifications.

Crespo, P. (2005). *Contraste Experimental y de las Variaciones Termincas en Puestes.* III Congreso de ACHE. Volumen I de Comunicaciones, 371-385.

Duffie, J. A., & Beckman, W. A. (1980). *Solar energy thermal processes.* New York: Wiley.

Elbadry, M. M., and Ghali, A. (1983). "Temperature variations in concrete bridges". Journal of Structural Engineering, 109(10), 2355-2374.

Elbadry, M., and Ghali, A. (1986). "Thermal stresses and cracking of concrete bridges". *American Concrete Institute (ACI) Journal*, 1001-1009.

Emerson, M. (1976). "Bridge temperature estimated from the shade temperature". Crowthorne: *TRRL Report SR 696*, Dept of Transport, Crowthorne, England.

European Committee for Standarization Eurocode. (2004). *Eurocode 1 Part 1-5 (CEN). General Thermal Actions.* Brussels, Belgium: European Committee for Standarization Eurocode.

Federal Highway Administration (FHWA). (2009). *National Bridge Inventory (NBI).* Washington, D.C.: Federal Highway Administration (FHWA).

Federal Highway Administration (FHWA). (2012). *California Pilot Bridge Preliminary Field Results.* Washington, D.C.: Federal Highway Administration (FHWA).

Federal Highway Administration (FHWA). (2012). *Utah Pilot Bridge Preliminary Field Results.* Washington, D.C.: Federal Highway Administration (FHWA).

Google Maps. (2013a). Aerial View of the California Bridge. https://www.google.com/maps/@38.3205179,-21.4648037,456m/data=!3m1!1e3

Google Maps. (2013b). Aerial View of the Utah Bridge. https://www.google.com/maps/@41.456846,-112.0552509,119m/data=!3m1!1e3

Halling, D., Barr, D., Womack, D., & Thurgood, T. (2010). *California bridge selection process.* Logan: Utah State University.

Hedegaard, B. D., French, C. E., and Shield, C. K. (2012). *Investigation of thermal gradients effects in the I-35W St. Anthony Falls Bridge.* American Society of Civil Engineers.

Hodson, D. J. (2010). "Live load test and finite element model analysis of a box girder bridge for the long term bridge performance program"*.* MS thesis. Logan: Utah State University.

Imbsen, R. A., Vandershaf, D. E., Schamber, R. A., and Nutt, R. V. (1985). "Thermal effects in concrete bridge superstructures". Washington, D.C.: *NCHRP Report 276*, Transportation Research Board, National Research Council.

Kuppa, S., and Roeder, C. (1991). *Thermal movements in bridges.* Final Report to NSF.

National Oceanic and Atmospheric Administration (NOAA). (1931-2013). Air Temperature Data of the Sacramento Executive Airport Weather Station. Sacramento, California, United States of America.

National Oceanic and Atmospheric Administration (NOAA). (1941-2013). Air Temperature Data of the Hill Air Force Base Weather Station. Clearfield, Utah, United States of America.

Ortega, M., Millanes, F., and Mansilla, J. L. (2010). *Analisis de la Instrumentacion de Temperaturas del Viaducto Mixto de Alta Velocidad Arroyo las Piedras.* HyA 258, 81-97.

Ortega, M., Millanes, F., and Mansilla, J. L. (2011). *Contraste Normativo y Experimental de los Efectos Termicos en Puentes de Hormigon, Metalicos y Mixtos.* Barcelona: V Congreso de ACHE.

Potgieter, I. C., and Gamble, W. L. (1983). "Response of highway bridges to nonlinear temperature distributions". Urbana-Champaign, Ill: *Rep. No. FHWA/IL/UI-201*, Univ. of Illinois at Urbana-Champaign.

Priestley, M. (1978). "Design of Concrete Bridges for Temperature Gradients". *American Concrete Institute (ACI) Journal,* 75(23), 209-217.

Roberts, C. L., Breen, J. E., and Kreger, M. E. (1993). "Measurement based revisions for segmental bridge design criteria". Austin, Tex.: Research Rep. 1234-3F, Center for Transportation Research, Univ. of Texas at Austin.

Roberts-Wollman, C. L., Breen, J. E., and Cawrse, J. (2002). "Measurements of Thermal Gradients and their Effects on Segmental Concrete Bridge". *Journal of Bridge Engineering,* 7(3), 166-174

Rodriguez, L. E. (2012). "Temperature effects on integral abutment bridges for the long-term bridge performance program". MS thesis. Logan: Utah State University.

Roeder, C. W. (2002). "Thermal movement design procedure for steel and concrete bridges". Seattle, WA: *Rep. to the National Cooperative Highway Research Program NCHRP 20-07/106*, University of Washington.

Shushkewich, K. W. (1998). "Design of segmental bridges for thermal gradient". *PCI Journal,* 43(4), 120-137.

Thompson, M. K., Davis, R. T., Breen, J. E., and Kreger, M. E. (1998). *Measured Behavior of a Curved Precast Segmental Concrete Bridge Erected by Balanced Cantilevering.* Austin, Tex.: Report No. FHWA/TX-98/1404-2, University of Texas at Austin.

Utah State Department of Highways - Structures Division. (1975). "3F 205 Bridge As-Built Drawings". Salt Lake City: Utah State Department of Highways.

Utah State Department of Highways - Structures Division. (2005). "3F 205 Bridge Inspection Report". Salt Lake City: Utah State Department of Highways.